

HUGHES

**DETERMINATION OF THE TRIBOLOGICAL FUNDAMENTALS OF
SILICON AND DIAMOND FOR MICRO- AND MACROMECHANISM
APPLICATIONS**

Final Report for the Period 01 November 1996 to 31 October 1997
AFOSR Contract No. F49620-95-C-0002

22 December 1997

DISTRIBUTION STATEMENT A

**Approved for public release
Distribution Unlimited**


Submitted by:
Components & Materials Laboratory
Sensors and Communications Systems
Hughes Aircraft Company
El Segundo, CA 90245

Prepared for:
Air Force Office of Scientific Research (AFOSR/NL)

Maj. Hugh C. De Long, Program Manager

DTIC QUALITY INSPECTION

Prepared by:



M.N. Gardos
Principal Scientist
Materials & Processes
Department

Approved by:



D.I. Basiulis
Manager
Materials & Processes
Department

19980116 112

2000 East El Segundo Boulevard
PO Box 902, El Segundo CA 90245
(310) 616-1375

REPORT DOCUMENTATION PAGE			Form Approved OMB No. 0704-0188	
Public reporting burden for this collection of information is estimated to average 1 hour per response, including the time for reviewing instructions, searching existing data sources, gathering and maintaining the data needed, and completing and reviewing the collection of information. Send comments regarding this burden estimate or any other aspect of this collection of information, including suggestions for reducing this burden, to: Washington Headquarters Services, Directorate for Information Operations and Reports, 1215 Jefferson Davis Highway, Suite 1204, Arlington, VA 22202-4302, and to the Office of Management and Budget, Paperwork Reduction Project (0704-0188), Washington, DC 20503.				
1. AGENCY USE ONLY (Leave blank)		2. REPORT DATE 22 December 1997		3. REPORT TYPE AND DATES COVERED Final Report, 01 Nov. 1996 - 31 Oct. 1997
4. TITLE AND SUBTITLE Determination of the Tribological Fundamentals of Silicon and Diamond for Micro- and Macromechanism Applications			5. FUNDING NUMBERS F49620-95-C-0002 2303/BS 61102F	
6. AUTHOR(S) Michael N. Gardos				
7. PERFORMING ORGANIZATION NAME(S) AND ADDRESS(ES) Hughes Aircraft Company Sensors & Communications Systems Components & Materials Laboratory P.O. Box 902;E1/C182 El Segundo, CA 90245			8. PERFORMING ORGANIZATION REPORT NUMBER	
9. SPONSORING / MONITORING AGENCY NAME(S) AND ADDRESS(ES) Air Force Office of Scientific Research AFOSR/NL 110 Duncan Avenue, Suite B115 Bolling AFB, DC 20332-0001			10. SPONSORING / MONITORING AGENCY REPORT NUMBER	
11. SUPPLEMENTARY NOTES Maj. Hugh C. De Long, Program Manager				
12a. DISTRIBUTION / AVAILABILITY STATEMENT Distribution Statement A. Approved for public release; distribution is unlimited.			12b. DISTRIBUTION CODE	
13. ABSTRACT (Maximum 200 words) SEM tribometry was performed with (a) various Si crystallinities [Si(100), Si(111) and poly-Si], and (b) polished, mostly C(100)-textured and acid-cleaned polycrystalline CVD diamond films [PCDC ₍₁₀₀₎] heated to 850°C (Si) or 950°C (PCD) then cooled to room temperature (RT). The initial test environment was $\sim 1 \times 10^{-5}$ Torr moderate vacuum of the SEM column containing $\sim 93\%$ water vapor in its residual gas environment, followed by 26 Pa (0.2 Torr) total pressure of 99.999%-pure H ₂ (dry PH ₂) as the second test environment, and the same dry PH ₂ containing 2.6 Pa (~ 0.02 Torr) partial pressure of water vapor (wet PH ₂) as the third environment. The data indicate that both H ₂ and H ₂ O can act as atomic level lubricants for Si and PCDC ₍₁₀₀₎ , but only from gas-phase dissociative chemisorption reactions at elevated temperatures well above the boiling point of water. The most effective thermal regions for reducing both the average and the maximum coefficient of friction are near the desorption temperatures of the hydrides, the -OH moieties as well as the bridge bonded Si-O-Si and C-O-C. The wet PH ₂ was particularly effective in reducing the wear rate of the various Si crystallinities from the 10^{-12} m ³ /N·m range found both in vacuum and in dry PH ₂ by one to two orders-of magnitude. The friction and wear of Si and PCD are dependent on the temperature- and gas-phase-induced dissociative chemisorption of H ₂ and H ₂ O passivating the sliding- and heating-induced dangling bonds. The results dispel the current belief that water is harmful under all conditions to Si MEMS surfaces and reinforces the contention the PCD is a far better MEMS bearing material than Si.				
14. SUBJECT TERMS Micromechanisms, friction, wear, SEM tribometry, vacuum, hydrogen, water, partial pressures, high temperatures, dangling bonds, reconstruction, poly-Si, Si(100), Si(111), polycrystalline diamond, C(100) texture, gas lubrication.			15. NUMBER OF PAGES 100	
			16. PRICE CODE	
17. SECURITY CLASSIFICATION OF REPORT Unclassified	18. SECURITY CLASSIFICATION OF THIS PAGE Unclassified	19. SECURITY CLASSIFICATION OF ABSTRACT Unclassified	20. LIMITATION OF ABSTRACT UL	

Table of Contents

	<u>Page</u>
1.0 EXECUTIVE SUMMARY.....	1
2.0 INTRODUCTION AND BACKGROUND.....	2
3.0 THEORETICAL AND EXPERIMENTAL BASIS FOR ESTABLISHING THE MODEL SEM TRIBOMETER EXPERIMENTS IN WET P_{H_2}	4
3.1 Static and Tribochemical Dissociative Chemisorption of H_2O on Silicon.....	4
3.1.1 Theoretical Treatment.....	4
3.1.2 Experimental Literature Data.....	5
3.2 Static and Tribochemical Dissociative Chemisorption of H_2O on Diamond.....	8
4.0 TEST SPECIMENS AND THE $P_{H_2} + P_{H_2O}$ TEST PROCEDURE.....	10
5.0 TEST RESULTS.....	12
5.1 Friction and Wear of Si vs. Si in Dry and Wet P_{H_2}	12
5.1.1 Friction Behavior.....	12
5.1.2 Wear Behavior.....	15
5.2 Friction and Wear of Polished $PCD_{C(100)}$ versus Itself in Dry and Wet P_{H_2}	16
6.0 DISCUSSION.....	18
6.1 Water as a Lubricant for Silicon.....	18
6.2 Water as a Lubricant for Diamond.....	21
7.0 CONCLUSIONS	22
8.0 RESEARCH PERSONNEL.....	23
9.0 TRANSITIONS.....	23
9.1 Hughes/JPL/Caltech Cooperative Technical Agreement.....	23
9.2 A Hughes/JPL/Argonne National Lab Response to a DARPA MEMS BAA.....	24
9.3 Technical Papers	25
REFERENCES.....	26
APPENDIX: M.N. Gardos, "Advantages and Limitations of Silicon as a Bearing Material for MEMS Applications," invited paper presented at the NSF/AFOSR/ASME Workshop <i>Tribology Issues and Opportunities in MEMS</i> , Nov. 9-11, 1997, Columbus, OH; to be published in a book by Kluwer Academic Publishers (in press).....	
	A1

FOREWORD

The main objective of this three-year AFOSR/NL program has been to determine the surface chemistry-driven tribological fundamentals of silicon (Si) and polycrystalline diamond (PCD) as bearing materials used in microelectromechanical systems (MEMS). The focus is on mitigating the high friction- and wear rate-induced failures of Si microelements by atomic-level lubrication with selected surface adsorbates, and by the replacement of Si with adsorbates-lubricated PCD as the preferred MEMS bearing material. The secondary objective has been to determine the possibility of using PCD films for reinforcing conventional macromechanism bearing and gear surfaces for a variety of extreme-environment engineering applications, where low friction and ultralow wear are required. The title of the program has been "Determination of the Tribological Fundamentals of Silicon and Diamond for Micro- and Macromechanism Applications", with a start date of 01 November 1994. This Final Report covers the work done during the third (and final) year of the present program, between 01 November 1996 and 31 October 1997.

List of Tables

- Table 1. Temperature or temperature range of well-defined COF/MAX.COF-reduction drops in Centigrades ($^{\circ}\text{C}$) with *poly-Si in dry and wet P_{H_2}* . Temperature values were read off the indicated illustrations, as guided by the arrows pointing out the COF reduction regions ("drops"), are rounded off to the nearest 50°C . The re(de)construction temperature peaks that follow the initial COF reductions are not marked by arrows to avoid confusion. COF reductions are indicated either by a temperature range or a discrete value, when the drop is sharp. All temperature peaks are indicated by a single value.
- Table 2. Temperature or temperature range of well-defined COF/MAX.COF-reduction drops in Centigrades ($^{\circ}\text{C}$) with *Si(100) in dry and wet P_{H_2}* . Temperature values were read off the indicated illustrations, as guided by the arrows pointing out the COF reduction regions ("drops"), are rounded off to the nearest 50°C . The re(de)construction temperature peaks that follow the initial COF reductions are not marked by arrows to avoid confusion. COF reductions are indicated either by a temperature range or a discrete value, when the drop is sharp. All temperature peaks are indicated by a single value.
- Table 3. Temperature or temperature range of well-defined COF/MAX.COF-reduction drops in Centigrades ($^{\circ}\text{C}$) with *Si(111) in dry and wet P_{H_2}* . Temperature values were read off the indicated illustrations, as guided by the arrows pointing out the COF reduction regions ("drops"), are rounded off to the nearest 50°C . The re(de)construction temperature peaks that follow the initial COF reductions are not marked by arrows to avoid confusion. COF reductions are indicated either by a temperature range or a discrete value, when the drop is sharp. All temperature peaks are indicated by a single value.
- Table 4. Wear rate of Si in dry and wet P_{H_2} during room temperature (RT) "grind" experiments.
- Table 5. Wear rate of Si in dry and wet P_{H_2} during thermally ramped (TR) experiments.
- Table 6. Wear rate (\mathcal{W}) of unpolished and polished PCD in vacuum and in dry P_{H_2} , from [2]. Wear of the pin tip was negligibly small after the dry P_{H_2} experiments, therefore the \mathcal{W} in wet P_{H_2} (attempted with the previously used specimen) could not be determined.

List of Figures

- Figure 1. The COF of the various Si crystallinities at the 15 g load in vacuum and in Round 1 dry P_{H_2} under standard thermal ramping conditions, with the associated unit Hertzian stresses calculated by the wear scar diameters.
- Figure 2. The COF of the polished $PCD_{C(100)}$ vs. itself at 28 g load in vacuum and at various levels of dry P_{H_2} , under standard thermal ramping.
- Figure 3. The COF and MAX.COF of the various Si crystallinities at the 15 g load in dry P_{H_2} under slow thermal ramping conditions, with the associated unit Hertzian stresses calculated by the wear scar diameters.
- Figure 4. The COF of the polished $PCD_{C(100)}$ vs. itself at 28 g load in dry P_{H_2} , under slow and standard thermal ramping conditions.
- Figure 5. The MAX.COF of the polished $PCD_{C(100)}$ vs. itself at 28 g load in dry P_{H_2} , under slow and standard thermal ramping conditions. Equivalent COF curves in Fig. 4.
- Figure 6. Potential energy diagrams for adsorbed water and its dissociation products; from [18].
- Figure 7. Enthalpy changes which accompany adsorption and dissociation of water, referenced to gas-phase hydrogen and oxygen; from [18].
- Figure 8. Suggested arrangements of -H and -OH surface groups on Si after dissociative chemisorption of water: (a) monohydride with OH nearest neighbor, (b) monohydride with O nearest neighbor, (c) pure monohydride, and (d) dihydride. Note that the angles are associated with the effective dynamic dipole moment rather than the geometric band; from [28].
- Figure 9. Bridged, hydrogen-bonded water clusters bonded to the hydrophilic sites of a Si surface; after [30].
- Figure 10. Wear rate and COF of PCD films in various atmospheric environments; from [15].
- Figure 11. Wear rate and COF of PCD films in distilled water; from [15].
- Figure 12. Water saturation apparatus for introducing wet P_{H_2} into the SEM tribometer.
- Figure 13. The COF of the various Si crystallinities at the 15 g load in vacuum and during the Round 3 dry P_{H_2} and the only round of wet P_{H_2} experiments, with the associated unit Hertzian stresses calculated by the wear scar diameters.
- Figure 14. The MAX.COF of the various Si crystallinities at the 15 g load in vacuum and during the Round 3 dry P_{H_2} and the only round of wet P_{H_2} experiments, with the associated unit Hertzian stresses calculated by the wear scar diameters. Equivalent COF curves in Fig. 13.
- Figure 15. COF and MAX.COF of the poly-Si shakedown test at a 15 g load in dry P_{H_2} using a preworn pin tip, as compared with the Round 1 dry P_{H_2} poly-Si test performed at the same 15 g load; from [72].

- Figure 16. COF and MAX.COF of the Round 1 dry P_{H_2} tests at a 15 g load for all Si crystallinities, generated with prepolished pin tip scars further ground by a 1000-cycle planarization procedure performed at a 15 g load; from [72].
- Figure 17. COF and MAX.COF of the Round 2 dry P_{H_2} tests tests at a 15 g load using poly-Si and Si(111) specimens only, with prepolished pin tip scars further ground by a 1000-cycle planarization procedure performed at a 15 g load; from [72].
- Figure 18. Predicted temperature-programmed desorption of hydrogen from a porous silicon surface, using experimental dihydride and monohydride desorption kinetics; from [74].
- Figure 19. Smoothed thermal desorption spectra from H-terminated Si(100). The temperature-programmed desorption spectroscopic (TDS) signatures are shown for (a) H_2 ($m/e = 2$), (b) CH_3 (15), (c) $CH_3(CH_2)_3$ (57), and (d) $CH_3(CH_2)_3CO$ (85). The ramp rate was $10^\circ C/s$; from [75].
- Figure 20. Measured temperature-induced desorption of hydrogen from (a) an oxygen deficient silicon grain boundary, (b) an oxygen-containing grain boundary; from [76].
- Figure 21. Measured temperature-programmed desorption of hydrogen (H_2) for as-deposited boron-doped, amorphous hydrogenated silicon (a-Si:H) films (solid line) and films annealed for 100 hours at $220^\circ C$ (dash-dotted line); from [77].
- Figure 22. SEM photomicrographs of Si pin tip wear scars at 100x mag., after the respective dry and wet P_{H_2} 15 g load RT "grind" + 15 g load standard thermal ramp experiments.
- Figure 23. SEM photomicrographs of Si flat wear scars at 100x and 2000x mags., after the respective 15 g load dry P_{H_2} RT "grind" + 15 g load standard thermal ramp experiments. Photos of matching pin tip scars at 100x mag. in Fig. 22.
- Figure 24. SEM photomicrographs of Si flat wear scars at 100x and 2000x mags., after the respective 15 g load wet P_{H_2} RT "grind" + 15 g load standard thermal ramp experiments. Photos of matching pin tip scars at 100x mag. in Fig. 22.
- Figure 25. SEM photomicrographs of Si flat wear scars at 2000x mag., after the respective 15 g dry and wet P_{H_2} RT "grind" + 15 g load standard thermal ramp experiments. Photos show typical tensile microcracking of the respective surfaces.
- Figure 26. SEM photomicrographs of poly-Si pin tip and flat wear scars at 100x and 500x mags., after the respective 15 g load RT "grind" + 15g load standard thermal ramp experiments in vacuum.
- Figure 27. SEM photomicrographs of Si(100) pin tip and flat wear scars at 100x and 500x mags., after the respective 15g load RT "grind" + 15g load standard thermal ramp experiments in vacuum.
- Figure 28. SEM photomicrographs of Si(111) pin tip and flat wear scars at 100x and 500x mags., after the respective 15g load RT "grind" + 15g load standard thermal ramp experiments in vacuum.

- Figure 29. Typical peak-type $\text{PCD}_{\text{C}(100)}$ COF curves taken from the various 28 g load dry PH_2 standard thermal ramp test rounds described more thoroughly in [2], not showing re(de)constructions troughs previously depicted in Fig. 2.
- Figure 30. Typical peak-type $\text{PCD}_{\text{C}(100)}$ MAX.COF curves taken from the various 28 g load dry PH_2 test rounds described more thoroughly in [2], not showing re(de)constructions troughs previously depicted in Fig. 2. Equivalent COF curves in Fig. 29.
- Figure 31. All $\text{PCD}_{\text{C}(100)}$ COF curves taken from the 28 g load wet PH_2 experiments.
- Figure 32. All $\text{PCD}_{\text{C}(100)}$ MAX.COF curves taken from the 28 g load wet PH_2 experiments.
- Figure 33. Temperature programmed desorption spectra (symbols) and first order fits (solid lines) off PCD for initial deuterium coverages of 0.27 ML (●), 0.40 ML (▼), 0.52 ML (■), and 0.57 ML (▲). The fit parameters are $E_a = 51$ kcal/mol and $\nu = 5 \times 10^7$ s⁻¹; from [78].
- Figure 34. Calculated coverage of atomic hydrogen on C(100) as a function of surface temperature for three values of H atom flux shown; from [79].
- Figure 35. Thickness of titanium oxide (1) and silicon oxide (2) layers produced by surface hydration as a function of temperature; from [82].
- Figure 36. Schematic representation of the types of water adsorbed on TiO_2 : Type I is hydrogen-bonded to surface hydroxyl groups, whereas Type II is hydrogen-bonded to a bridging oxygen atom; from [83].
- Figure 37. Modeled schemes of surface hydroxylations and partial dehydroxylations; from [84].

1.0 EXECUTIVE SUMMARY

SEM tribometry was performed with (a) various Si crystallinities [Si(100), Si(111) and poly-Si], and (b) polished, mostly C(100)-textured and acid-cleaned polycrystalline CVD diamond films [PCD_{C(100)}] heated to 850°C (Si) or 950°C (PCD) then cooled to room temperature (RT). The initial test environment was $\sim 1 \times 10^{-5}$ Torr moderate vacuum of the SEM column with $\sim 93\%$ water vapor in its residual gas environment, followed by 26 Pa (0.2 Torr) total pressure of 99.999%-pure H₂ (dry P_{H₂}) as the second test environment, and the same dry P_{H₂} containing ~ 2.6 Pa (~ 0.02 Torr) partial pressure of water vapor (wet P_{H₂}) as the third environment.

The data indicate that both H₂ and H₂O can act as atomic level lubricants for Si and PCD_{C(100)}, but only from gas-phase dissociative chemisorption reactions at elevated temperatures well above the boiling point of water. The most effective thermal regions for reducing both the average and the maximum coefficient of friction (COF and MAX.COF, respectively) are near the desorption temperatures of the dihydrides, monohydrides, the -OH moieties and the most stable oxygenated surface groups (e.g., the bridge bonded Si-O-Si and C-O-C). The wet P_{H₂} was particularly effective in reducing the wear rate (\mathcal{W}) of the various Si crystallinities from the 10^{-12} m³/N·m range found both in moderate vacuum and in dry P_{H₂} by one to two orders-of magnitude. However, this reduction occurs only at low Hertzian stresses, on the order of 10 MPa or less. At RT only (no thermal ramping) and under the high starting Hertz stresses of near 430 MPa, there was essentially no difference in the wear rate of Si in either dry or wet P_{H₂}. In contrast, the \mathcal{W} of PCD_{C(100)} remained at or below $\sim 10^{-16}$ m³/N·m in any and all test environments and thermal regions at loads ranging from 1.7 GPa down to 5 MPa, with COF and MAX.COF values below those of the respective Si tests.

The three-year program has conclusively demonstrated that the friction of wear of Si and diamond are highly dependent on the temperature- and gas-phase-induced dissociative chemisorption of hydrogen and water vapor passivating the sliding-and heating-induced dangling bonds on the interacting surfaces. The most surprising finding has been that a low partial pressure of ~ 0.02 Torr of water vapor is a better atomic level lubricant than its dry hydrogen carrier. The results dispel the current belief that water is harmful under all conditions to Si MEMS surfaces due to "stiction" effects, and reinforces our original contention the PCD is a far better MEMS bearing material than Si.

2.0 INTRODUCTION AND BACKGROUND

As shown in a recently presented paper now in press [1] (attached here as an APPENDIX), during wide temperature range SEM tribometry in the benign atmospheric environment of a 0.2 Torr partial pressure of 99.9999%-pure hydrogen gas (P_{H_2} ; Matheson Research Purity, typical water content <0.5 ppm; actual water analysis of source cylinder content $<0.05 \text{ ppm} \leq 3.8 \times 10^{-5}$ Torr P_{H_2O} in 760 Torr = 1 atm. of the hydrogen gas), the COF of the various Si crystallinities was as high or higher than in vacuum, and significantly higher than the COF of the $PCD_{C(100)}$. However, there was a remarkably repeatable reduction in COF in a narrow thermal range just below the desorption temperature of hydrogen (Fig. 1, right column, see arrows), indicating the same type of heating- and sliding-catalyzed dissociative chemisorption of H_2 previously observed with PCD [2] (Fig. 2, right column, see arrows).

The presence of this chemisorptive thermal-atmospheric region was confirmed by slow-thermal-ramp SEM tribometry both with Si (Fig. 3) and polished $PCD_{C(100)}$ (Figs. 4 and 5). Unlike PCD, however, deconstructed (dangling) Si bonds did not seem to react with H_2 on cooling, leaving the COF at high values at or near RT (Fig. 1). Only the Si(100) appeared to benefit somewhat from P_{H_2} in terms of some wear rate reduction. The other crystallinities exhibited essentially the same wear rates in vacuum and P_{H_2} on thermal ramping to 850°C (near $10^{-12} \text{ m}^3/\text{N}\cdot\text{m}$, 10^4 -times higher than PCD), although the wear rates were reduced during testing only at RT by about an order-of-magnitude or more. The wear rates could be further lowered by keeping COF the least by staying within the temperature range of the tribocatalytic thermal-atmospheric reaction region.

These SEM tribometer results agreed with the reported ability of *molecular* hydrogen to passivate dangling Si bonds on heating. As more thoroughly described in [1], an early 1967 paper dealing with the passivation of dangling Si bond defects at the Si/SiO₂ interface demonstrated that baking in H_2 at temperatures between 1000° and 1200°C negated the effects of electron trapping at the interface. A patent was granted along the same lines in 1979, showing that passivation could already be achieved between 650° and 950°C . Since then, others have also examined this method Si/SiO₂ trap reduction at even lower temperatures. For example, annealing of Si solar cells in H_2 at 300°C already significantly improved device performance. In fact, both atomic and molecular hydrogen passivated the dangling bonds at the grain boundaries of poly-Si. The H_2 deactivated the free radicals during elevated temperature annealing, although not as effectively as H.

Our concept of using water vapor as an atomic-level lubricant for Si began to germinate when the COF data generated with Si crystallinities in moderate vacuum were compared with those obtained in P_{H_2} . The starting COF of the high-wear-rate pin/flat specimens (i.e., those exhibiting wear-induced dangling bonds on their rubbing surfaces) always seemed to be lower in the $\sim 1 \times 10^{-5}$ Torr atmosphere of the SEM column containing 93% water vapor in the residual gases (Fig. 1, left column) than the same type of specimens tested in of 0.2 Torr of 99.9999% P_{H_2} (Fig. 1, right column). In addition, retrospectively, the slight but perceptible reduction of COF at the onset of heating the poly-Si and the Si(100) during the low-load (15 g) testing in the same type of moderate vacuum (see arrows in Fig. 1, left column), and the equally slight but also quite perceptible reduction in COF of the polished $PCD_{C(100)}$ (see arrows in Fig. 2, left column) may have also signalled the presence of a similar "water-lubrication" mechanism. Not having been sufficiently clarified at the time, the slight RT COF reduction peaks in both atmospheres were dismissed as typical variations in friction not attributable to any particular input parameter. As will be shown later here with a larger number of test results, the residual water vapor in both vacuum and in 99.9999% P_{H_2} does leave a small but recurring tribochemical imprint behind at RT and even more at elevated temperatures, with significantly more pronounced signatures on heating where the P_{H_2} contains more water vapor.

In spite of the fact that the MEMS literature is awash with reports of the harmful effects of either ordered molecular layers of hydrogen-bonded H_2O or capillary (bulk) water trapped within the exceedingly small clearances of Si MEMS moving mechanical assemblies (MMAs), the validity of employing such a mechanism for lubricating Si MEMS-MMAs with some water under certain conditions was further strengthened by the experimental facts that (a) heating in the presence of water vapor can also annihilate Si dangling bonds at the Si/SiO₂ interface [1,3-5], and (b) boiling in water alone, in the absence of any other HF- or NH_3F -type rinsing procedures, can completely hydrogenate Si surface bonds [6-9]. The advantageous effects of water on the tribological properties of diamond have already been known for some time [10-15], in agreement with the results of SEM tribometry on various forms of PCD in the water vapor-laden residual atmosphere of the SEM column at $\sim 1 \times 10^{-5}$ Torr [16,17].

The remarkable parallel between the apparent ability of both molecular hydrogen and water vapor to passivate dangling Si and diamond bonds prompted a closer look at the theoretical and experimental aspects of tribothermal water sorption onto Si and polished $PCD_{C(100)}$. The existing knowledge was meant to serve as the basis for establishing an SEM tribometry regimen performed with both specimen types in wet P_{H_2} .

3.0 THEORETICAL AND EXPERIMENTAL BASIS FOR ESTABLISHING THE MODEL SEM TRIBOMETER EXPERIMENTS IN WET P_{H_2}

3.1 Static and Tribochemical Dissociative Chemisorption of H_2O on Silicon

The adsorption of H_2O on Si surfaces is important in semiconductor technology, being the initial step in the wet-oxidation of Si. As shown in Thiel and Maddey's thorough 1987 overview dealing with the interaction of water with solid surfaces [18], this subject has been studied both theoretically and experimentally for years. Their treatise includes ample experimental evidence of water dissociatively chemisorbing on Si, especially on the highly reactive Si(100)-(2x1). The initial absorption probability (the sticking coefficient S_0) of H_2O on Si(111)-(7x7) at 300 K is at least two-orders-of-magnitude lower than on Si(100)-(2x1), where it is about unity. The S_0 on a cleaved Si(111)-(2x1) surface represents an intermediate case, with a value about 10-times lower than on the Si(100)-(2x1). Hydrogen termination of the Si(100) surface atoms reduces the rate of sorption, at low coverages, on the Si(100) surface by at least 10 (and perhaps as much as 14) orders of magnitude. At the time of Thiel and Maddey's publication it was still questionable, however, whether or not dissociation occurs at RT, and what the mechanism of H_2O -Si interaction might be at elevated temperatures.

3.1.1 Theoretical Treatment

In general, the experimental findings in [18] were in accordance with simple thermodynamic arguments explained with the help of Figs. 6 and 7. In Fig. 6, the potential energy curve of adsorbed H_2O can have a minimum, which is either higher in energy than the dissociated products (Curve No. 1) or lower than the adsorbed hydrogen and oxygen (Curve No. 2). In the first case, dissociative chemisorption is thermodynamically favored; in the second, it is not. If the activation energy barrier to dissociative chemisorption ($E_{act/dcs}$) is sufficiently high, dissociation may be prevented due to kinetic limitations, even though it may be thermodynamically favored.

The respective energies are schematically depicted in Fig. 7, using atomic hydrogen and oxygen as the products of dissociation. The change in enthalpy (ΔH) which is associated with the *nondissociative* adsorption of H_2O is simply the negative of the heat of desorption (assuming no barrier to adsorption).

Using the classical approach of $\Delta H_{dcs} = \Delta H_f$ (dissociation products) - ΔH_f (H_2O gas), Thiel and Maddey [18] estimated ΔH_f of the dissociation products from (a) the strength of the Si-O bond in crystalline SiO_2 [-453 kJ/mol (\sim -108 kcal/mol)], and (b) Si-H bond strength of

chemisorbed hydrogen [-240 to -336 kJ/mol (~ -58 to -81 kcal/mol)]. As defined in Fig. 7, this leads to $\Delta H_{\text{dcs}} \equiv -700$ to -892 kJ/mol (~ -168 to -214 kcal/mol), a value much more negative than the chemisorption bond strength of molecular water (-50 kJ/mol (~ -12 kcal/mol)). As such, dissociative chemisorption is indeed strongly favored.

3.1.2 Experimental Literature Data

In order to design and control surface structures by adsorbates on the atomic scale, it is very important to characterize and understand the charge transfer between an adsorbate and the substrate and, as a prerequisite, know the influential local electronic structures of the surface. This is also the case with the sorption of various gases and vapors on Si. For example, the initial reactive sites and subsequent reactions of oxygen and ammonia molecules are governed by the local electronic structure of the Si surface. This mechanism is largely determined by the type of reconstruction cell(s) present as a function of surface treatment [19-21]. Indeed, during examination in an SEM, the secondary electron intensity changed depending on the direction of the dimer rows on Si(100) [1×2 = light contrast; 2×1 = dark contrast], and between the 7×7 (light) and unreconstructed 1×1 structures (dark) on Si(111) [21]. Essential semiconductor industry processes such as atomic layer epitaxy and initial growth of semiconductors (e.g., Si) depend on the understanding of these fundamental aspects of adsorbate versus surface interactions.

As also described in [21], the Si(111) surface structure undergoes a transformation between the reconstructed (7×7) and the unreconstructed (1×1) at 830°C , and that these structures co-exist at the transition temperature. Heating the Si(111) to 1300 K (1027°C) produces a clean and well-ordered (7×7) surface [22].

The reconstruction of the Si(111)-(7×7) surface is a subject of continued interest. The Si(111)-(7×7) has been probably the most complex and most widely studied surface of a solid [23], mainly because its stability constitutes ubiquitous problems (a) during the CVD growth of Si, and (b) as to the reactivity of Si surfaces with a variety of substances at elevated temperatures. For example, the characteristically high stability of the Si(111)-(7×7) surface is manifested by the low sticking coefficient S_0 of SiCl_4 (a CVD growth precursor) as a function of temperature (~ 0.18 at 160 K to ~ 0.03 at 600 K) [24]. The initial reactive S_0 of diethylsilane (another growth precursor) on Si(111)-(7×7) decreased versus the surface temperature from $\sim 1.7 \times 10^{-3}$ at 200 K to $\sim 4 \times 10^{-5}$ at 440 K. At 300 K this adsorbate began to be dissociatively chemisorbed, however, producing Si-H and Si- C_2H_5 surface species. Annealing at temperatures to 700 K revealed that *hydride coverage increased* as the hydrocarbon decomposed at progressively higher temperatures, with ethylene and molecular hydrogen as the desorbed byproducts [25].

The stable Si(111)-(7x7) must be heated to high temperatures to render it reactive. Temperatures above ~750 °C were needed to provide the required activation energy for the generation of surface dangling bonds by restructuring the Si(111)-(7x7) surface for reaction with CaF₂ [26]. Annealing the Si(111)-(7x7) surface to 1020 K causes C₆₀ fullerene cages applied onto this surface to open and thereby cover more of the reconstructed surface. The cage opening was correlated with an increase in Si-C bonding [27].

As to dissociative chemisorption mechanisms of water on Si, early suggested arrangements of the dissociated H and OH moieties on the Si surface [28] are shown in Fig. 8. The off-normal direction of the surface bonds (i.e., the Si-OH bond is tilted off-normal on the surface) has since been confirmed [29]. Then, in water vapor-containing atmospheric environments, H₂O molecules can sorb onto the hydroxylated Si surface atoms, forming water bridges with the relatively high hydrogen bond energy of ~5 kcal/mol (Fig. 9, after [30]). The strength of this bond leads to liquid water condensing between oxidized Si surfaces in air, at sufficiently high relative humidities. The subsequent generation of ultrathin layers of grease-like hydrated silica generated by the reaction $\text{SiO}_2 + 2\text{H}_2\text{O} \rightarrow \text{Si}(\text{OH})_4$ [31,32] is believed to cause the highly undesirable "stiction" of oxidized, hydroxylated then hydrated Si MEMS-MMA components.

The dissociative chemisorption steps of water on Si are highly temperature dependent. Since Thiel and Madey's days it has been determined that water dissociates upon adsorption at 300 K (27 °C) to form Si-H and Si-OH surface species. On water-saturated surfaces, the the Si-OH groups decompose between 460 and 860 K (187 ° and 307 °C) to form Si-O-Si species and additional surface hydrogen between 460 and 580 K (187 ° and 314 °C). The Si-H surface species decreased as H₂ desorbed above 700 K (427 °C) [33]. The hydroxyl and hydride groups are chemically stable at RT under ultrahigh vacuum. Above ~420 K (~147 °C) the Si-OH was found to decompose gradually into silicon oxide and more hydride. Finally, above 600 K (~327 °C), hydrogen desorbs from the surface to leave the oxygen behind [34]. On heating, the surface -OH is eventually converted to bridge-bonded oxygens at temperatures ≥550 K (~277 °C), which finally penetrates to form SiO₂ at T ≥ 750 K (~477 °C) in a strongly disturbed bond configuration [35].

On further heating close to 900 °C in high vacuum or at low partial pressures of oxygen, any SiO₂ is removed from the Si surface by decomposition to the volatile SiO. This removal exposes regions of atomically clean Si [36-39]. It has already been established that at these high temperatures even the stable Si(111)-(7x7) reconstruction will break up into dangling bonds. Under low PO₂ environmental conditions, the surfaces of both Si₃N₄ and the various SiC polytypes become similarly depleted of their passivating SiO₂ layers by the same "active oxidation" [40-42].

More importantly, Watanabe et al [7-9] demonstrated that aqueous HF- and NH_4F solutions were not necessary for complete surface hydrogenation of Si bonds. Boiling in water for periods as short as 5 minutes resulted in the dissolution of any SiO_2 , followed by complete surface hydride formation. There was a complete absence of hydroxyl termination. Where the oxide layer was thicker or more tenacious, longer boiling times (up to 60 minutes) were necessary to obtain the same condition.

In an interesting parallel, temperature-programmed desorption (TPD) studies of two different types of raw and water-Soxhlet -extracted Si_3N_4 powders (for 405 hours) indicated, that the surface energy of the extracted powders was far lower than the raw versions. In each case, the TPD spectra showed that the raw powders lost a great deal of water starting at temperatures between 300 and 400 K (27 ° and 127 °C) somewhat diminishing at higher temperatures, along with the evolution of lesser amounts of H_2 . Hydrogen desorbed with progressively higher intensity as the temperature was further increased. In contrast, the water-washed samples lost much smaller amounts of water between 300 and 400 K, with very low continuing water loss at temperatures to as high as 900 K (627 °C). The associated hydrogen loss was very high (higher than in the previous case), with the rate of loss increasing sharply above 700 K (427 °C). Ammonia loss at elevated temperatures was also significantly higher with the water-washed samples [43]. These data make sense only if the dissolution of the silicon oxides from the powder particle surfaces during the Soxhlet extraction process was followed by hydrogenation of the dangling Si surface bonds, with the attendant reduction of surface energy.

In terms of tribochemistry of water with Si surfaces, Si wafers are routinely polished in slurries containing fumed silica suspension dispersed in aqueous KOH (pH~10), whereby the tribochemically formed silicon oxide/hydroxide is continually dissolved-abraded away. The chemical part of the removal rate depends on the tribocatalytic effect of the load and the speed, affecting the rubbing-induced generation of active sites (dangling bonds) on the surface [44]. Other energy input (e.g., ion-sputtering with argon) equally capable of dangling bonds formation also increases the hydration (ergo the water-wettability) of Si surfaces [45]. Silicon oxide formation beneath an AFM tip by applying a negative bias voltage between the p^+ silicon tip and a Si surface through tip-induced anodization in the presence of adsorbed water was assumed to be the cause of the surface transformations [46]. The above results agree with the basic tribochemical formation and removal mechanisms of the hydrated silica from the surfaces of Si, SiC and Si_3N_4 [47-51].

The overly generalized statements that "water also decreases the wear and friction coefficients of oxide ceramics" and "amorphous hydroxide layers serve as lubricants during friction of Al_2O_3 and SiO_2 in water" [52] must be viewed with caution, however, when referring to surface hydration of Si. For example, in spite of the facts that ball-on-flat Si versus Si tribometry was done in dry argon at RT [53], the native oxides combined with the residual sorbed water and the H_2O remaining in the dried argon or originating from the test chamber walls turned the surface oxides-hydroxides into micro-rolls between the sliding specimens. The formation of these rolls is akin to the rolls generated by rubbing an eraser against paper. The coefficient of friction (COF) was reduced from the relatively high 0.45 to about half that value (still high by MEMS standards) at a 2.65 N normal load. Above that load, the reduced COF fluctuated between 0.2 and 0.4, meaning that the "lubricating" rolls had limited load-carrying capacity.

Roll formation occurs especially readily by (a) compaction of a tribofilm consisting of silica platelets containing some minimally adsorbed water, which enhances the adhesion between the platelets, and (b) delamination of the wetted platelets into rolled aggregates by the shear forces that develop during sliding. The COF was lowered from 0.5 - 0.6 (no rolls at 100 °C) to ~0.2 (rolls at 600 °C), with the reduction maintained far better at an H_2O partial pressure ($P_{\text{H}_2\text{O}}$) of 0.034 MPa (~200 Torr) than at $P_{\text{H}_2\text{O}} = 0.008$ MPa (~50 Torr). The wear of the Si was also progressively reduced by an increase in temperature from 100 °C to 300 °C, and finally to 600 °C [54]. Not only hydrated silica on a variety of hydrated SiO_2 -containing ceramics, but other relatively soft debris particles of different chemistry can undergo similar roll formation during sliding [55].

During benchtop tribometry, however, where the available power to continue sliding (and to generate the "lubricative" rolls) is usually available regardless of the COF magnitude, is not the same tribosystem as MEMS gears and bearings rotated by e.g., an electrostatic micromotor. A sufficient amount of capillary water and/or hydrated silica in the narrow clearances of MEMS-MMAs can bind up the mechanisms due to the limited power available to drive the motor.

3.2 Static and Tribochemical Dissociative Chemisorption of H_2O on Diamond

Since the use of PCD for microelectronics and other applications is more recent than that of Si, the literature contains less information on the chemisorption of adsorbates and, in particular water, on diamond surfaces. In addition to the early water sorption data collected in [16], Struck and D'Evelyn's IR spectroscopy [56,57] has identified hydroxyl, ether and carbonyl groups on C(100) as water dissociatively chemisorbed on cooling from 770 °C in 1×10^{-7} Torr $P_{\text{H}_2\text{O}}$. It was hypothesized that H_2O has another role besides being an oxygen carrier to promote growth of pure

PCD films at lower temperatures. Because it dissociatively chemisorbs on diamond, it can also saturate dangling bonds on the surface in the form of C-OH groups [58,59].

Inasmuch as the bond energy of the C-OH (85 kcal/mol) is lower than that of the C-H (107 kcal/mol), the -OH group should be easier to desorb than the less stable carbonyl and the more stable ether groups [60]. These moieties begin to leave the diamond surface above 400 °C as CO and above 500 °C as CO₂ [61]. At PCD growth temperatures below 680 °C, H₂O simultaneously inhibits diamond oxidation. A small increase in relative humidity can result in a significant reduction in the rate of diamond etching by O₂ at typical deposition temperatures [59,62]. The addition of water below 800 °C and the attendant retardation of etching of the diamond phase by molecular oxygen was attributed to the formation of C-OH bonds.

In contrast, hydrogen does not desorb in large quantities until about 1000 °C. Since it requires greater energy to desorb it, the CVD growth temperatures in the presence of only hydrogen have to be above 850 °C. The lower bond strength of -OH thus permits the deposition of PCD at lower temperatures, along with the ready removal of sp²-bonded (nondiamond) contaminant by the same addition of water [63-65].

Vacuum annealing of as-grown CVD-PCD films removed all hydrides from the surface at 1470 K (1197 °C). Subsequent air exposure to surface saturation resulted in the adsorption of atmospheric gases such as oxygen and water. On reheating the film, hydrogen was released between 1100 and 1470 K (827 ° and 1197 °C). The thermal desorption spectrum of hydrogen had two peaks at 1170 and 1320 K (897 ° and 1047 °C, respectively). Up to 70% of the bonded hydrogen was attributed to water adsorption on the diamond during air exposure [66].

As previously mentioned, friction and wear tests of single-crystal diamond pins sliding against single-crystal and CVD-PCD flats in various environments indicated that H₂O is an excellent lubricant. The COF was reversibly reduced/increased from ~0.08 to 0.06 to below 0.02 going from air to water and back to air [10,11], and in similar experiments from ~0.15 to as low as 0.05 going again from air to water [12]. In other recent experiments with polished PCD-coated pins sliding against similarly coated flats in the water-wetted test mode, Miyoshi [13-15] reported unusually low friction and wear rate values (Figs. 10 and 11). These data agree with the low-friction and low-wear SEM tribometer experiments we have conducted to date with polished PCD_{C(100)} specimens in ~1x10⁻⁵ Torr vacuum, where over 90% of the residual gases consisted of water vapor [16,17].

4.0 TEST SPECIMENS AND THE $P_{H_2} + P_{H_2O}$ TEST PROCEDURE

The literature data presented above indicate that water vapor should act as an atomic level lubricant (a) for Si above the boiling point of water, where condensed liquid could not cause excessive COF in MEMS-MMAs or perhaps even in benchtop tribometry, and (b) for diamond in any reasonable test environment. As such, the SEM tribometer test technique developed for testing in a dry P_{H_2} atmosphere would be fully applicable in the present case, provided water vapor could be introduced into P_{H_2} kept at ~ 0.2 Torr in some manner. Mixing water into P_{H_2} would be particularly suitable, because Burt and Matthies [4] have found by testing Si in wet hydrogen that the atomic hydrogen species on the Si mainly appeared to be due to the reaction of water supplied by the annealing gas with the active sites on its oxide surface. The contribution of the molecular hydrogen of the annealing ambient to the observed annealing kinetics of the Si/SiO₂ interface traps seemed to be of lesser importance.

A clean, 4 cm diameter, 9 cm long 304 stainless steel gas filter vessel (Scott Model 53-45H5) with the fibrous gas filter cartridge removed served as a water saturation device for the gently flowing hydrogen (Fig. 12). Since the hydrogen was passing through the needle valve at extremely slow flow rates to provide the ~ 0.2 Torr total pressure of $H_2 + H_2O$ in the tribometer subchamber, the conventional method of testing materials in wet hydrogen by bubbling the dry gas through distilled water [67-69] could not be accomplished. Instead, the gas mixture was allowed to come to saturated equilibrium with water vapor in the stainless steel vessel at RT without any special thermostated state, prior to introduction into the preferentially pumped tribometer subchamber. This methodology was similar to the one used in [70].

Using Fig. 12 as a guide, the detailed water introduction procedure is as follows:

1. Close needle valve.
2. Pump down the SEM column to $\sim 1 \times 10^{-5}$ Torr.
3. Half-fill stainless steel water saturation vessel.
4. Heat thermostated needle valve to $\sim 50^\circ \text{C}$ and keep at that temperature until the entire experiment is completed.
5. Adjust gas regulator pressure to 10 psig H_2 , with the regulator outlet valve closed.
6. Pressurize water vessel with the 10 psig H_2 by opening the regulator valve.
7. Close regulator valve.
8. Evacuate dead air space of water vessel to -25 psig (Max. vacuum level) through the needle valve, very slowly. *CAUTION: evacuation to less than -25 psig will cause the water to degas and boil. Slow evacuation is absolutely necessary to*

prevent liquid water from entering the needle valve and thus the SEM tribometer subchamber.

9. Close needle valve.
10. Repeat Steps 6 through 9 ten times.
11. Pressurize water vessel to 10 psig H_2 , then close regulator outlet valve and needle valve.
12. Allow water vapor to reach equilibrium with the H_2 -filled water vessel and transport tube volume overnight under 10 psig H_2 .
13. On following morning, crack needle valve until the subchamber Baratron pressure gage registers 0.2 Torr and proceed with the experiment.

Note in Step 4 that the Joule-Thomson expansion of the gas mixture exiting the needle valve into the subchamber has chilled the water vapor to the point of ice formation, stopping the gas flow. The needle valve had to be wrapped with a heating tape and thermostated to the lowest possible temperature ($\sim 50^\circ C$) to melt/vaporize the ice and reinstate the flow.

The P_{H_2O} in the total of 0.2 Torr pressure of the gas mixture was estimated by (a) shutting off the flow of the mixture into the subchamber, (b) measuring the subchamber pressure during continued pump-down (note that the mechanical pump is always assisted by the turbomolecular pump helping in the evacuation of the subchamber through the lid orifice), and (c) determining the inflection pressure, where the characteristically rapid evacuation of hydrogen was followed by the more slowly developing pressure change attributed to the more difficult-to-pump residual water vapor. This methodology resulted in estimating a ~ 0.02 Torr P_{H_2O} in ~ 0.2 Torr (actually, 0.18 Torr by Dalton's Law) P_{H_2} . A similar technique of P_{H_2O} approximation was practiced in [71].

Prior to tribometry, all Si specimens received an aqueous HF treatment to remove all surface oxides and to cap all surface bonds with hydrogen, as before. The polished $PCDC(100)$ pin and flat previously employed to repeatedly test this combination in vacuum [17] and then in P_{H_2} [2] were again reused a number of times for the wet hydrogen tests, but only after the customary hot chromic acid solution cleaning step to remove all surface contaminants. All other test technique steps previously used for P_{H_2} experimentation of Si or $PCDC(100)$ were also employed here. These additional steps have been adequately described in [1,2,72].

5.0 TEST RESULTS

5.1 Friction and Wear of Si vs. Si in Dry and Wet P_{H_2}

5.1.1 Friction Behavior

The COF and the associated MAX.COF charts of the last round (Round 3) of the dry and the only round of wet P_{H_2} tests are shown in Figs. 13 and 14, respectively, as a function of temperature. These data are compared with all the other previous rounds of dry P_{H_2} experiments described in [1,72] and summarized here in Figs. 15 through 17. The results must be viewed in light of the fact that the sapphire reaction barrier plate between the Si flat and the Pt heater strip is thermally insulative. Combined with the position of the thermocouple unavoidably located *below* the heater strip, *the recorded heater temperatures are always below the actual surface temperature of the Si flat* during heating and sliding. In vacuum, this ΔT value was estimated to be 200°C [73]. In P_{H_2} it is less due to the higher thermal conductivity of the P_{H_2} test atmosphere, estimated to be ~100 °C [1,2]. As a consequence, all temperatures read off the charts and subsequently included in tables were increased by 100 °C.

The most important observation from the data in Figs. 13 through 17 is that the remarkable reduction in COF and MAX.COF previously observed in dry hydrogen at the estimated surface temperatures of between 250° and 450°C also occurs in the wet gas. There are distinct similarities and a few significant differences between the dry and wet friction data, as measured by sudden thermally- and sliding-induced changes in the COF and MAX.COF. The inflection temperatures taken from the above illustrations, representing measurable and often abrupt decreases or increases in COF-MAX.COF, are summarized in Tables 1, 2 and 3. The COF inflection points and regions are always reconciled with the respective MAX.COF inflections for the most representative data possible. The data from all dry P_{H_2} tests are averaged (where prudent and applicable), because the best overall and most reliable Third Round of the dry P_{H_2} experiments juxtapositioned with the *only* round of wet ones in Figs. 13 and 14 are not completely representative of all the other dry tests depicted in Figs. 15 through 17.

To compare the best inflection temperatures associated with the dry and wet friction reduction zones (3 ea. with all crystallinities), and the peaks hypothesized to be the results of re(de)construction (2 ea. with all crystallinities), the temperatures within each dry round were averaged. Averaging was accomplished by reading off the inflection temperature values and/or ranges from Figs. 13 through 17, as guided by the arrows pointing out the COF/MAX.COF change boundaries rounded off to the nearest 50°C. The re(de)construction temperature peaks that follow the

initial COF reductions preceding these peaks are not marked by arrows to avoid confusion. The reductions in friction (called "drops" in Tables 1 through 3) were logged either as temperature ranges where the reduction persisted or by a discrete value, when the friction drop was sharp. All re(de)construction temperature peaks, by definition, are indicated by a single number.

The friction drops compared in Tables 1 through 3, containing the summary of the thermal inflection points or regions taken from the COF-MAX.COF data presented in Figs. 13 through 17, exhibit remarkable similarities and a few significant differences as the function of absence or presence of water vapor in hydrogen:

1. Poly-Si: As previously described in detail in [1,72], the largest number of dry P_{H_2} experiments were run with this crystallinity, providing the most reliably averaged values in Table 1. As depicted there, the first friction drop was at RT, manifested as a slight but noticable reduction during each test, in both atmospheres. This drop may be related to some tribochemical reaction of the residual water vapor remaining behind in the 99.9999% H_2 , as discussed later in this report. The second and third friction drops in both atmospheres compare well with the temperatures where the dihydrides and the monohydrides desorb from Si (see Figs. 18 through 21 taken from [74 through 77], respectively). During the Third Round dry test, the second and third COF drops in Fig. 13 appeared to have coalesced into one single trough, although the associated MAX.COF values in Fig. 14 did indicate some bifurcation.

These findings should be compared not only with the hydrogen desorption temperatures, but with the thermal history of Si surfaces previously discussed in 3.1.2: on water-saturated surfaces the Si-OH groups decompose between 187° and 307 °C to form Si-O-Si groups, along with the generation of additional hydrides.

The 700°C reconstruction peak No. 1 also agrees with the desorption temperatures depicted in Figs. 18 through 21, beyond which no hydrogen is expected to remain on the surface. The reconstruction temperature of Peak No. 1 did shift, however, by a significant amount from 700°C (dry P_{H_2}) to 850°C (wet P_{H_2}). As also discussed in 3.1.2, the second friction drop range of 500 ° to 600 °C agrees not only with the removal temperature of the monohydride, but also with the formation of stable SiO_2 , followed by a volatile decomposition into SiO at some higher temperature. However, SiO does not evaporate until ~900 °C. At that point, all surface bonds will become unsaturated. Reconstruction occurs at a significantly higher temperature, therefore, than if the last vestiges of only the less stable monohydrides

were removed. After the hypothesized deconstruction, the friction remain high, indicating the lack of dissociative chemisorption of either H_2 or H_2O on cooling to RT. The general levels of high friction are extremely stable at or near RT, except in the single case of the poly-Si shakedown experiment.

2. Si(100): The first (RT) COF-MAX.COF drop of the wet test is broader and more intensive than the dry equivalents, and certainly better defined than in the case of all parallel poly-Si tests. In the same vein, the second drop of both type of atmospheric tests also appear to be better defined than that of poly-Si. The third drop of the wet Si(100) test was equally more intensive and better defined than with dry Si(100) or dry poly-Si. The temperature range of this final drop definitely shifted upward compared to the poly-Si tests, although a small wet-poly-Si peak in the same thermal range (not marked with an arrow in Fig. 13) can also be observed. The third friction drop of the wet Si(100) test is definitely higher than that of the comparable dry experiment, possibly indicating the persistence of greater amounts of relatively low-friction surface oxides that developed in hydrogen containing the larger amount of water.

The sharper friction drops in the case of Si(100) should be examined in light of a Si(100) surface theoretically containing better defined sets of di- and monohydrides than the more disordered poly-Si surface or the essentially monohydrides-covered Si(111). This should be generally true in practice as well, notwithstanding any miscut surface disorder invariably induced during specimen fabrication to some degree.

3. Si(111): The lubricating effects of water at unexpectedly high elevated temperatures are remarkable with this crystallinity. While at RT the usual tribochemical COF-MAX.COF (first) drops have also been observed both in the dry and the wet cases (as before), the second and third friction drop temperatures are significantly higher during the wet experiments. *In fact, the Si(111) surface exhibited the unusually low COF of ~0.05 and MAX.COF of ~0.2 near 800 °C!* The reconstruction temperature is by far the highest observed among all the crystallinities tested, indicating the extreme stability of the the bridge-bonded oxygens on the Si(111). The 950 °C reconstruction temperature agrees extremely well with the reported ~900 °C decomposition temperature of SiO_2 .

5.1.2 Wear Behavior

The wear rate (\mathcal{W}) data in Table 4 indicates that during the RT "grind" experiments inherently performed under the highest Hertzian stresses, the \mathcal{W} of all crystallinities remained about the same, regardless of the environment. The ability of wet P_{H_2} to act as an atomic-level lubricant does not manifest itself until the contact stresses are significantly reduced (Table 5). As previously reported in [1] and presented again in Table 5, the \mathcal{W}_{Si} during the thermally ramped tests is roughly the same in vacuum and in 0.2 Torr dry P_{H_2} , with the exception of Si(100). This crystallinity showed a factor of ~ 5 reduction in wear rate in dry P_{H_2} . *In contrast, the presence of ~ 0.02 Torr $\text{P}_{\text{H}_2}\text{O}$ in the 0.18 Torr hydrogen environment drastically reduces the \mathcal{W}_{Si} in each and every case: by a factor of 100 with the Si(111), a factor of ~ 30 with the poly-Si and about a factor of 3 with the Si(100).*

This order of wear reduction agrees with the COF-MAX.COF data in Figs. 13 through 17. The extremely low overall friction of the wet Si(111) is commensurate with the largest wear rate reduction attributed to the water vapor. The most persistently high COF-MAX.COF values of the Si(100) come with the lowest water-induced wear reduction, with the poly-Si exhibiting intermediate values in-between.

SEM photomicrographs of the dry and wet P_{H_2} experiment pin tip scars are compared in Fig. 22. Although the photos reveal the cohesive nature of the wear debris in both atmospheric environments, the wet debris shows a tendency to agglomerate more on the entry-and-discharge regions of the tip. The wet debris also tends to remain more within the scars. The lowest \mathcal{W} Si(111) had the most, and the highest \mathcal{W} Si(100) the least included debris there, with the poly-Si representing an intermediate state. It is equally significant that plowing of the debris caused scalloping the dry P_{H_2} wear scar edges, while the "wet" scar edges exhibit essentially no crenellation.

The wear scar photomicrographs of the respective flats in Figs 23 through 25 corroborate these findings. The frosty appearance of the scars are attributed to relatively homogeneous tensile microcracking of the substrates normal to the direction of sliding, with the wet P_{H_2} scars showing considerably more homogeneity with smaller cracks of shallower depth. In parallel with the behavior of the debris in the pin tip scars, it is apparent under the highest (2000 x) magnification that more microdebris particles remained in the wet flat scars than in the dry ones.

However, none of these pin or flat scar photos reveal any evidence of eraser-like rolls. As previously discussed, these type of rolls were as large as 10 μm in length and 1 μm in cross-section during 600 °C testing in a 0.034 MPa (~ 200 Torr) $\text{P}_{\text{H}_2}\text{O}$ environment [54]. Equally long but far thinner rolls were generated in "dry" argon, presumably originating from residual hydrated

silica rolled up from the sliding surfaces [53]. The absence of such "bearing rollers" notwithstanding, it appears that the moisture-induced malleability of the super-fine Si wear debris smeared into the wear scars during the present experiments imparts properties similar to a semi-solid lubricant.

Our hypothesis associating low wear with the solid lubricating nature of the wet debris is further strengthened by the appearance of the pin and flat wear scars of the 15 g thermally-ramped *vacuum* tests previously described in [72,73]. Their appearance is depicted here in Figs. 26 through 28. The relatively high \mathcal{W} in vacuum versus the much lower \mathcal{W} in wet P_{H_2} described in Table 5 may be better understood by observing that the pin tips are *not* decorated with debris after the vacuum experiments. This indicates considerable non-adherence to the Si tip substrate and non-coherence of the microparticles to form aggregates, their large surface area-to-mass ratios notwithstanding. Comparing the morphology of the debris generated in wet versus dry P_{H_2} , the particles left behind in the flat scars of the vacuum tests appear dry, powdery and inhomogeneously agglomerated, where small clumps of powder could be found at all in the first place. The resulting pin scars are much rougher, exhibiting the degree of grain pull-out not observed after the wet P_{H_2} experiments. The flat scars associated with the vacuum tests also appear more damaged.

5.2 Friction and Wear of Polished $PCD_{C(100)}$ vs. Itself in Dry and Wet P_{H_2}

The COF and MAX.COF of polished $PCD_{C(100)}$ tested in dry versus wet P_{H_2} in Figs 29 through 32 depict a similar lubrication mechanism via reactions of water vapor with the hot PCD surfaces from the gas phase. However, the results are more subtle than in the case of Si:

1. During testing in dry P_{H_2} [2], 27 ea. $PCD_{C(100)}$ tests were completed with as many COF curves generated. Note that the MAX.COF curves were not given in [2], but are presented in this report. One significant finding in [2] was that individual experiments within each test round, consisting of anywhere from 2 to 6 tests per round, exhibited either the re(de)construction trough-containing stepfunction (the ideal friction signature) or the stepfunction without the trough (only a friction peak). These differently shaped curves have been previously shown in Fig. 2 (right column). The typical peak-only curves taken from the test rounds where both shapes manifested themselves are given in Fig. 29. The fact that the stepfunctions-and-troughs one would ideally expect during each test did not occur every time was attributed to wear path-to-wear path crystallinity disorder, to differences in surface temperature of the PCD as a function of hydrogen pressure, and to some other yet unrecognized influences.

During the test rounds where both curve shapes have been found, the distribution of the peak-only tests versus the trough-type COF-curved tests were as follows: Round 1 = 1 out of 2 was peak shaped; Round 3 = 1 out of 4; Round 4 = 3 out of 6; Round 5 = 2 out of 6; and Round 6 = 2 out of 5. Statistically, out of any 4 consecutive experiments run, at least 1 out of the 4 COF curves should be peak-shaped. As shown in Fig. 31, the 4 ea. wet P_{H_2} experiments performed with the same (but acid-cleaned) rubbing surfaces *all* had peak shapes. At the same time, the highest COF value was attained at the highest surface temperature in each case, although the wet P_{H_2} values were measurably less than the dry P_{H_2} cases.

2. The corresponding MAX.COF curves in Figs. 30 and 32 are more revealing in terms of water effects. The highest MAX.COFs of the dry P_{H_2} tests range from 0.3 to as high as 1.0, with most of the values clustering around 0.5 to 0.6. In contrast, the corresponding maximums of the wet P_{H_2} tests are always below 0.3. In fact the heated MAX.COF are always lower above 600 °C than below it, indicating some sign of a beneficial gas-phase reaction that occurs in wet P_{H_2} , which does not occur in dry P_{H_2} . It is suspected that these reactions prevent the formation of the re(de)construction troughs depicted in Fig. 2. There are indications in Figs. 2, 4, 5, and 29 through 32 that the most advantageous temperature range, in terms of MAX.COF reduction, is around 700° to 1000 °C in both dry and wet P_{H_2} . As shown by a TPD study in Fig. 33 taken from [78], this temperature range agrees with the desorption range of hydrogen from PCD surfaces.

The fact that the gas phase reactions do have an excellent opportunity of occurring is reinforced by the data in Fig. 34 [79], where the incoming flux of *atomic* hydrogen is plotted as a function of temperature and coverage on a C(100) diamond surface. If we now calculate the impingement rate v of *molecular* hydrogen flux on the polished $PCD_{C(100)}$ as a function of the 0.2 Torr P_{H_2} and temperature of ~1000 °C \equiv 1300 K by the well-known formula of $v = (3.513 \times 10^{22})(P)/(MT)^{0.5}$ from [80], we find a value of $(3.513 \times 10^{22})(0.2)/(2600)^{0.5} = 1.38 \times 10^{20} \text{ cm}^{-2} \cdot \text{cm}^{-1}$. The data indicate that this flux agrees with a complete monolayer of H_2 coverage at that temperature. The impingement rate of the water molecules at ~0.02 Torr present in the introduced hydrogen is $(3.513 \times 10^{22})(0.02)/(2600)^{0.5} = 4.59 \times 10^{18} \text{ cm}^{-2} \cdot \text{cm}^{-1}$. According to Fig. 34, this is also enough for a monolayer coverage at ~1000 °C. The S_0 sticking coefficients of the respective species should be near unity at the active sites.

Examination of the pin tip previously used for the dry P_{H_2} experiments has found that the size of the scar remained essentially the same after the 8000 cycles of additional sliding (represented by the data in Figs. 31 and 32) in wet P_{H_2} , under the average stress of ~ 7 MPa (~ 1000 psi). Therefore, the previously summarized wear rates of polished $PCD_{C(100)}$ in dry P_{H_2} [2] are the best available \mathcal{W} , as presented in Table 5. At the present time, one can only approximate the \mathcal{W} of $PCD_{C(100)}$ in wet P_{H_2} as $< 2 \times 10^{-16} \text{ m}^3/\text{N}\cdot\text{m}$.

6.0 DISCUSSION

Even in the absence of any in-situ surface analytical capability in the SEM tribometer, there is now ample evidence that both hydrogen and water enters into a gas phase, tribochemical reaction with the Si and diamond surfaces. The hydrides and in the case of water the -OH and -O- groups and/or their possible reactive intermediates passivate the dangling bonds created by wear. These reactions occur at well defined temperature ranges generally agreeing with the desorption temperature of these groups from the respective surfaces. At the beginning of this study, the ideal water content in hydrogen for optimum lubrication of Si was not known. The convenience of water saturation of the H_2 by a simple apparatus at RT (Fig. 12) was an important factor driving the creation of the test regimen. It is fortunate that the resulting P_{H_2O} content of ~ 0.02 Torr in the ~ 0.2 Torr dry P_{H_2} gave such promising results. Therefore, the question remains: if too much water is harmful due to capillary condensation and the ensuing, tribocatalyzed formation of hydrated silica leading to stiction of Si-based MEMS-MMAs, would P_{H_2O} values higher or lower than 0.02 Torr be ideal for the atomic-level lubrication of Si?

6.1 Water as a Lubricant for Silicon

The data indicate that H_2O can act as an atomic level lubricant for Si, but only from gas-phase reactions well above the boiling point of water. However, both its partial pressure in the environment as well as the temperature of the surface play an important part in this mechanism.

As depicted by the friction data presented in this report, neither the $\sim 10^{-5}$ Torr residual P_{H_2O} in the SEM column, nor the $< 10^{-7}$ Torr P_{H_2O} in 0.2 Torr of the dry 99.9999%-pure H_2 or its wet ~ 0.2 Torr version containing ~ 0.02 Torr P_{H_2O} was enough to substantially reduce the starting friction by whatever dissociative chemisorption water did undergo at the wear-generated dangling bonds, at RT. It appears, that the competitive, preferential adsorption of larger molecules such as N_2 also containing less than 1 ppm of water is more effective onto hydrophilic surfaces than any similar action of the smaller H_2 molecules [81]. The water molecules, just like the hydrogen molecules, have to come in contact with the Si surface heated to sufficiently high temperatures to induce

the formation of either reactive intermediates or the fully formed hydrides (from hydrogen) and hydroxyls, hydrides and oxides (from water vapor). The dangling bonds thus become passivated via these gas-phase reactions, until these groups desorb at some even higher temperatures.

At a P_{H_2O} of 0.2 Torr, 0.9 monolayer of water was formed on quartz (SiO_2) powder at RT [80]. If we presumed that the surface of the silica was already hydroxylated, then this nearly monomolecular layer of water would be hydrogen-bonded to the surface hydroxyls as depicted schematically in Fig. 9. Since it has been determined that the Si-OH surface bonds are off-normal, see [28,29] and Fig. 8, the architecture of the actual water bridges may be somewhat different from the simplified schematic, as discussed later herein. Nevertheless, as gathered by examining even the simplified Fig. 9, the arrangement of a monomolecular water layer under static (i.e., non-sliding) conditions should be such that the outermost region would either be rich in the hydrides or in oxygen.

Such surface arrangements on Si can be discussed in terms of water sorption on TiO_2 , since the oxide growth and hydration/dehydration of SiO_2 and TiO_2 are similar, see Fig. 35 [82]. Molecular water adsorbs on a TiO_2 surface as one of two types (Fig. 36), leading to two different temperature ranges of water desorption. In the Type I adsorption in Fig. 36, molecular water is physisorbed onto the hydroxylated surface (which results from chemisorbed water in the first place). In Type II adsorption, molecular water sorbs onto bridge-bonded oxygens. This latter step is followed by dissociation of the water molecules into surface hydroxyls. While Type I can sorb more than one monolayers of water (and thus forming the water bridges depicted in Fig. 9, Type II water is limited to a monolayer. Type I water desorbs from 70°C to 130 °C, while the Type II version from 190 °C to 250 °C [83]. In either case, statically contacting surfaces identically terminated with just one monolayer should experience *repulsion* and not *attraction*. Even in the Type I monolayer case, the repulsive nature of the hydroxylated Si surface depends on the actual configuration and interactions between the characteristically aligned surface -OH moieties.

The early suggestions of Si surface hydroxylation depicted in Fig. 8 have since been complemented by examining the synergistic or antagonistic effects of the various cleavage planes to hydroxylation and further hydration [84]. Hydroxylation of the Si(100) leads to geminal $Si(OH)_2$ groups, which form hydrogen-bonded chains with neighboring geminal groups, as depicted in Fig. 37. This arrangement would render the surface even more homogeneously repulsive, either before or after further baking to remove some molecular water. As also shown in Fig. 37, dehydroxylation readily occurs to form siloxane bridges. In contrast, there would be no hydrogen-bonding between neighboring hydroxyls on the Si(111) surface, because of the large distance separating them (about 4 to 6 Å; a characteristic of the (111) surface). Dehydroxylation is unlikely

due to the lack of surface-bound clusters that otherwise form on Si(100). Therefore, the Si(111) exhibits greater thermal stability against losing such surface moieties.

As to the effects of third bodies on wear, it is known that a large amount of submicron particles can serve as a form of solid lubrication, redistributing the contact stresses. Tribochemical reactions with water vapor can form films and rollers, lubricating the tribocontact. As the load in the contact approaches a threshold value characteristic to the structural integrity (mainly tensile strength) of the ceramic, the micro-Hertzian stresses between the contacting asperities and the friction-induced tensile stresses increase to the point where a large number of microtensile cracks will form in the wear scar [85]. It was already shown in [53,54] that the formation of a compacted silica microdebris film requires the adsorption of some minimum amount of water, which enhances the adhesion between the particles. The sliding stress then first delaminates then agglomerates the wet debris, culminating in the formation of rolls in the tribocontact. As previously mentioned, there is available power to continue sliding (and form the "lubricative" rolls) during the tribometry of Si regardless of the COF magnitude. However, a tester is not the same tribosystem as MEMS gears and bearings rotated by an electrostatic micromotor. The hydrated silica in the narrow clearances of the MEMS-MMAs will bind them up due to the limited power of the locomotor.

What is then the ideal mechanism of lubricating Si with water?

During sliding and generation of microsized wear particles, the above-discussed repulsive forces would act as a lubricant layer, providing low COF and MAX.COF values. However, this mechanism of lubrication would be different from that offered by the grease-like behavior of $\text{Si}(\text{OH})_4$. Stoichiometric silicon hydroxide can be formed only if all the Si backbonds of each surface atom had been completely cleaved and capped with hydroxyls. There is no need, however, for such a complete reaction to form a grease-like layer, as indicated by the behavior of hydrated fumed (extremely small particle size) silica. There, the wear debris microparticles are so small that their hydroxylated surfaces, especially when capped with one or more molecular layer(s) of water, will coalesce into a highly malleable, grease-like gel via micelle formation. If, on the other hand, the surface bonds of each partially or fully oxidized Si microparticle generated by the wear process were not hydroxylated but hydrogenated instead, the surface energy would also be just as low or even lower. There would be some van der Waals attraction between the hydrogenated or hydroxylated particles, although not as strong as the hydrogen bond of fully formed water bridges.

When the debris particles and their aggregates associated with the dry and wet P_{H_2} tests (or the vacuum experiments) were photographed in the SEM (Figs. 22 through 28), they had already been exposed to atmospheric air and moisture. Therefore, their initial conditions in the original test

environments immediately after termination of the experiments (i.e., prior to exposing the used specimens to air) either retarded or enhanced the sorption of any additional atmospheric moisture. The minimally cohesive debris observed after the vacuum tests, the cohesive nature after the dry P_{H_2} experiments, and the even more cohesively aggregated microdebris after testing in wet P_{H_2} can be understood better by viewing the additional atmospheric moisture sorbing onto the respective debris types as some "internal standard".

As depicted in the COF and MAX.COF data, neither the $\sim 10^{-5}$ Torr residual P_{H_2O} in the SEM column, nor the $< 10^{-7}$ Torr P_{H_2O} in 0.2 Torr of the dry 99.9999%-pure H_2 or its wet ~ 0.2 Torr version containing ~ 0.02 Torr P_{H_2O} was enough to substantially reduce the friction by whatever dissociative chemisorption water did undergo at the wear-generated dangling bonds during RT sliding at the beginning of each test. Water, just like the dry hydrogen before, has to be heated to high (to 400 °C) temperatures to induce the formation of either reactive intermediates or the actual hydrides (from hydrogen) and hydroxyls, hydrides and oxides (from water vapor) capable of passivating the dangling bonds on the sliding and heated Si surfaces. The surprising difference in the lubricating ability of water vapor seems to consist of the low-friction-providing role of the highly stable surface siloxane (Si-O-Si) moieties, capable of reducing the friction of the most stable Si(111) surfaces to the unusually low COF of ~ 0.05 and MAX.COF of ~ 0.2 near 800 °C. Even the less stable Si(100) could provide some reduction in friction just before that temperature.

6.2 Water as a Lubricant for Diamond

Water is an excellent atomic level lubricant for diamond. In view of (a) the general dearth of surface analytical data as complete as those found for Si, and (b) the lack of in situ surface analytical capabilities of the SEM tribometer, the likely reactions leading to the COF and MAX.COF reductions are not speculated here. At best, one can invoke analogies with the hydrogen and water vapor reactions and gas desorption occurring with/from the Si surfaces, plus the experimental fact that water reduces the oxidative etching of diamond. It is strongly suspected that the gas-phase reactions with water vapor reactions prevent the formation of the re(de)construction troughs at the highest test temperatures. In spite of the substantial lubricating effects of water for Si, the friction and wear behavior of PCD is still far better for MEMS-MMA applications than the various crystallinities of Si.

The SEM tribometric data of $\mathcal{W}_{PCD} < 2 \times 10^{-16} \text{ m}^3/\text{N}\cdot\text{m}$ agrees well with Miyoshi's results presented in Fig. 10.

7.0 CONCLUSIONS

For the past three years, SEM tribometry has been performed with (a) various Si crystallinities [Si(100), Si(111) and poly-Si], and (b) polished, mostly C(100)-textured and acid-cleaned polycrystalline CVD diamond films [PCD_{C(100)}] heated to 850°C (Si) or 950°C (PCD) then cooled to room temperature (RT). The initial test environment was $\sim 1 \times 10^{-5}$ Torr moderate vacuum of the SEM column containing $\sim 93\%$ water vapor in its residual gas environment, followed by 26 Pa (0.2 Torr) total pressure of 99.999%-pure H₂ as the second test environment, and the same dry P_{H₂} containing ~ 0.02 Torr partial pressure of water vapor as the third environment.

The results to date indicate that both H₂ and H₂O can act as atomic level lubricants both for Si and PCD_{C(100)} via gas-phase dissociative chemisorption reactions well above the boiling point of water. The most effective thermal regions for reducing both the average and the maximum coefficient of friction (COF and MAX.CVOF) are near the desorption temperatures of the dihydrides, monohydrides, the -OH moieties and the most stable oxygenated surface groups (e.g., the bridge bonded Si-O-Si and C-O-C). The wet P_{H₂} was particularly effective in reducing the wear rate (\mathcal{W}) of the various Si crystallinities from the 10^{-12} m³/N·m range found in moderate vacuum and in dry P_{H₂} by one to two orders-of magnitude in the wide temperature range thermal ramping environment of the SEM tribometer, but only at low Hertzian stresses on the order of 10 MPa or less. At RT and under the high starting Hertz stresses of near 430 MPa, there was essentially no difference in the wear rate of Si in either dry or wet P_{H₂}. In contrast, the \mathcal{W} of PCD_{C(100)} remained at or below $\sim 10^{-16}$ m³/N·m, with COF and MAX.COF values substantially below those of Si.

The present three-year program has conclusively demonstrated that the friction of wear of Si and diamond are highly dependent on the temperature- and gas-phase-induced dissociative chemisorption effects of hydrogen and water vapor passivating the sliding-and heating-induced dangling bonds on the sliding surfaces. The most surprising finding has been that a low partial pressure of ~ 0.02 Torr of water vapor is a better atomic level lubricant than its dry hydrogen carrier not only for diamond but for silicon as well. The best reactive thermal region is well above the boiling point of water (where the "stiction" caused by capillary water disappear in the first place), near the desorption temperatures of the dihydrides, monohydrides, the surface -OH and -O- groups.

The results dispel the current belief that water is harmful under all conditions to Si MEMS surfaces due to "stiction" effects, and reinforces our original contention the PCD is a far better MEMS bearing material than Si.

8.0 RESEARCH PERSONNEL

This research has been performed by selected members of the Hughes tribology team, under the direction of Dr. Michael N. Gardos as the Program Manager and Principal Investigator, e-mail: mngardos@ccgate.hac.com ; Ph.: (310) 616-9890, and FAX: (310) 616-2628. He is being supported by Ms. Patricia Schmidt as the Hughes Contracts Administrator. Messrs. Lindon Melton, Bruce W. Buller, Gerald R. Meldrum, Stephen A. Gabelich, and Dr. Daniel A. Demeo were responsible for the tribological and chemical characterization of single-crystal and polycrystalline Si and crystallographically textured, polycrystalline diamond films.

Key subcontractor representatives helping the Hughes efforts were Drs. K.V. Ravi (formerly with Lockheed-Martin and now with Intel) and A. Joshi of Lockheed-Martin R & D (Palo Alto, CA) growing the diamond films, Mr. Thomas F. Wilson of Meller Optics, Inc. (Providence, RI) responsible for cutting and polishing the Si tribospecimens, and Mr. Richard Palicka of Cercom Inc. (Vista, CA) supplying the polycrystalline α -SiC tribopins as substrates for CVD diamond deposition.

This program has been guided by Maj. Hugh C. De Long, AFOSR/NL Program Manager.

9.0 TRANSITIONS

In addition to the establishment of a Hughes/JPL/Caltech Technical Cooperative Agreement (TCA), the submittal of 4 ea. draft copies of papers and the publication of three others, as well as the presentation 5 ea. seminars and papers in Europe described in the '97 Progress Report, there are several additional Transitions items worth mentioning (see below).

9.1 Hughes/JPL/Caltech Technical Cooperative Agreement

The TCA work is now ongoing, where most of the accomplishments consisted of (a) the successful completion of the present AFOSR program, (b) establishing the improved molecular dynamics calculation routines for single-crystal diamond surfaces at Caltech, and (c) developing deep reactive ion etching techniques at JPL to prepare hollow molds for the deposition of hollow diamond rotors for upcoming JPL experiments testing Si and PCD rotors side-by-side in various harmful and advantageous atmospheric and thermal environments. These environments will be determined by the findings of the presently completed AFOSR MEMS Tribology Program.

9.2 Hughes/JPL/Argonne National Lab Response to a DARPA MEMS BAA

Building on the plans and accomplishments of the TCA and the present AFOSR program, the TCA team involved the nanocrystalline diamond growers of the Argonne National Laboratory in jointly responding with a Proposal Abstract to DARPA BAA 97-43, entitled "Microelectromechanical Systems (MEMS)". A three-year, ~\$3.5 M program was suggested, as described below.

The proposed research and development program contains three main innovations:

- The use of a novel form of nanocrystalline diamond (Argonne NanoCrystalline Diamond; ANCD) developed at Argonne National Laboratory (ANL) as an essential multi-purpose material for tribological, chemical and the associated electronic functions of MEMS-MMA devices. From the tribological point of view, it is expected that ANCD will reduce by a factor of ten the wear rate compared with polished conventional microcrystalline diamond (with 1-10 μm grain size), which itself has been demonstrated to have a wear rate 10,000 times lower than that of Si. The work on ANCD has been recognized in the form of one of three 1997 awards given by the U. S. Department of Energy for "Most Significant Implications for Energy Technology".
- The use of an innovative, Si-compatible fabrication technology as a means of forming diamond MEMS-MMA structures, and integrating them with Si-based devices.
- A continued systematic study of ANCD-ANCD, ANCD-Si and Si-Si nanotribology directed toward the understanding and control of component-gas phase and solid phase interactions in order to reduce friction and wear, as well as toward controlling the chemical and electronic properties both on the surface and in the bulk of MEMS-MMAs.

Robust low-friction, long-life actuators, which perform useful work, require a material with significantly longer life than those made of Si. The primary purpose of this program will be to focus on the development of long life, low friction ANCD actuators for MEMS applications. These actuators can move currently available sensors or their components, using fabrication methods which are compatible with Si-based technology. We hope to achieve these goals by:

- building model ANCD actuators driven by micromotor - gear train combinations capable of moving a real or simulated load representing e. g., a pointing and tracking sensor.

- developing fabrication techniques based on methods originated by JPL for the integration of existing Si lithographic methods with selective deposition and reactive ion etching to create hollow ANCD parts (e. g., gears and rotors) of sufficient structural integrity. In order to prove the efficacy of the proposed hybrid Si-ANCD technology, we intend to minimize some of the complications of micron-scale fabrication by working in the millimeter to sub-millimeter size range in the overlapping region of MEMS and mesoscale MMAs for ease of assembly and testing.
- elucidating the surface chemical properties of ANCD which controls the tribological and electronic performance of the devices, using the special test equipment and surface engineering (lubrication) techniques developed at Hughes Aircraft Company and ANL.

DARPA will inform those who are found worthy of submitting a full fledged proposal, just before or immediately after the Holidays.

9.3 Technical Papers

Reference [1] has been presented and is now in press, expected to be published early next year in a book form. Reference [2] will appear in the next issue of Tribology Letters. Based on the results of this Final Report and the early PO_2 tests to be performed under the auspices of the follow-on AFOSR Tribology Program entitled: "Surface-Chemistry-Driven Tribological Fundamentals of Diamond and SiC for Extreme Environment MEMS Applications," an invited paper is now under preparation for the Tribology Symposium of the 1998 International Conference of Metallurgical Coatings (ICMC), to be held in San Diego, CA in Apr. '98. The tentative title of the paper is "Tribological Fundamentals of Polycrystalline Diamond Films".

REFERENCES

1. M.N. Gardos, "Advantages and Limitations of Silicon as a Bearing Material for MEMS Applications," invited paper presented at the NSF/AFOSR/ASME Workshop *Tribology Issues and Opportunities in MEMS*, Nov. 9-11, 1997, Columbus, OH; to be published in a book by Kluwer Academic Publishers (in press).
2. M.N. Gardos, "Re(de)construction-induced Friction Signatures of Polished Polycrystalline Diamond Films in Vacuum and Hydrogen," *Tribol. Lett.*, (in press).
3. Y. Nishi, "Study of Silicon-Silicon Dioxide Structure by Electron Spin Resonance I," *Jap. J. Appl. Phys.*, 10, pp. 52-62 (1971).
4. E.P. Bulte, and P. Matthies, "The Influence of Water on the Annealing Behavior of Midgap Traps at the Silicon Oxide-Silicon Interface," *J. Appl. Phys.*, 64, pp. 1927-1930 (1988).
5. J-i. Takahashi, K. Machida, N. Shimoyama, and K. Minegishi, "Water Trapping of Point Defects in Interlayer SiO₂ Films and its Contribution to the Reduction of Hot-carrier Degradation," *Appl. Phys. Lett.*, 62, pp. 2365-2366 (1993).
6. Y. Ohmura, Y. Otomo, Y. Tago, N. Terakado, and T. Satoh, "Enhanced Hydrogenation and Acceptor Passivation in Si by Pressurized Water Boiling," *Appl. Phys. Lett.*, 67, pp. 64-66 (1995).
7. S. Watanabe, N. Nakayama, and T. Ito, "Homogeneous Hydrogen-terminated Si(111) Surface Formed Using Aqueous HF Solution and Water," *Appl. Phys. Lett.*, 59, pp. 1458-1460 (1991).
8. S. Watanabe, K. Hoiuchi, and T. Ito, "Atomic Step Structure on Vicinal H/Si(111) Surface Formed by Hot Water Immersion," *Jpn. J. Appl. Phys.*, 32, pp. 3420-3425 (1993).
9. S. Watanabe, and Y. Sugita, "Appearance of Vertical Dihydrides on a Silicon Surface While Dissolving the Surface Oxide Layer in Hot Water," *Appl. Phys. Lett.*, 66, pp. 1797-1799 (1995).
10. Z. Feng, and J.E. Field, "Friction of Diamond on Diamond and Chemical Vapour Deposition Diamond Coatings," *Surf. Coat. Technol.*, 47, pp. 631-645 (1991).

11. Z. Feng, and J.E. Field, "The Friction and Wear of Diamond Sliding on Diamond," J. Phys. D: Appl. Phys., 25, pp. A33-A37 (1992)].
12. Y. Enomoto, S. Miyake, and S. Yazu, "Friction and Wear of Synthetic Diamond with and without N⁺ Implantation and CVD Diamond Coating in Air, Water and Methanol," Tribol. Lett., 2, pp. 241-246 (1996).
13. K. Miyoshi et al., "Physical and Tribological Characteristics of Ion-Implanted Diamond Films," NASA-TM-106682, 1995.
14. K. Miyoshi, "Friction and Wear Properties of As-Deposited and Carbon Ion-Implanted Diamond Films, NASA-TM-106759, 1995.
15. K. Miyoshi, "Friction and Wear of As-polished, Nitrogen Ion-implanted, and Fluorinated Diamond in Water," Paper No. E6.08 presented at the 1996 Int. Conf. on Metall. Coatings and Thin Films (ICMCTF), Apr. 22-26, 1996, San Diego, CA.
16. M.N. Gardos, "Tribology and Wear Behavior of Diamond," Chapter 12 in *Synthetic Diamond: Emerging CVD Science and Technology* (Eds. K.E. Spear, and J.P. Dismukes), ISBN 0-471-53589-3, Electrochem. Soc. Monograph, John Wiley and Sons, N.Y. NY, 1994, pp. 533-580.
17. M.N. Gardos, "Tribological Behavior of Polycrystalline Diamond Films," in *Protective Coatings and Thin Films*, "Proc. NATO Adv. Res. Workshop, May 30 - June 5, 1996, NATO ARW Series, eds. Y. Pauleau and P.B. Barna, (Kluwer Academic Publishers, Dordrecht, The Netherlands, 1997), pp.185-196.
18. P.A. Thiel, and T.E. Madey, "The Interaction of Water with Solid Surfaces: Fundamental Aspects," Surf. Sci. Reports, 7, pp. 211-385 (1987) and references therein.
19. Ph. Avouris, and R. Wolkow, "Atom-resolved Surface Chemistry Studied by Scanning Tunneling Microscopy and Spectroscopy," Phys. Rev. B., 39, pp. 5091-5100 (1989).
20. K. Miyake, H. Shigekawa, and R. Yoshizaki, "Electronic Structure of Si(111)-7x7 Phase Boundary Studied by Scanning Tunneling Microscopy," Appl. Phys. Lett., 66, pp. 3468-3470 (1995).

21. Y. Homma, M. Suzuki, and M. Tomita, "Atomic Configuration Dependent Secondary Electron Emission from Reconstructed Silicon Surfaces," *Appl. Phys. Lett.*, 62, pp. 3276-3278 (1993).
22. M. Balooch, and A.V. Hamza, "Observation of C₆₀ Cage Opening on Si(111)-(7x7)," *Appl. Phys. Lett.*, 63, pp. 150-152 (1993).
23. L. Stauffer, S. Van, D. Bolmont, J.J. Koulmann, and C. Minot, "Non-equivalence of the Adatoms in the DAS Model of the Si(111)-(7x7) Surface. An Extended Hückel Model Calculation," *Solid State Commun.*, 85, pp. 935-940 (1993).
24. P. Gupta, P.A. Coon, B.G. Koehler, and S.M. George, "Adsorption and Desorption Kinetics for SiCl₄ on Si(111)7x7," *J. Chem. Phys.*, 93, pp. 2827-2835 (1990).
25. P.A. Coon, M.L. Wise, A.C. Dillon, M.B. Robinson, and S.M. George, "Diethylsilane on Silicon Surfaces: Adsorption and Decomposition Kinetics," *J. Vac. Sci. Technol.*, B10, pp. 221-227 (1992).
26. Ph. Avouris, and R. Wolkow, "Scanning Tunneling Microscopy of Insulators: CaF₂ Epitaxy on Si(111)," *Appl. Phys. Lett.*, 55, pp. 1074-1076 (1989).
27. M. Balooch, and A.V. Hamza, "Observation of C₆₀ Cage Opening on Si(111)-(7x7)," *Appl. Phys. Lett.*, 63, pp. 150-152 (1993).
28. Y.J. Chabal, "Hydride Formation on the Si(100): H₂O Surface," *Phys. Rev. B*, 29, pp. 3677-3680 (1984).
29. R. Lindsey, P.L. Wincott, C.A. Muryn, G. Thornton, S.P. Frigo, J.K. Simons, and R.A. Rosenberg, "An Oxygen K-edge NEXAFS Study of H₂O Adsorption on Si(111)," *Jpn. J. Appl. Phys.*, 32 (Suppl. 32-2), pp. 347-349 (1993).
30. R.K. Iler, *The Chemistry of Silica*, John Wiley & Sons, New York, 1979, p.651.
31. R.S. McDonald, "Study of the Interaction between Hydroxyl Groups of Aerosil Silica and Adsorbed Non-polar Molecules by Infrared Spectrometry," *J. Am. Chem. Soc.*, 74, pp. 850-854 (1957).
32. R.W. Tillman, M. Radmacher, and H.E. Gaub, "Surface Structure of Hydrated Amorphous Silicon Oxide at 3 Å Resolution by Scanning Force Microscopy," *Appl. Phys. Lett.*, 60, pp. 3111-3113 (1992).

33. A.C. Dillon, P. Gupta, M.B. Robinson, A.S. Bracker, and S.M. George, "FTIR Studies of Water and Ammonia Decomposition on Silicon Surfaces," Rept. No. SU-TR-18 (AD-A234637), Stanford Univ., CA, 12 Apr.1991.
34. H. Ibach, H. Wagner, and D. Bruchmann, "Dissociative Chemisorption of H₂O on Si(100) and Si(111) - A Vibrational Study," Solid State Commun., 42, pp. 457-459 (1982).
35. W. Ranke, and Y.R. Xing, "Orientation Dependent Adsorption on a Cylindrical Silicon Crystal I. Water," Surf. Sci., 157, pp. 339-352 (1985).
36. R. Tromp, G.W. Rubloff, P. Balk, F.K. LeGoues, and E.J. van Loenen, "High-Temperature SiO₂ Decomposition at the SiO₂/Si Interface," Phys. Rev. Lett., 55, pp. 2332-2335 (1985).
37. N. Miyata, M. Shigeno, Y. Arimoto, and T. Ito, "Thermal Decomposition of Native Oxide on Si(100)," J. Appl. Phys., 74, pp. 5275-5276 (1993).
38. H. Watanabe, K. Fujita, and M. Ichikawa, "Thermal Decomposition of Ultrathin Oxide Layers on Si(111) Surfaces Mediated by Surface Si Transport," Appl. Phys. Lett., 70, pp. 1095-1097 (1997).
39. K. Fujita, H. Watanabe, and M. Ichikawa, "Nanometer-scale Si Selective Epitaxial Growth on Si(001) Surfaces using the Thermal Decomposition of Ultrathin Oxide Films," Appl. Phys. Lett., 70, pp. 2807-2809 (1997).
40. S.C. Singhal, "Thermodynamics and Kinetics of Oxidation of Hot-Pressed Silicon Nitride," J. Mat. Sci., 11, pp. 500-509 (1976).
41. H.-E. Kim, and A.J. Moorhead, "Effects of Active Oxidation on the Flexural Strength of α -Silicon Carbide," J. Am. Ceram. Soc., 73, pp. 1868-1872 (1990).
42. T. Narushima, T. Goto, Y. Iguchi, and T. Hirai, "High-Temperature Active Oxidation of Chemically Vapor-Deposited Silicon Carbide in an Ar-O₂ Atmosphere," J. Am. Ceram. Soc., 74, pp. 2583-2586 (1991).
43. M. Kawamoto, C. Ishizaki, K. Ishizaki, "Fluidity-increasing Behavior of Silicon Nitride Powder by Aqueous Washing," J. Mat. Sci. Lett., 10, pp. 279-281 (1991).

44. W.-T. Tseng, and Y.-L. Wang, "Re-examination of Pressure and Speed Dependences of Removal Rate during Chemical-Mechanical Polishing Processes," J. Electrochem. Soc., 144, pp. L15-L17 (1997).
45. N. Inoue, M. Kikuchi, T. Shima, M. Iwase, and Y. Nishi, "Change in Wettability of Water on Si after Ion Treatment by Aging under Water and Air," Phys. Lett. A, 157, pp. 299-300 (1991).
46. D. Wang, L. Tsau, and K.L. Wang, "Nanometer-structure Writing on Si(100) Surfaces Using a Non-contact-mode Atomic Force Microscope," Appl. Phys. Lett., 65, pp. 1415-1417 (1994).
47. K. Mizuhara and S.M. Hsu, "Tribocchemical Reaction of Oxygen and Water on Silicon Surfaces," in *Wear Particles*, Eds. D. Dowson et al., Elsevier Sci. Publ. B.V., pp. 323-328 (1992).
48. S. Kitaoka, T. Tsui, Y. Yamaguchi and K. Kashiwagi, "Tribocchemical Wear Theory of Non-oxide Ceramics in High-Temperature and High-Pressure Water," Wear, 205, pp. 40-46 (1997).
49. J. Xu, K. Kato and T. Hirayama, "The Transition of Wear Mode during the Running-in Process of Silicon Nitride Sliding in Water," Wear, 205, pp. 55-63 (1997).
50. T. Saito, Y. Imada, and F. Honda, "An Analytical Observation of the Tribocchemical Reaction of Silicon Nitride Sliding with Low Friction in Aqueous Solutions," Wear, 205, pp. 153-159 (1997).
51. Y.-M. Gao, L. Fang, J.-Y. Su, and Z.-G. Xie, "Investigation on the Components and the Formation of a Tribocchemical Film in the Si₃N₄ - Gray Iron Sliding Pair Lubricated with Distilled Water," Wear, 206, pp. 87-93 (1997).
52. Y.G. Gogotski, and M. Yoshimura, "Water Effects on Corrosion Behavior of Structural Ceramics," MRS Bulletin, XIX(10), pp. 39-45 (1994).
53. E. Zanoria, and S. Danyluk, "Ball-on-flat Reciprocating Sliding Wear of Single-crystal, Semiconductor Silicon at Room Temperature," Wear, 162-164, pp. 332-338 (1993).

54. E.S. Zanoria, S. Danyluk, and M.J. McNallan, "Formation of Cylindrical Sliding-Wear Debris on Silicon in Humid Conditions and Elevated Temperatures," *Tribol. Trans.*, 38, pp. 721-727 (1995).
55. K. Hiratsuka, "Environmental Effects on the Formation Process of Adhesive Wear Particles," *Tribol. Int.*, 28, pp. 279-286 (1995).
56. L.M. Struck, and M.P. D'Evelyn, "Infrared Spectroscopy of Hydrogen and Water on Diamond (100)," *The Electrochem. Soc. Proc. Vol. 93-17*, pp. 674-681 (1993).
57. L.M. Struck, and M.P. D'Evelyn, "Interaction of Hydrogen and Water with Diamond (100): Infrared Spectroscopy," *J. Vac. Sci. Technol.*, A11, pp. 1992-1997 (1993).
58. S.I. Shaw, and M.M. Waite, "The Effect of Oxygen on the Nucleation and Growth of Diamond Thin Films," *Appl. Phys. Lett.*, 61, pp. 3113-3115 (1992).
59. Z. Li Tolt, L. Heatherly, R.E. Clausing, and C.S. Feigerle, "The Role of H₂O in Enhancing Hot Filament Assisted Diamond Growth at Low Temperatures," *J. Appl. Phys.*, 81, pp. 1536-1545 (1997).
60. P. Badziag and W.S. Verwoerd, "MNDO Analysis of the Oxidized Diamond (100) Surface," *Surf. Sci.*, 183, pp. 469-483 (1987).
61. E.P. Smirnov, O.K. Semchinova, A.M. Abyzov and D. Uffman, "The Surface Radicals of Diamond," *Carbon*, 35, pp. 31-34 (1997).
62. C.J. Chu, C. Pan, J.L. Margrave, and R.H. Hauge, "F₂, H₂O, and O₂ Etching Rates of Diamond and the Effects of F₂, HF and H₂O, on the Molecular O₂ Etching of (110) Diamond," *Dia. and Related Mater.*, 4, pp. 1317-1324 (1995).
63. S.J. Harris, and A.M. Weiner, "Effects of Oxygen on Diamond Growth," *Appl. Phys. Lett.*, 55, pp. 2179-2181 (1989).
64. N. Uchida, T. Kurita, H. Ohkoshi, K. Uematsu, and K. Saito, "Thermochemical Etching Effect of H₂O Vapor on CVD Diamond Film," *J. Cryst. Growth*, 114, pp. 565-568 (1991).
65. R.A. Rudder, G.C. Hudson, J.B. Posthill, R.E. Thomas, R.C. Hendry, D.P. Malta, and R.J. Markunas, "Chemical Vapor Deposition of Diamond Films from Water Vapor RF-plasma Discharges," *Appl. Phys. Lett.*, 60, pp. 329-331 (1992).

66. I.I. Arkhipov, B.V. Spitsyn, A.E. Gorodetsky, A.P. Zakharov, G. Popovici, T. Sung, M.A. Prelas, and S. Khasawinah, "Thermal Desorption Study of Bonded Hydrogen in Diamond Films," *Dia. and Related Mater.*, 5, pp. 121-123 (1996).
67. H.-E. Kim, and A.J. Moorhead, "Effect of Hydrogen-Water Atmospheres on Corrosion and Flexural Strength of Sintered α -Silicon Carbide," *J. Am. Ceram. Soc.*, 73, pp. 694-699 (1990).
68. H.-E. Kim, and A.J. Moorhead, "High-Temperature Gaseous Corrosion of Si_3N_4 in H_2 - H_2O and Ar-O_2 Environments," *J. Am. Ceram. Soc.*, 73, pp. 3007-3014 (1990).
69. H.-E. Kim, and A.J. Moorhead, "Corrosion and Strength of SiC-Whisker-Reinforced Alumina Exposed at High Temperatures to H_2 - H_2O Atmospheres," *J. Am. Ceram. Soc.*, 74, pp. 1354-1359 (1991).
70. C. Leyens, K. Fritscher, R. Gehrling, M. Peters, and W.A. Kaysser, "Oxide Scale Formation on an MCrAlY Coating in Various H_2 - H_2O Atmospheres," *Surf. Coat. Technol.*, 82, pp. 133-144 (1996).
71. B.S. Podol'skiĭ, V.A. Ukraintsev, and A.A. Chernov, "Kinetics of Slow Adsorption of H_2O on Si(111)-7x7," *Sov. Phys. Solid State*, 33, pp. 65-67 (1991).
72. M.N. Gardos, "Determination of the Tribological Fundamentals of Silicon and Diamond for Micro- and Macromechanism Applications," Final Report for the period 01 November 1994 to 31 October 1995, AFOSR Contract No. F49620-95-C-5909, Hughes Aircraft Company, El Segundo, CA, 20 December 1995.
73. M.N. Gardos, "Tribological Behavior of Polycrystalline and Single-Crystal Silicon," *Tribol. Lett.*, 2, pp.355-373 (1996).
74. P. Gupta, V.L. Corbin, and S.M. George, "Hydrogen Desorption Kinetics from Monohydride and Dihydride Species on Silicon Surfaces," *Phys. Rev. B.*, 37, pp. 8234-8243 (1988).
75. S.R. Kasi, M. Liehr, P.A. Thiry, H. Dallaporta, and M. Offenbergl, "Hydrocarbon Reaction with HF-Cleaned Si(100) and Effects on Metal-Oxide-Semiconductor Device Quality," *Appl. Phys Lett.*, 59, pp. 108-110 (1991).

76. Kazmerski, L. L., "Investigation of Impurity Neutralization and Defect Passivation in Polycrystalline Silicon Solar Cells," Mat. Res. Soc. Symp. Vol. 106, pp. 199-211 (1988).
77. Asano, A., "Slow Structural Transitions of Hydrogen in Hydrogenated Amorphous Silicon During Low Temperature Annealing," Physica B., 170, pp. 277-280 (1991).
78. M.T. Schulberg, C.A. Fox, G.D. Kubiak, and R.H. Stulen, "Hydrogen Desorption from Chemical Vapor Deposited Diamond Films," J. Appl. Phys., 77, pp. 3484-3490 (1995).
79. Kubiak, G. D., Hamza, A. V., Stulen, R. H., Sowa, E. C., Kolasinski, K. W., "Hydrogen Desorption and Subsequent Reconstruction on Natural Diamond Surfaces," *New Dia. Sci. and Technol.*, Proc. Int. Conf. Nat. Dia. Sci. and Technol., Mat. Res. Soc. Symp. pp. 21-28 (1991).
80. S. Dushman, *Scientific Foundations of Vacuum Technique*, John Wiley & Sons, Inc., New York, 1949.
81. M.N. Gardos, "Anomalous Wear Behavior of MoS₂ Films in Moderate Vacuum and Dry Nitrogen," Tribol. Lett., 1, pp. 67-85 (1995).
82. S.I. Koltsov, A.N. Kriulkin, V.K. Gromov, "Dehydroxylation and Rehydroxylation of Silicon Surface," Zhurnal Fizicheskoy Khimii, 61(4), pp. 1101-1104 (1987) (Russ.).
83. J.L. Keddie, P.V. Braun, and E.P. Gianellis, "Relationship between Water Desorption and Low-Temperature Densification of Colloidal Anatase Thin Films," J. Am. Ceram. Soc., 76, pp. 2529-2533, (1993).
84. L.-Y. Hsu, S.G. Shore, L. D'Ornelas, A. Choplin, and J.-M. Basset, "Models for Partially Hydroxylated Silica and Alumina and the Modeling of Metal-Support Interaction of Triosmium Clusters on Silica and Alumina," J. of Catal., 149, pp. 159-170 (1994).
85. T.N. Ying, M.C. Shen, Y.S. Wang, and S.M. Hsu, "Tribology of Si-Based Ceramics: Wear Mechanisms," Tribol. Trans., 40, pp. 685-693 (1997).

Table 1. Temperature or temperature range of well-defined COF/MAX.COF-reduction drops in Centigrades (°C) with *poly-Si in dry and wet PH₂*. Temperature values were read off the indicated illustrations, as guided by the arrows pointing out the COF reduction regions ("drops"), are rounded off to the nearest 50°C. The re(de)construction temperature peaks that follow the initial COF reductions are not marked by arrows to avoid confusion. COF reductions are indicated either by a temperature range or a discrete value, when the drop is sharp. All temperature peaks are indicated by a single value.

DRY

Test Round	Fig. No.	1st Drop	2nd Drop	3rd Drop	Peak No.1	Peak No.2
Shakedown	15	None	250-400	550	750	RT*
First	15,16	RT	300-400	600	800	650
Second	17	RT	200-300	550	700	300
Third	13,14	RT	200-550	None	600	400
AVERAGE	N/A	RT	250-400	550	700	450

* Not used in averaging values.

† Averaging is not appropriate here.

WET

Test Round	Fig. No.	1st Drop	2nd Drop	3rd Drop	Peak No.1	Peak No.2
One only	13,14	RT	350-400	500-600	850	450

Table 2. Temperature or temperature range of well-defined COF/MAX.COF-reduction drops in Centigrades ($^{\circ}\text{C}$) with *Si(100)* in dry and wet PH_2 . Temperature values were read off the indicated illustrations, as guided by the arrows pointing out the COF reduction regions ("drops"), are rounded off to the nearest 50°C . The re(de)construction temperature peaks that follow the initial COF reductions are not marked by arrows to avoid confusion. COF reductions are indicated either by a temperature range or a discrete value, when the drop is sharp. All temperature peaks are indicated by a single value.

DRY

Test Round	Fig. No.	1st Drop	2nd Drop	3rd Drop	Peak No.1	Peak No.2
First	16	RT*	400-500	600-700	800	650*
Third	13,14	RT-300*	350	700-800*	800	150*
AVERAGE	N/A	--†	400	650-750	800	--†

* Not used in averaging values.

† Averaging is not appropriate here.

WET

Test Round	Fig. No.	1st Drop	2nd Drop	3rd Drop	Peak No.1	Peak No.2
One only	16	RT-150	600-700	800	800	650

Table 3. Temperature or temperature range of well-defined COF/MAX.COF-reduction drops in Centigrades (°C) with *Si(111)* in dry and wet P_{H_2} . Temperature values were read off the indicated illustrations, as guided by the arrows pointing out the COF reduction regions ("drops"), are rounded off to the nearest 50°C. The re(de)construction temperature peaks that follow the initial COF reductions are not marked by arrows to avoid confusion. COF reductions are indicated either by a temperature range or a discrete value, when the drop is sharp. All temperature peaks are indicated by a single value.

DRY

Test Round	Fig. No.	1st Drop	2nd Drop	3rd Drop	Peak No.1	Peak No.2
First	16	RT	400	650	800	550
Second	17	RT	250	400-450	600	350
Third	13,14	RT	300-350	400-500	550	RT*
AVERAGE	N/A	RT	350	500	700	450

* Not used in averaging values.

WET

Test Round	Fig. No.	1st Drop	2nd Drop	3rd Drop	Peak No.1	Peak No.2
One only	13,14	RT	350-450	750-800	950	550

Table 4. Wear rate of Si in dry and wet P_{H_2} during room temperature (RT) "grind" experiments.

Pin/Flat	Atm./Test Type	Stress (MPa)		Pin Wear Rate ($m^3/N \cdot m$)
		Start	End	
poly-Si	dry P_{H_2} /RT	430	132	1×10^{-14}
		430	3.5	3×10^{-14}
	wet P_{H_2} /RT	430	10.6	3×10^{-14}
Si(100)	dry P_{H_2} /RT	430	3.3	3×10^{-14}
		430	108	$3 \times 10^{-17}^*$
	wet P_{H_2} /RT	430	10.6	3×10^{-14}
Si(111)	dry P_{H_2} /RT	430	2.5	2.9×10^{-13}
		430	2.8	8×10^{-14}
	wet P_{H_2} /RT	430	2.5	9×10^{-14}

* Wear rate reported to a larger number of significant figures due to the extremely small value, see [1].

Table 5. Wear rate of Si in dry and wet P_{H_2} during thermally ramped (TR) experiments.

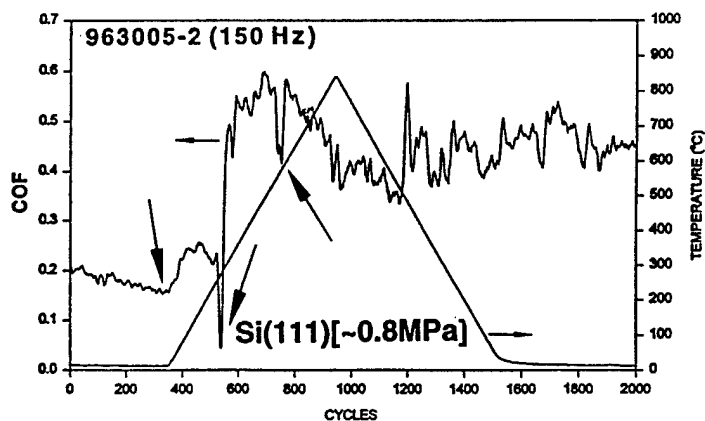
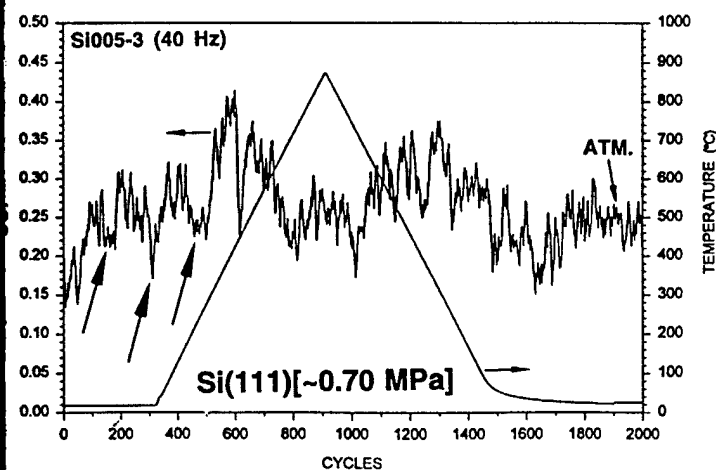
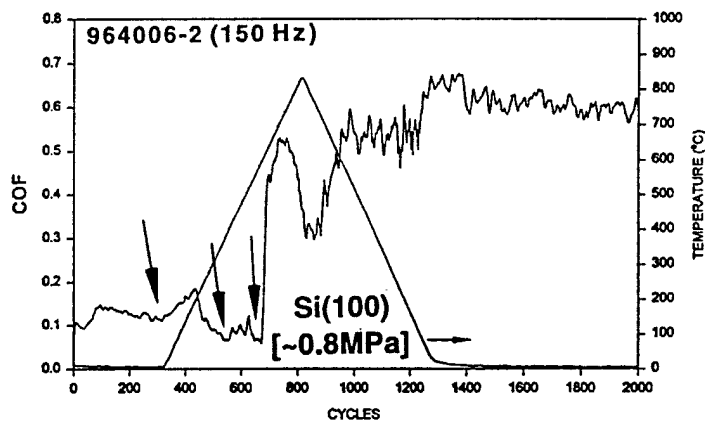
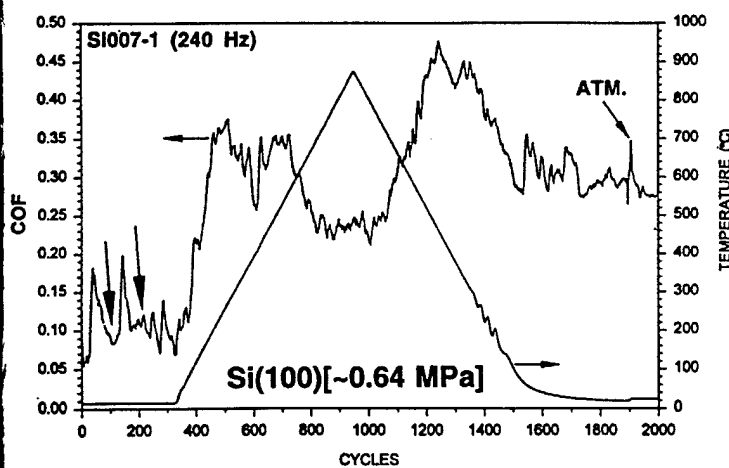
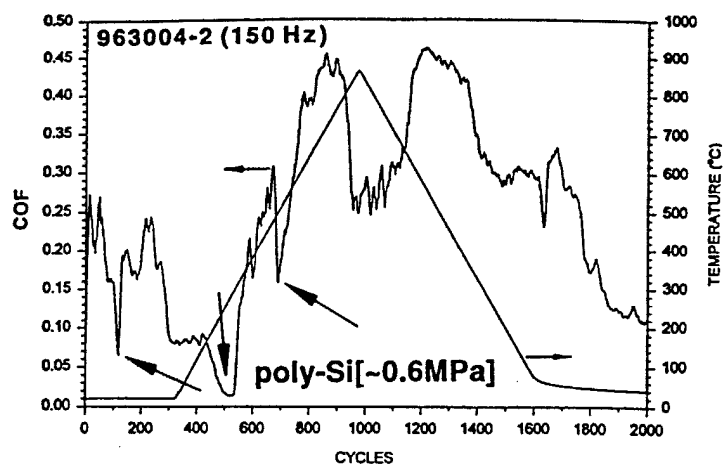
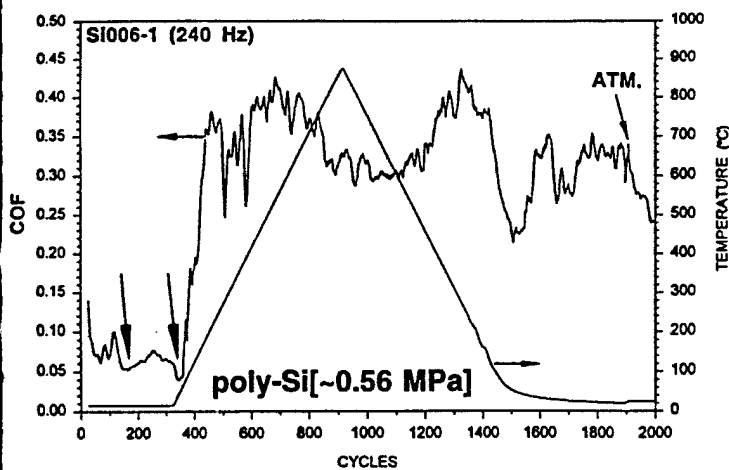
Pin/Flat	Atm./Test Type	Stress (MPa)		Pin Wear Rate ($m^3/N \cdot m$)
		Start	End	
poly-Si	Vac./TR	0.8	0.6	1.62×10^{-12}
	dry P_{H_2} /TR	132	1.1	1.27×10^{-12}
	wet P_{H_2} /TR	10.6	2.1	5×10^{-14}
Si(100)	Vac./TR	0.8	0.5	2.82×10^{-12}
	dry P_{H_2} /TR	3.3	0.8	6.2×10^{-13}
	wet P_{H_2} /TR	10.6	1.3	1.8×10^{-13}
Si(111)	Vac./TR	1.0	0.8	9.7×10^{-13}
	dry P_{H_2} /TR	2.5	0.9	1.45×10^{-12}
	wet P_{H_2} /TR	2.5	1.8	1×10^{-14}

Table 6. Wear rate (\mathcal{W}) of unpolished and polished PCD in vacuum and in dry P_{H_2} , from [2].
Wear of the pin tip was negligibly small after the dry P_{H_2} experiments, therefore the \mathcal{W} in wet P_{H_2} (attempted with the previously used specimen) could not be determined.

Pin	Flat	Stress (MPa)		Pin Wear Rate ($m^3/N \cdot m$)	No. of Cycles	Atm.
		Start	End			
PCD _{fine-caulifl.} (unpolished)	PCD _{fine-caulifl.} (unpolished)	2.9x10 ³	300	4.3x10 ⁻¹⁶	8000	vac.
PCD _{C(100)} (polished)	PCD _{C(100)} (unpolished)	26.5	25.5	8.5x10 ⁻¹⁶	2200	vac.
PCD _{C(100)} (polished)	PCD _{C(100)} (polished)	1.7x10 ³	8.6	3.9x10 ⁻¹⁶	14,000	vac. + dry P_{H_2}
PCD _{C(100)} (polished)	PCD _{C(100)} (polished)	8.6	4.8	2.2x10 ⁻¹⁶	49,200	dry P_{H_2}
PCD _{C(100)} (polished)	PCD _{C(100)} (polished)	1.7x10 ³ (averaged)	4.8 (averaged)	2.6x10 ⁻¹⁶ (averaged)	63,200	dry P_{H_2}

in $\sim 1 \times 10^{-5}$ Torr vac.

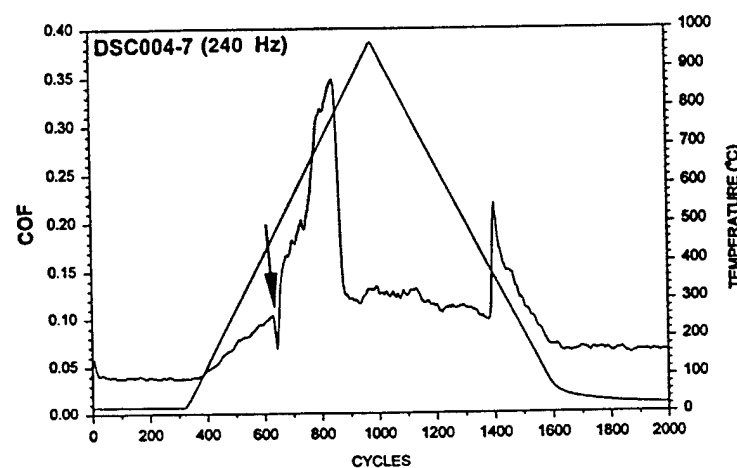
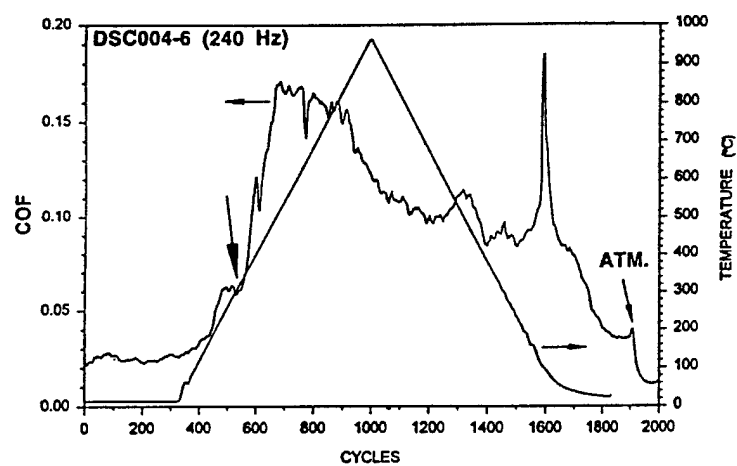
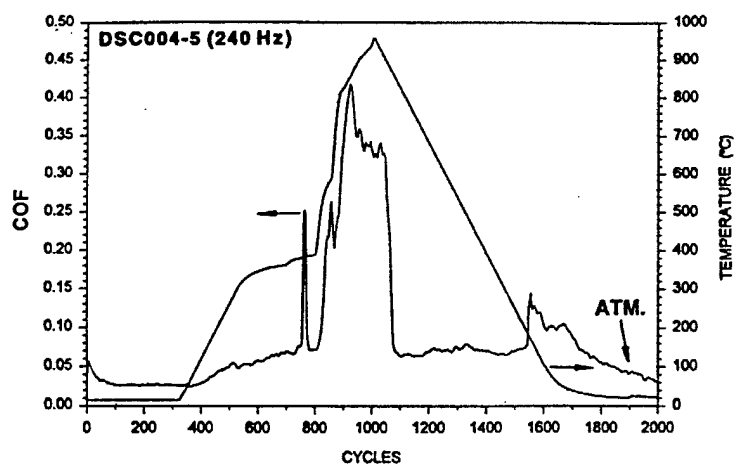
in 0.2 Torr dry H_2



15 g LOAD

Figure 1. The COF of the various Si crystallinities at the 15 g load in vacuum and in Round 1 dry PH_2 under standard thermal ramping conditions, with the associated unit Hertizian stresses calculated by the wear scar diameters.

VACUUM ($\sim 1 \times 10^{-5}$ Torr)



0.1 and 0.3 Torr P_{H_2}

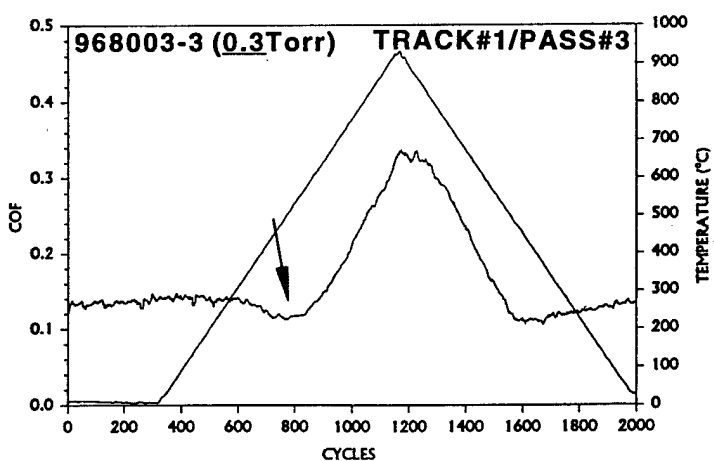
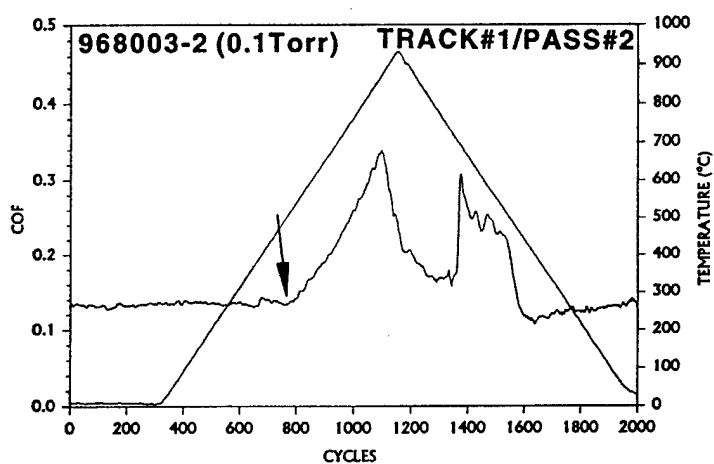
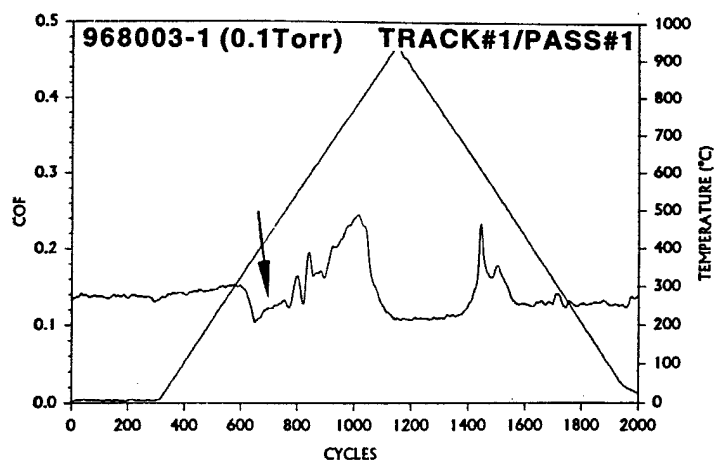
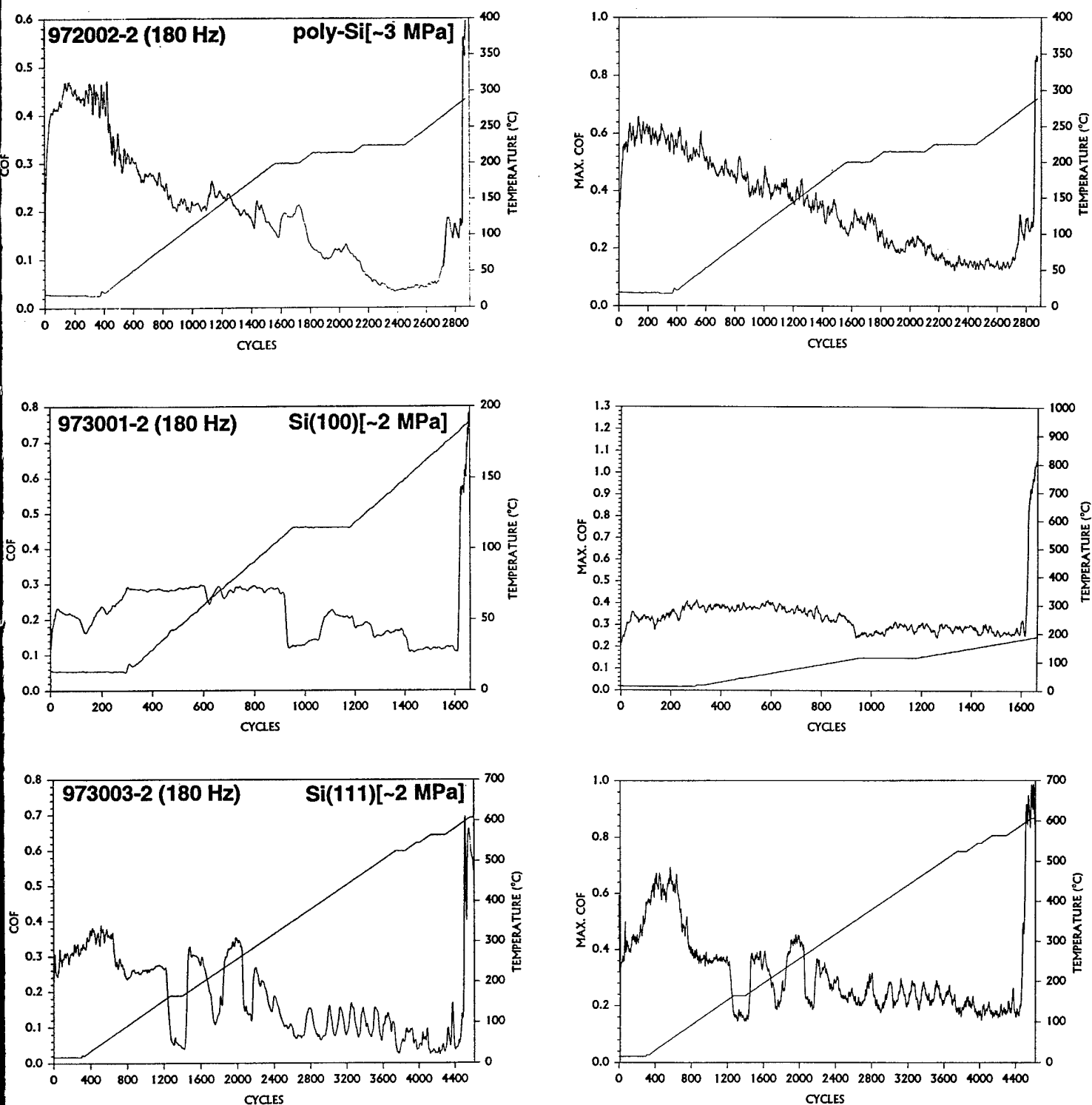


Figure 2. The COF of the polished $PCD_{C(100)}$ vs. itself at 28 g load in vacuum and at various levels of dry P_{H_2} , under standard thermal ramping.

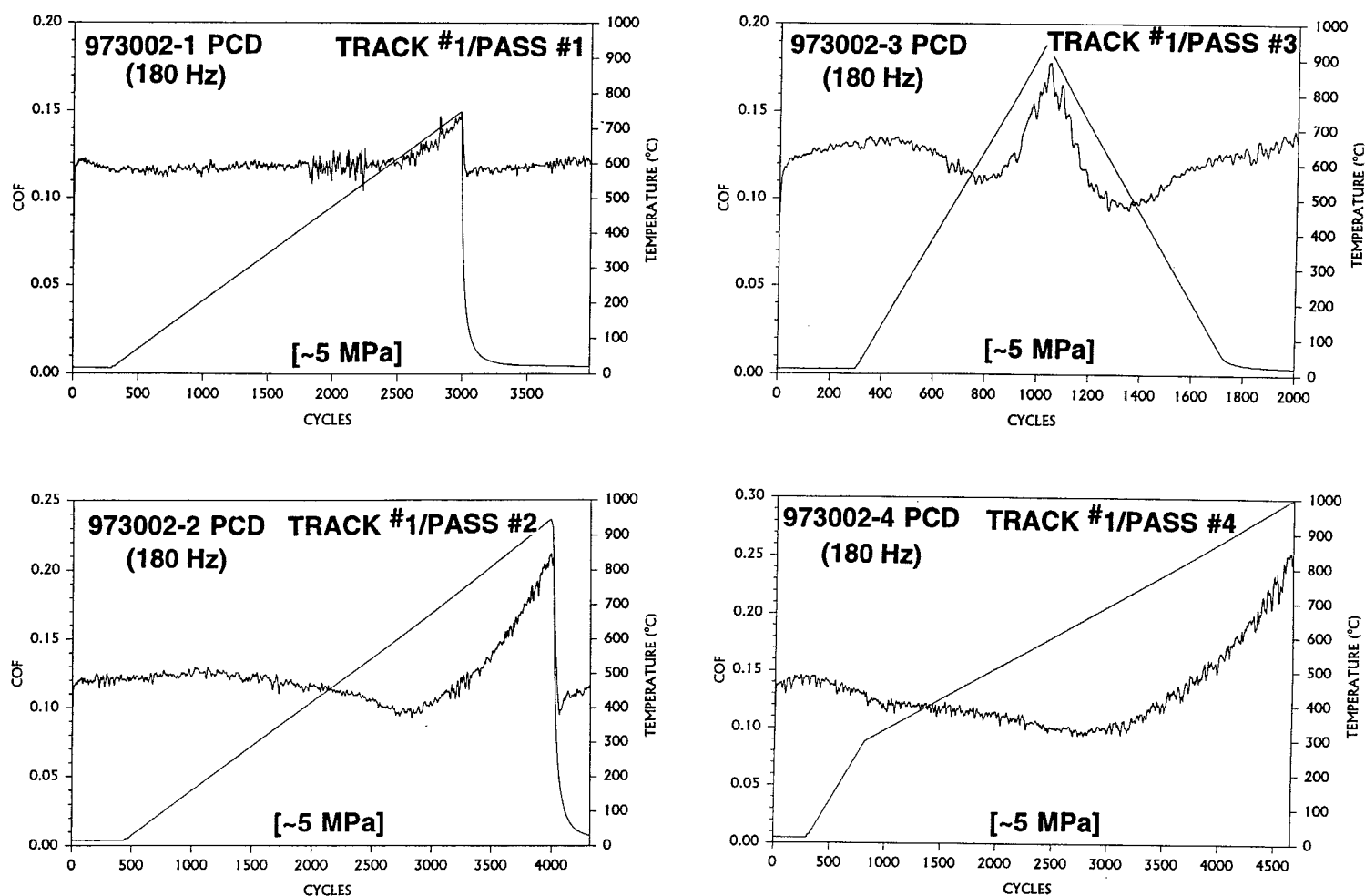
HF/H₂O-washed Si in 0.2 Torr dry H₂



15 g load

Figure 3. The COF and MAX.COF of the various Si crystallinities at the 15 g load in dry PH₂ under slow thermal ramping conditions, with the associated unit Hertzian stresses calculated by the wear scar diameters.

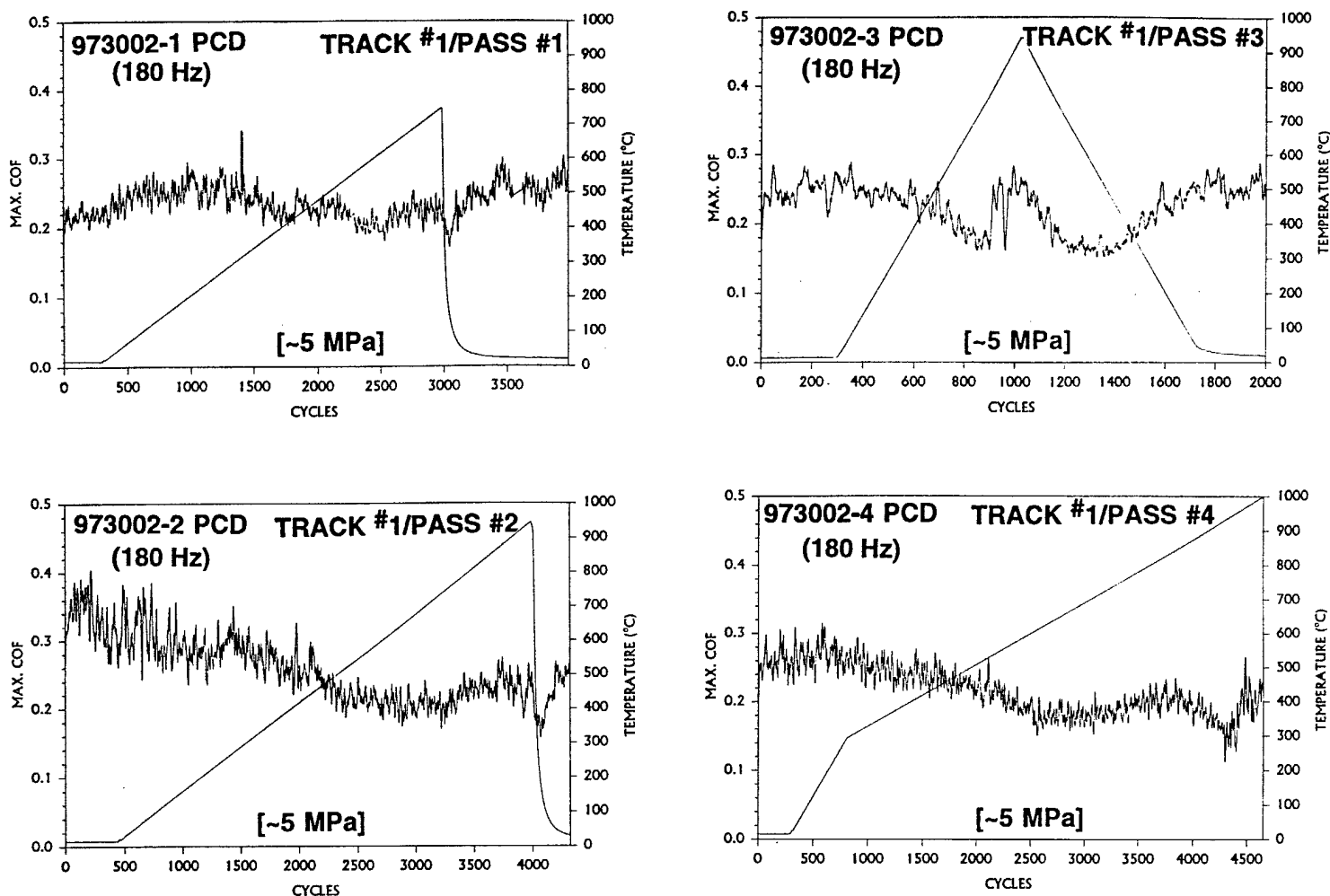
acid-washed PCD in 0.2 Torr dry H₂



28 g LOAD

Figure 4. The COF of the polished PCD_{C(100)} vs. itself at 28 g load in dry P_{H₂}, under slow and standard thermal ramping conditions.

acid-washed PCD in 0.2 Torr dry H₂



28 g LOAD

Figure 5. The MAX.COF of the polished PCD_{C(100)} vs. itself at 28 g load in dry P_{H₂}, under slow and standard thermal ramping conditions. Equivalent COF curves in Fig. 4.

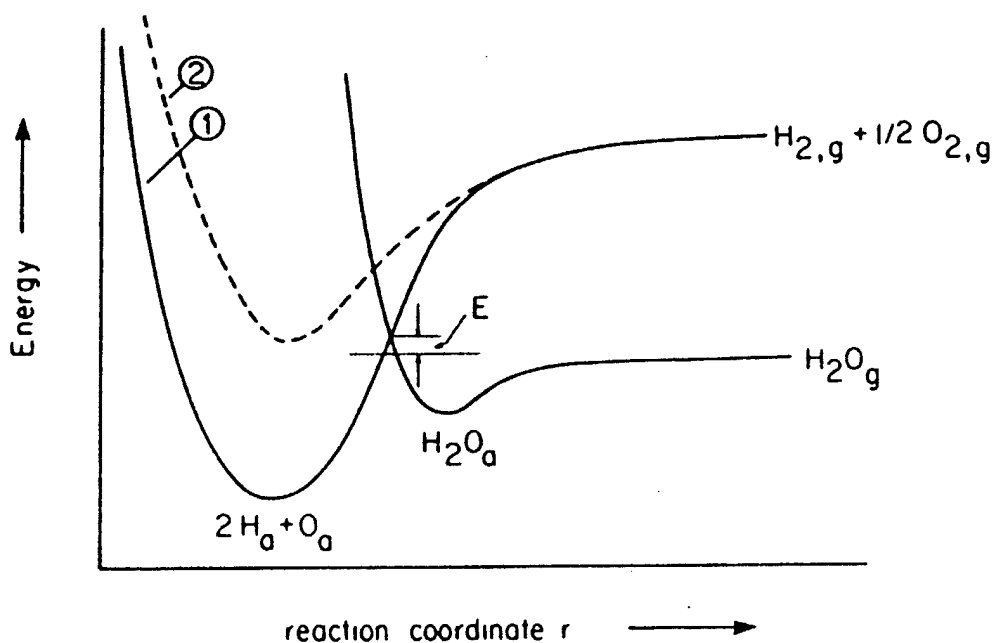


Figure 6. Potential energy diagrams for adsorbed water and its dissociation products; from [18].

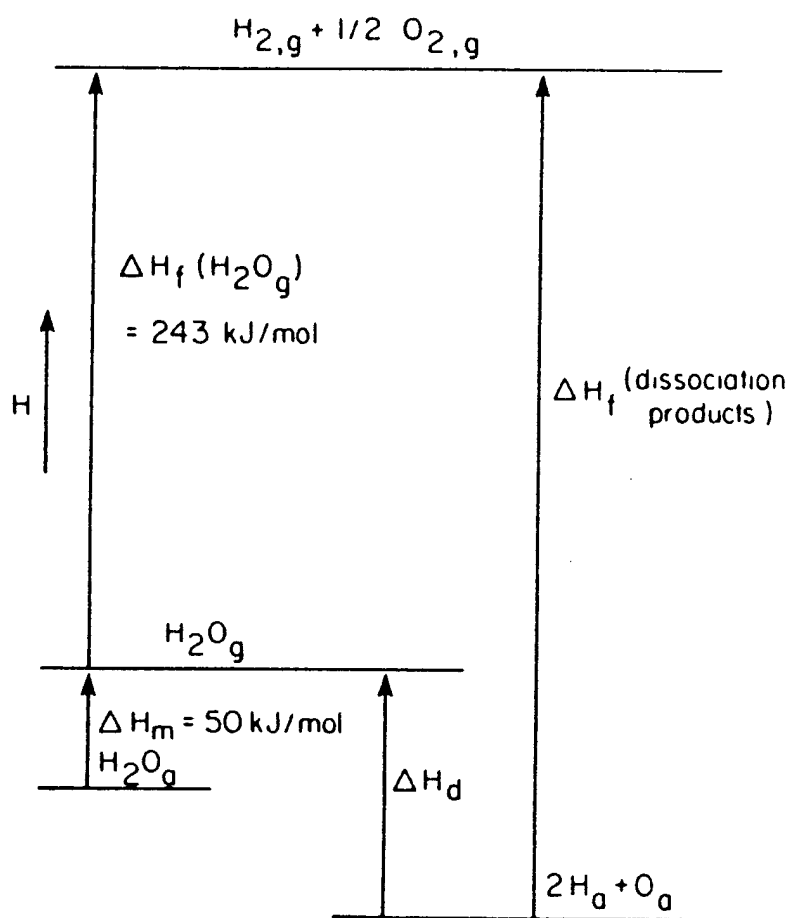


Figure 7. Enthalpy changes which accompany adsorption and dissociation of water, referenced to gas-phase hydrogen and oxygen; from [18].

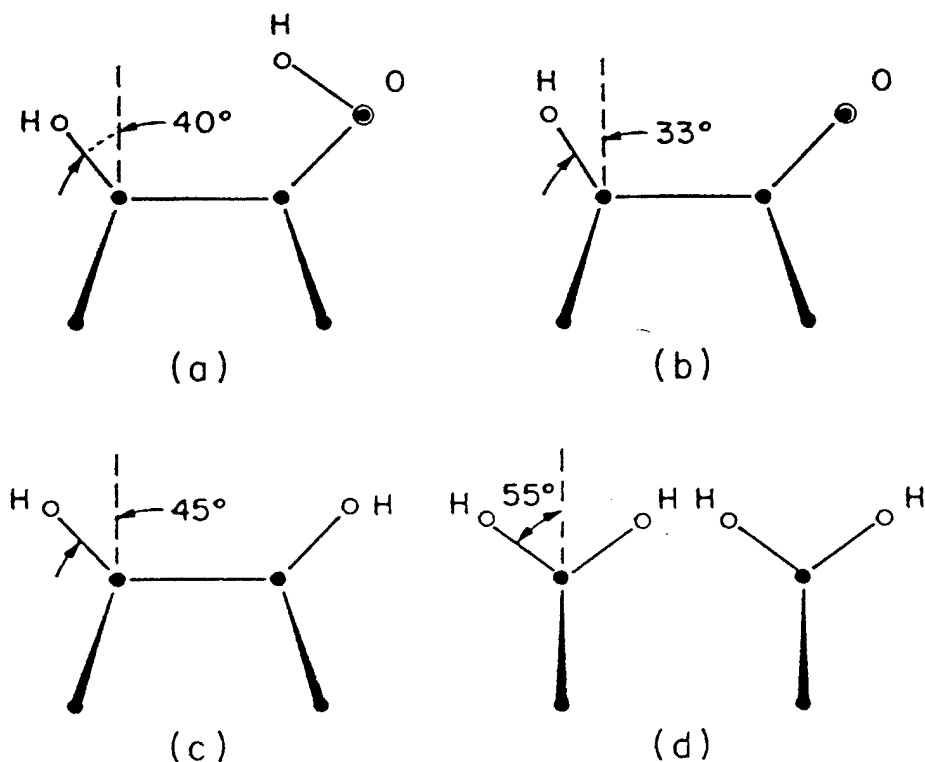


Figure 8. Suggested arrangements of -H and -OH surface groups on Si after dissociative chemisorption of water: (a) monohydride with OH nearest neighbor, (b) monohydride with O nearest neighbor, (c) pure monohydride, and (d) dihydride. Note that the angles are associated with the effective dynamic dipole moment rather than the geometric bond; from [28].

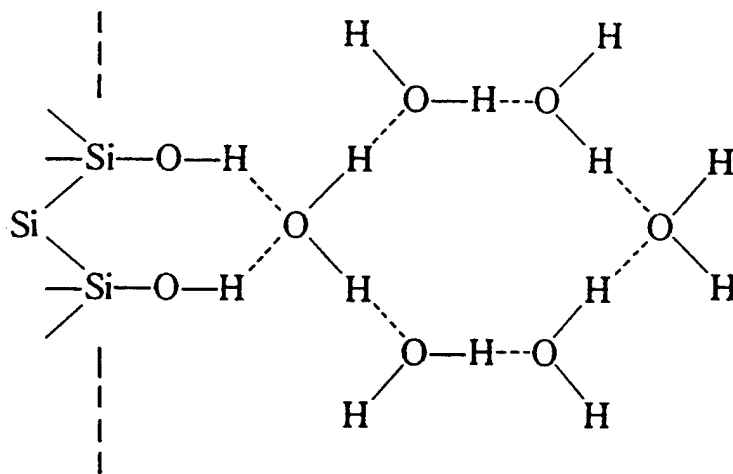


Figure 9. Bridged, hydrogen-bonded water clusters bonded to the hydrophilic sites of a Si surface; after [30].

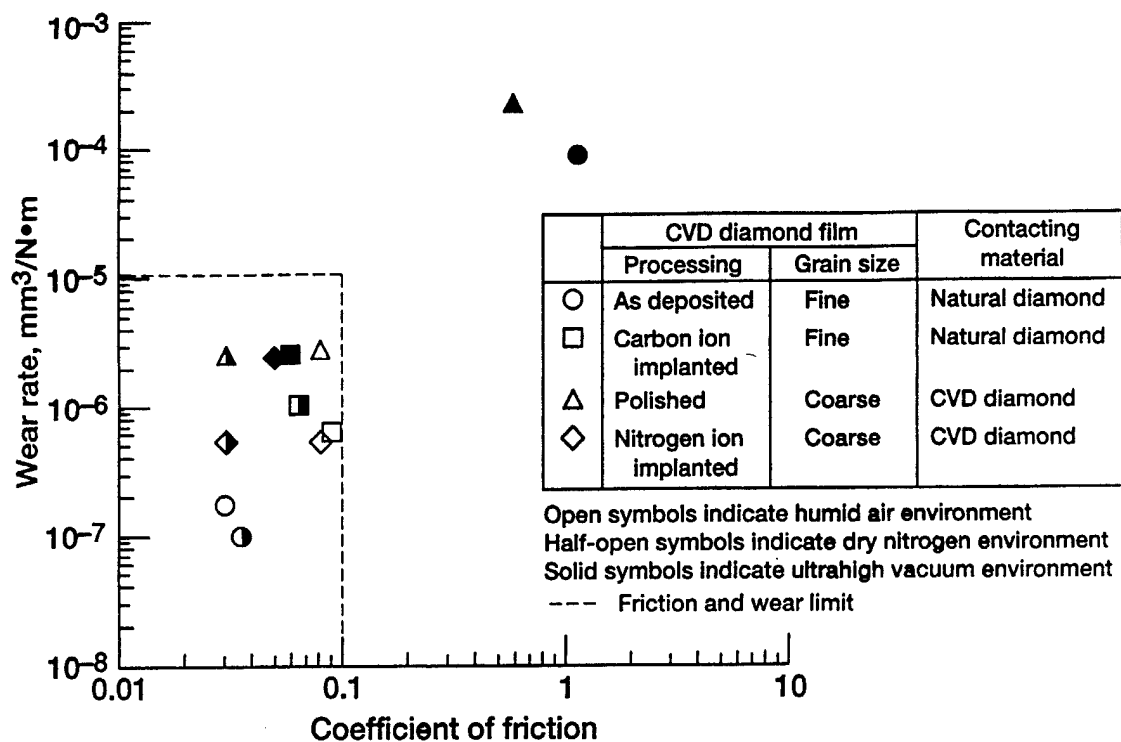


Figure 10. Wear rate and COF of PCD films in various atmospheric environments; from [15].

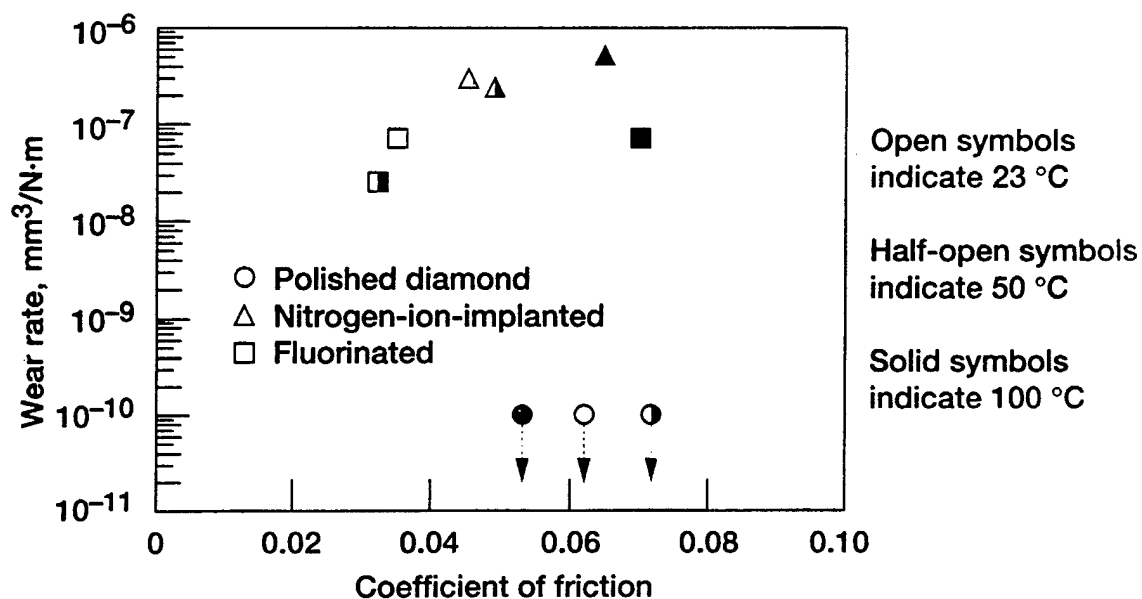


Figure 11. Wear rate and COF of PCD films in distilled water; from [15].

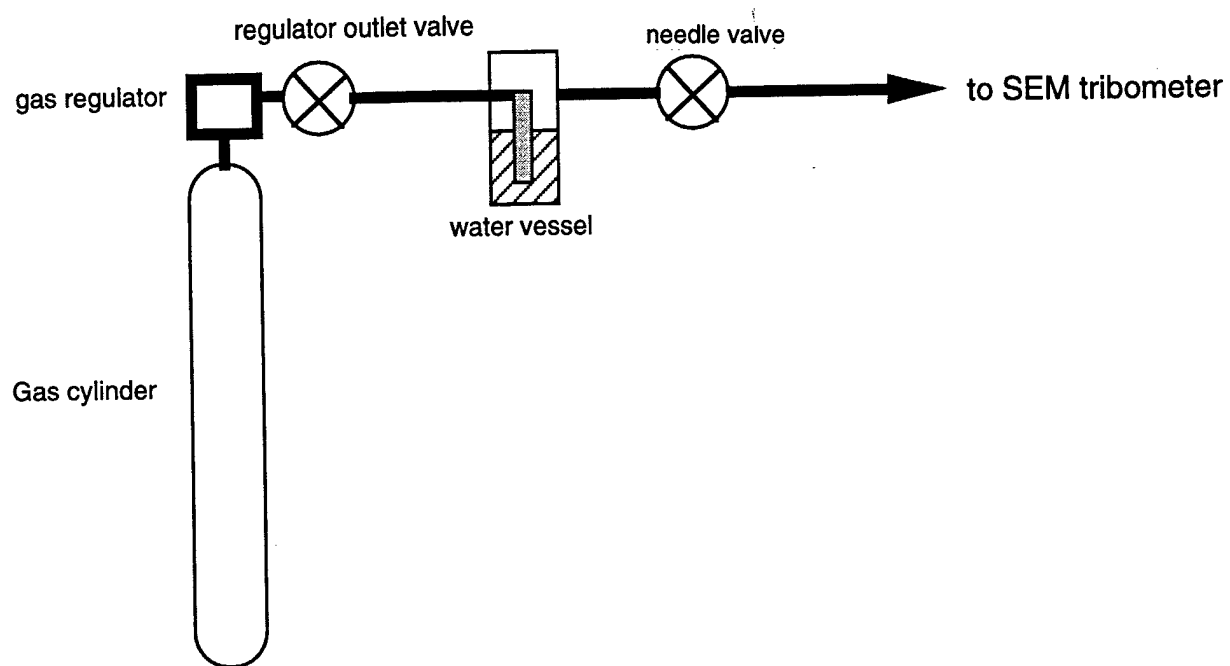
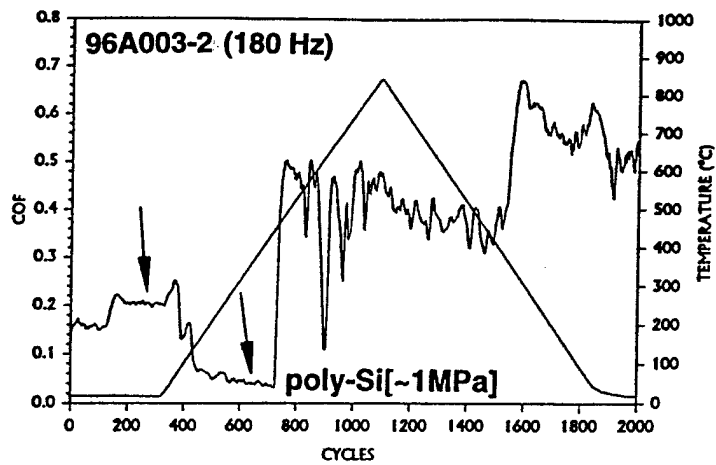
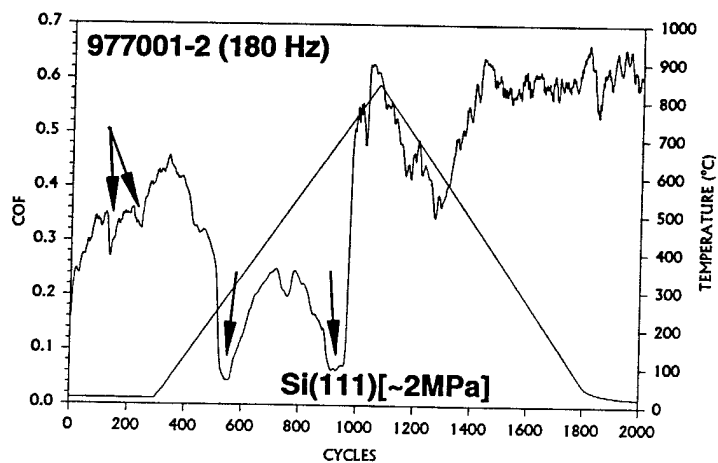
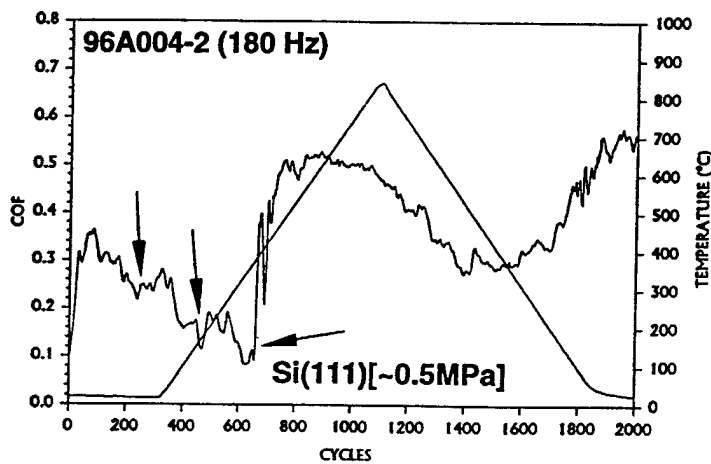
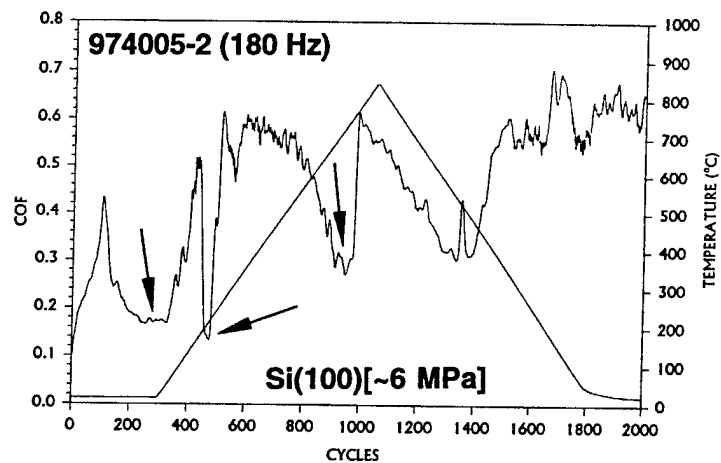
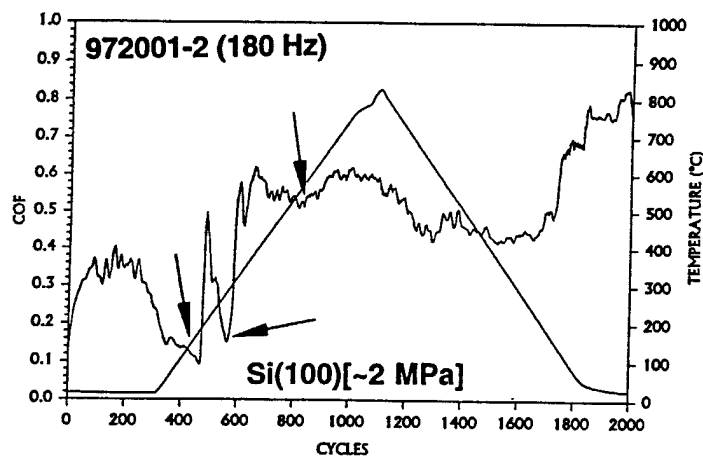
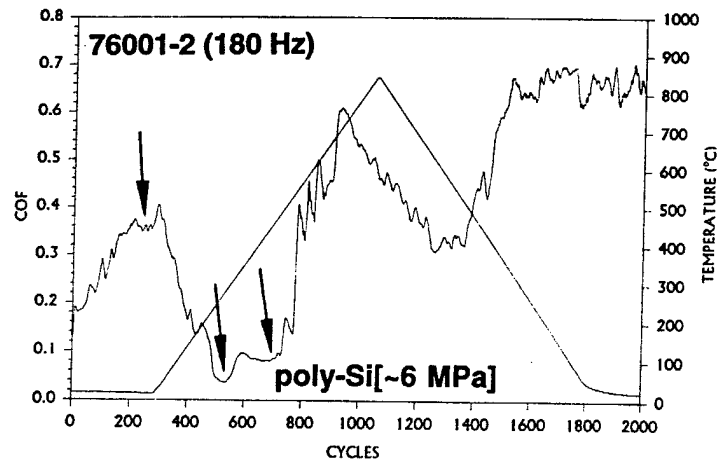


Figure 12. Water saturation apparatus for introducing wet P_{H_2} into the SEM tribometer.

in 0.2 Torr dry H_2



in ~0.2 Torr wet H_2
($P_{H_2O} \approx 0.02$ Torr)

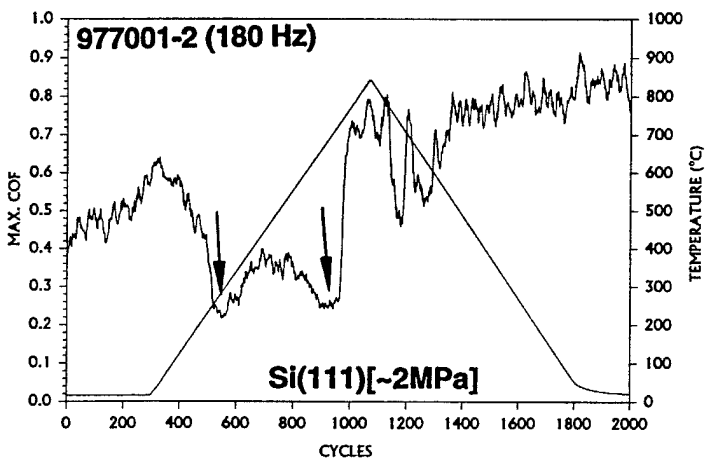
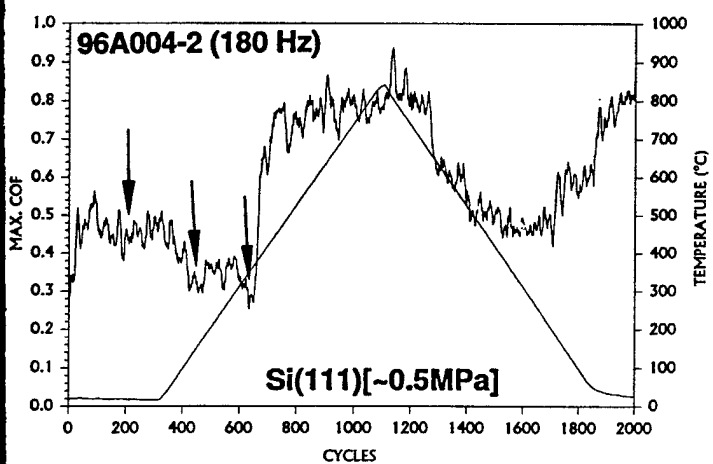
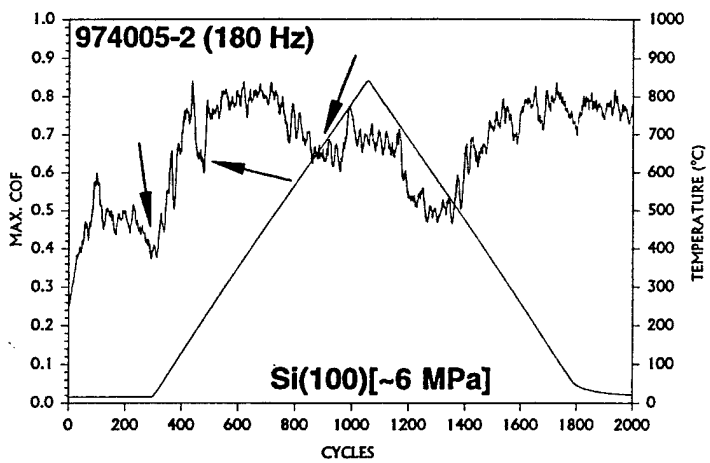
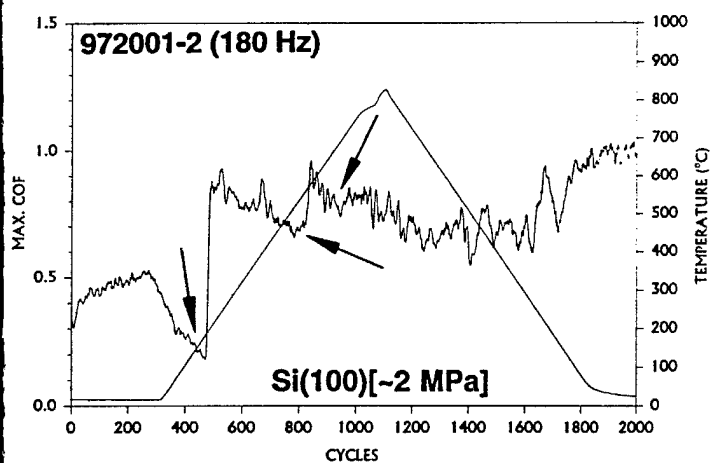
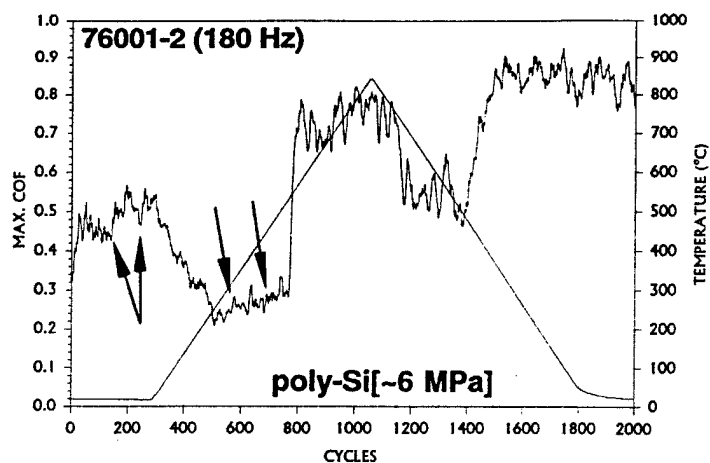
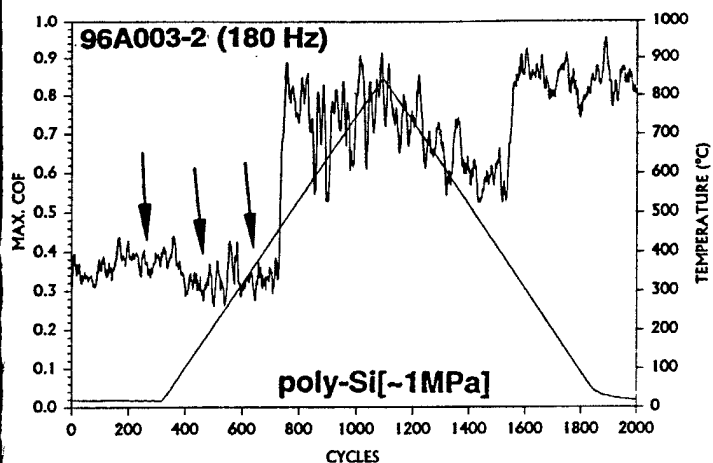


15 g load

Figure 13. The COF of the various Si crystallinities at the 15 g load in vacuum and during the Round 3 dry P_{H_2} and the only round of wet P_{H_2} experiments, with the associated unit Hertzian stresses calculated by the wear scar diameters.

in 0.2 Torr dry H_2

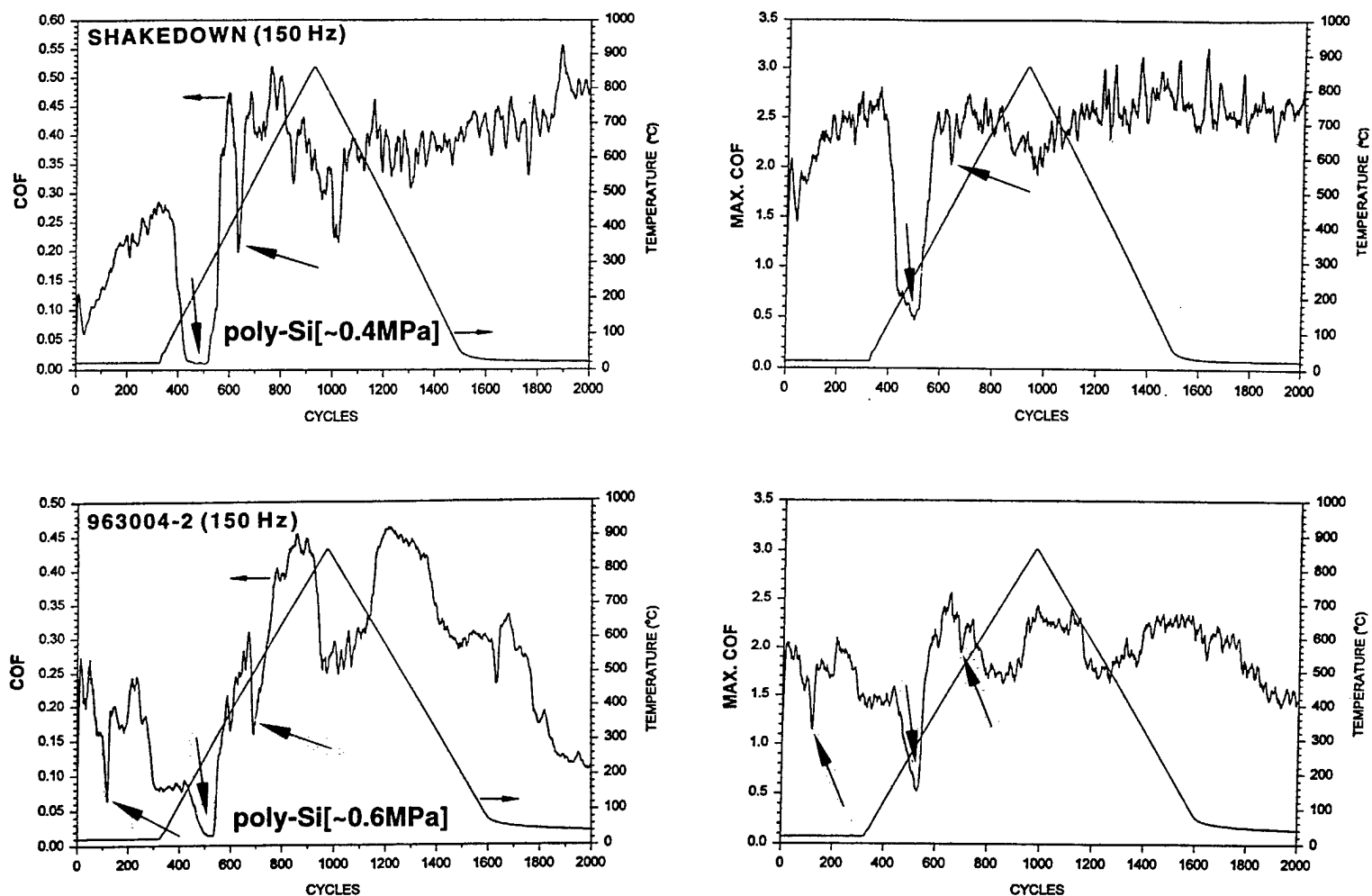
in ~0.2 Torr wet H_2
($P_{H_2O} \cong 0.02$ Torr)



15 g load

Figure 14. The MAX.COF of the various Si crystallinities at the 15 g load in vacuum and during the Round 3 dry P_{H_2} and the only round of wet P_{H_2} experiments, with the associated unit Hertzian stresses calculated by the wear scar diameters. Equivalent COF curves in Fig. 13.

in 0.2 Torr H₂



15 g LOAD

Figure 15. COF and MAX.COF of the poly-Si shakedown test at a 15 g load in dry P_H₂ using a preworn pin tip, as compared with the Round 1 dry P_H₂ poly-Si test performed at the same 15 g load; from [72].

in 0.2 Torr H₂

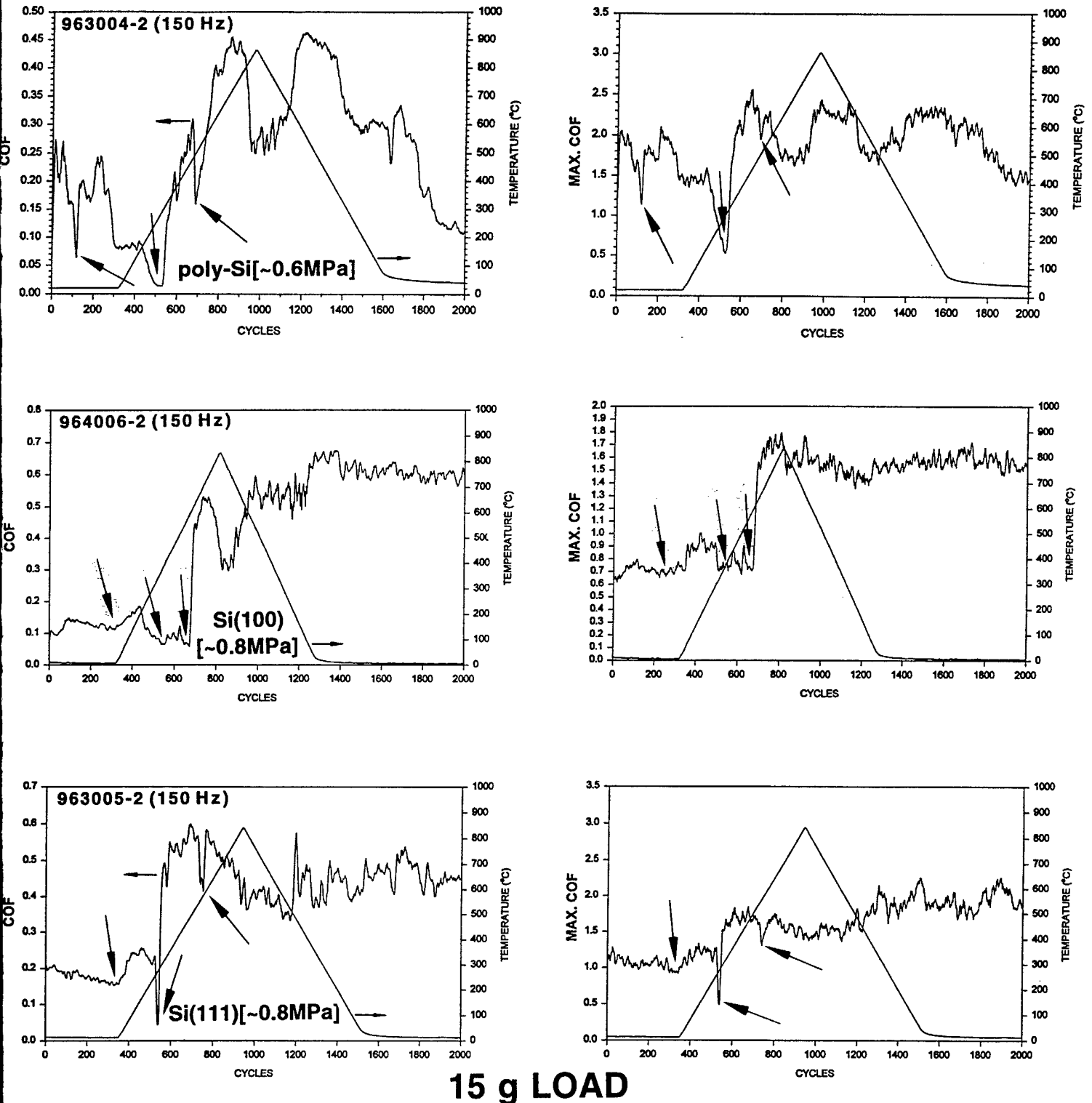
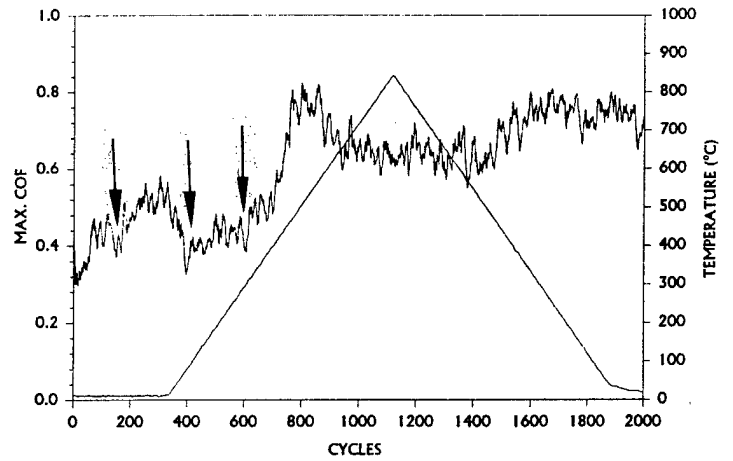
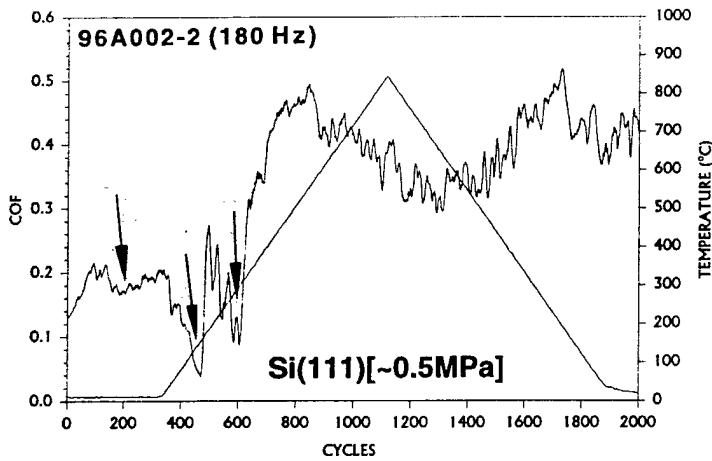
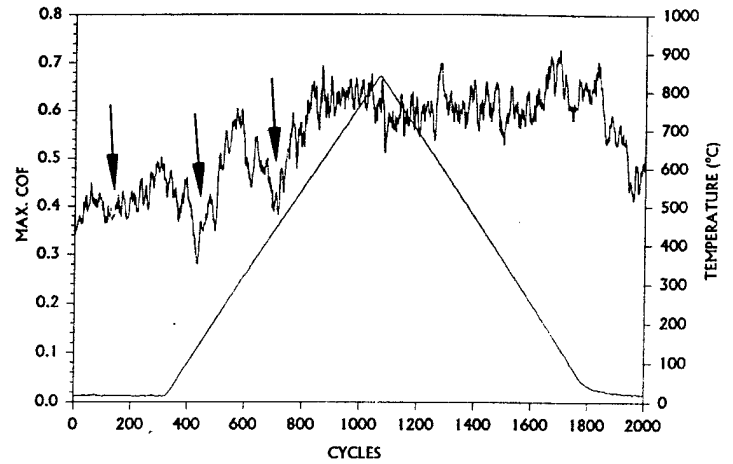
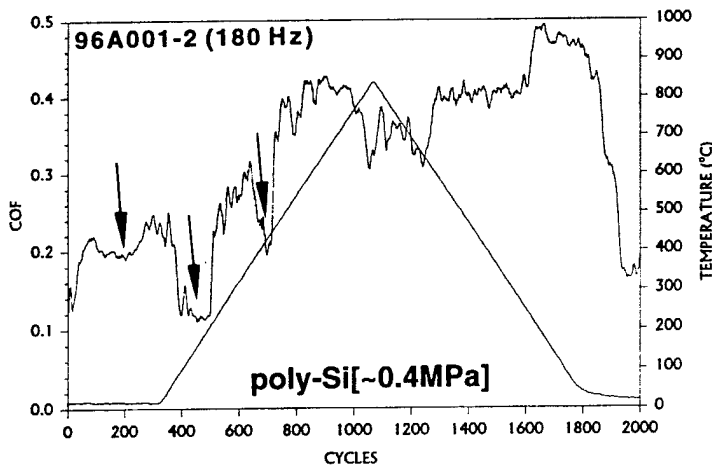


Figure 16. COF and MAX.COF of the Round 1 dry P_{H2} tests at a 15 g load for all Si crystallinities, generated with prepolished pin tip scars further ground by a 1000-cycle planarization procedure performed at a 15 g load; from [72].

in 0.2 Torr H₂



15 g LOAD

Figure 17. COF and MAX. COF of the Round 2 dry P_{H₂} tests tests at a 15 g load using poly-Si and Si(111) specimens only, with prepolished pin tip scars further ground by a 1000-cycle planarization procedure performed at a 15 g load; from [72].

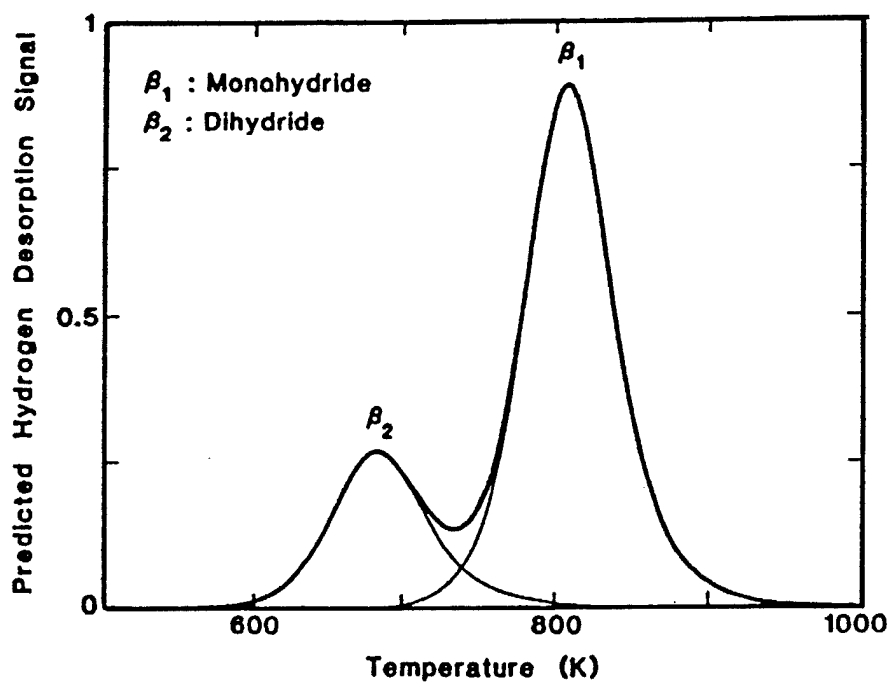


Figure 18. Predicted temperature-programmed desorption of hydrogen from a porous silicon surface, using experimental dihydride and monohydride desorption kinetics; from [74].

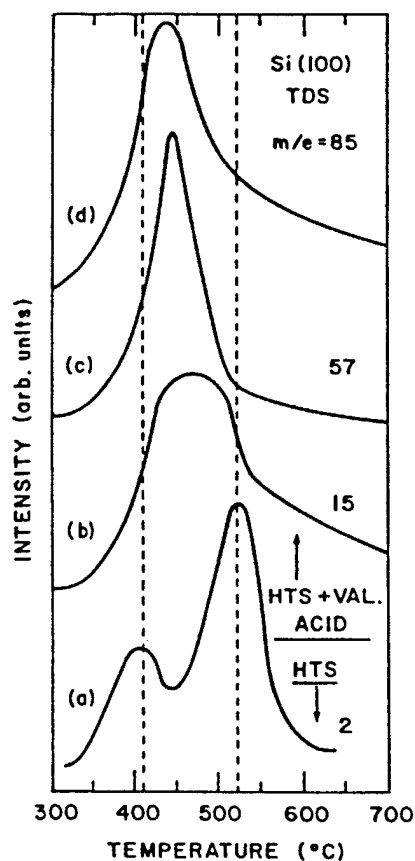


Figure 19. Smoothed thermal desorption spectra from H-terminated Si(100). The temperature-programmed desorption spectroscopic (TDS) signatures are shown for (a) H_2 ($m/e = 2$), (b) CH_3 (15), (c) $CH_3(CH_2)_3$ (57), and (d) $CH_3(CH_2)_3CO$ (85). The ramp rate was 10°C/s ; from [75].

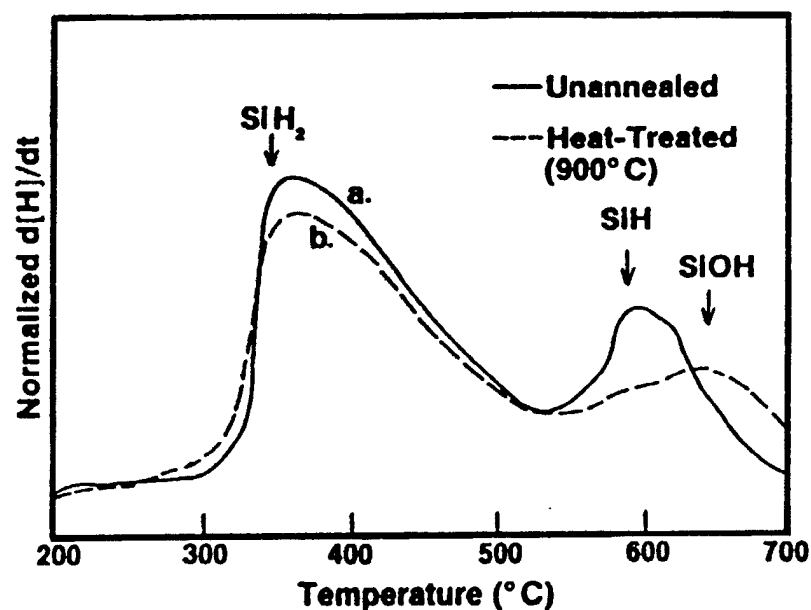


Figure 20. Measured temperature-induced desorption of hydrogen from (a) an oxygen deficient silicon grain boundary, (b) an oxygen-containing grain boundary; from [76].

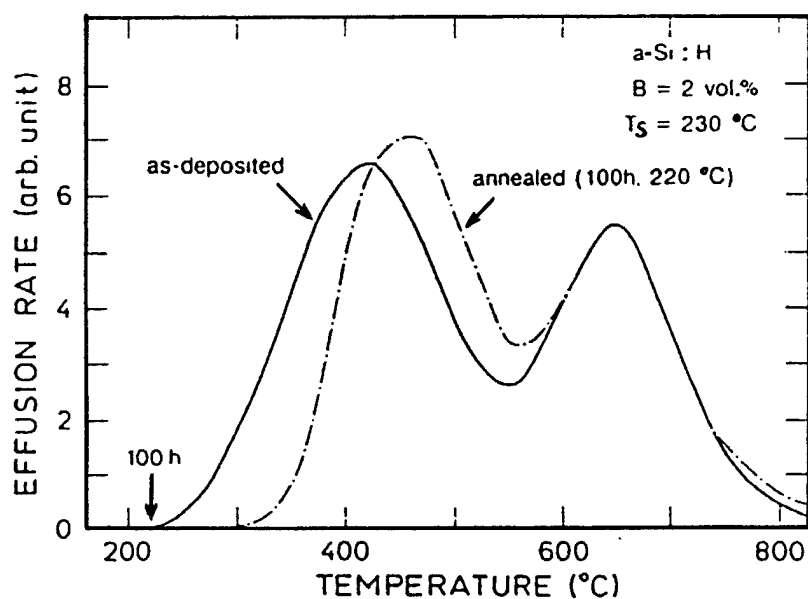


Figure 21. Measured temperature-programmed desorption of hydrogen (H_2) for as-deposited boron-doped, amorphous hydrogenated silicon (a-Si:H) films (solid line) and films annealed for 100 hours at 220°C (dash-dotted line); from [77].

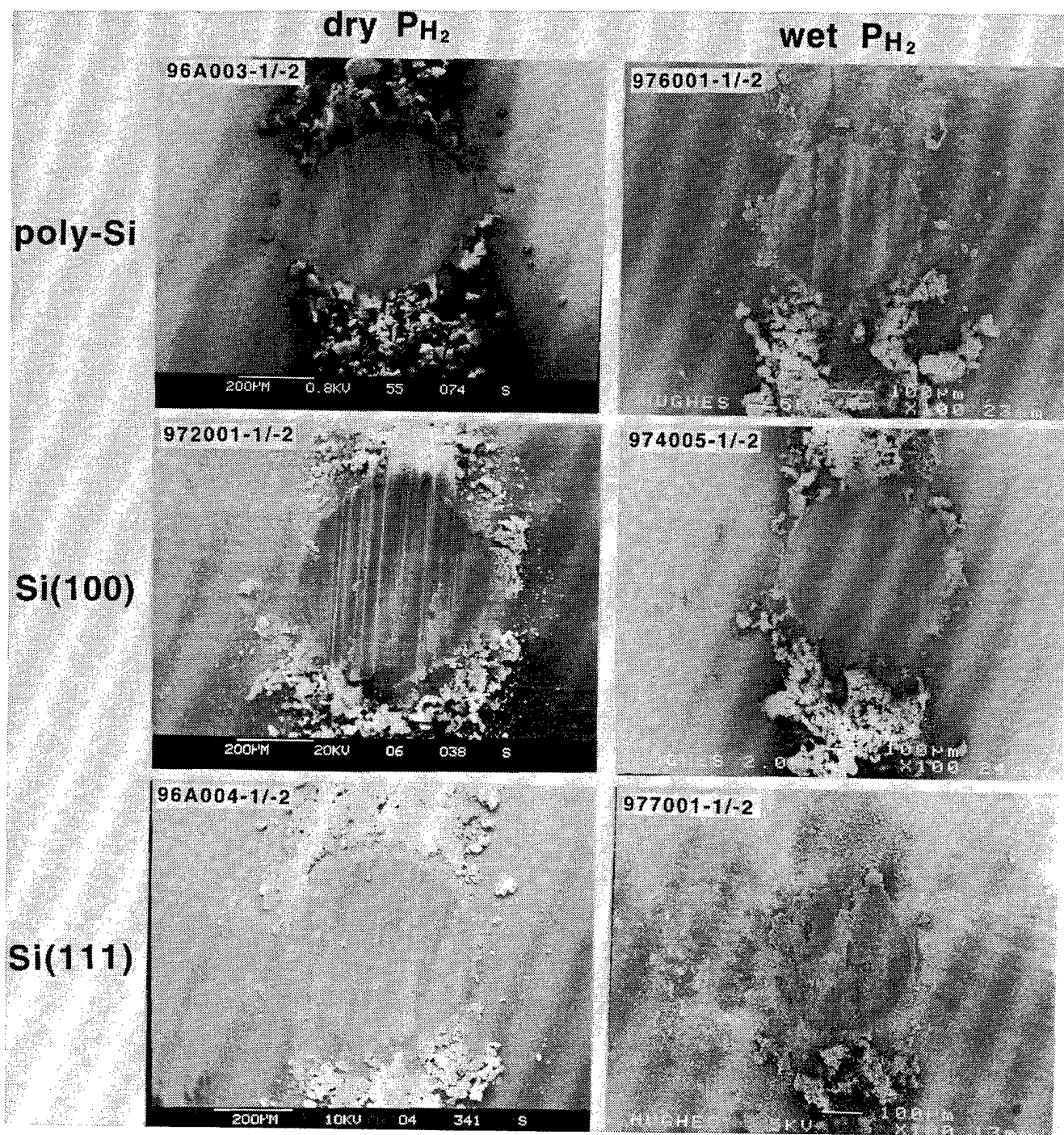


Figure 22. SEM photomicrographs of Si pin tip wear scars at 100x mag., after the respective dry and wet PH_2 15 g load RT "grind" + 15 g load standard thermal ramp experiments.

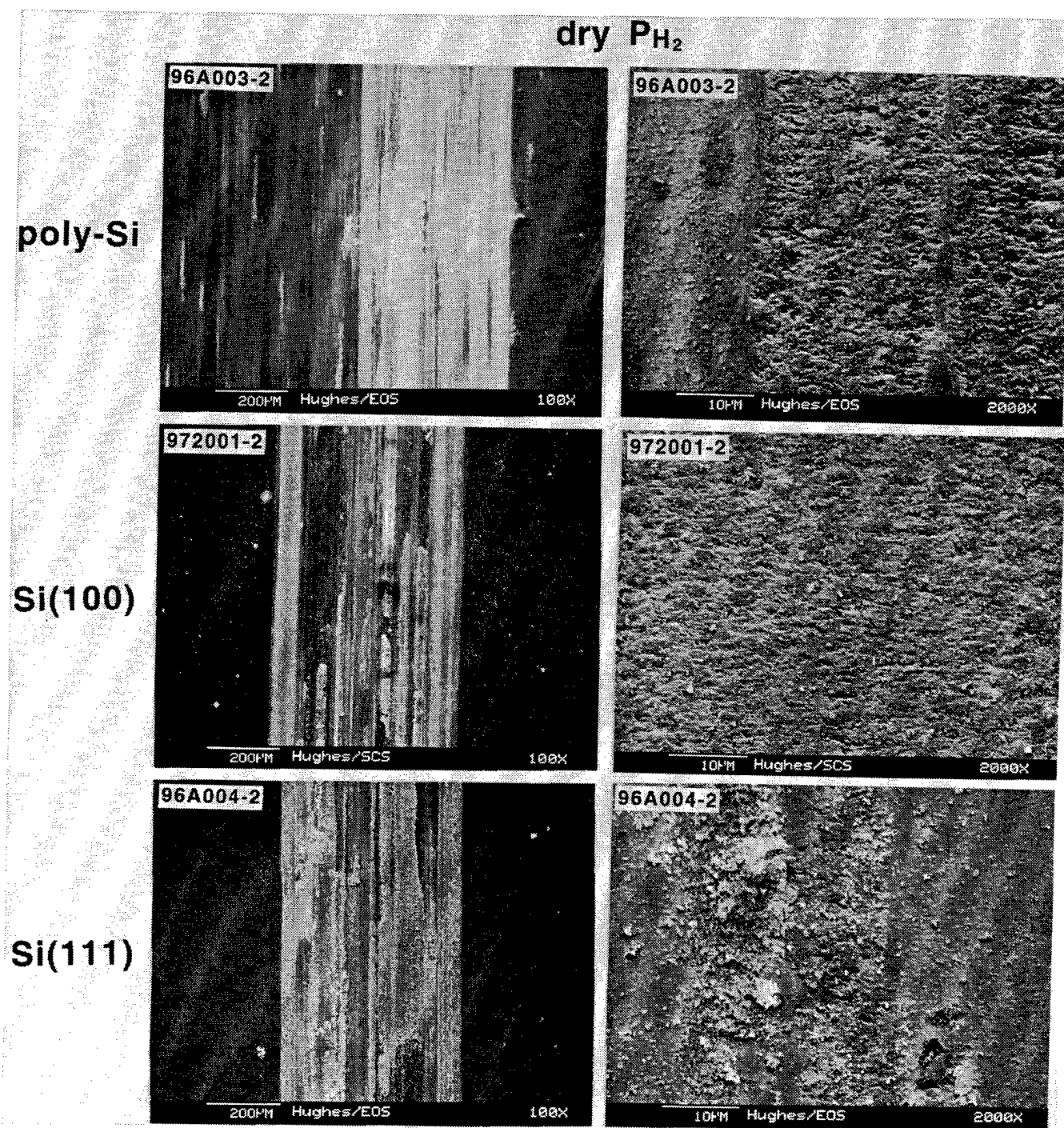


Figure 23. SEM photomicrographs of Si flat wear scars at 100x and 2000x mags., after the respective 15 g load dry P_{H_2} RT "grind" + 15 g load standard thermal ramp experiments. Photos of matching pin tip scars at 100x mag. in Fig. 22.

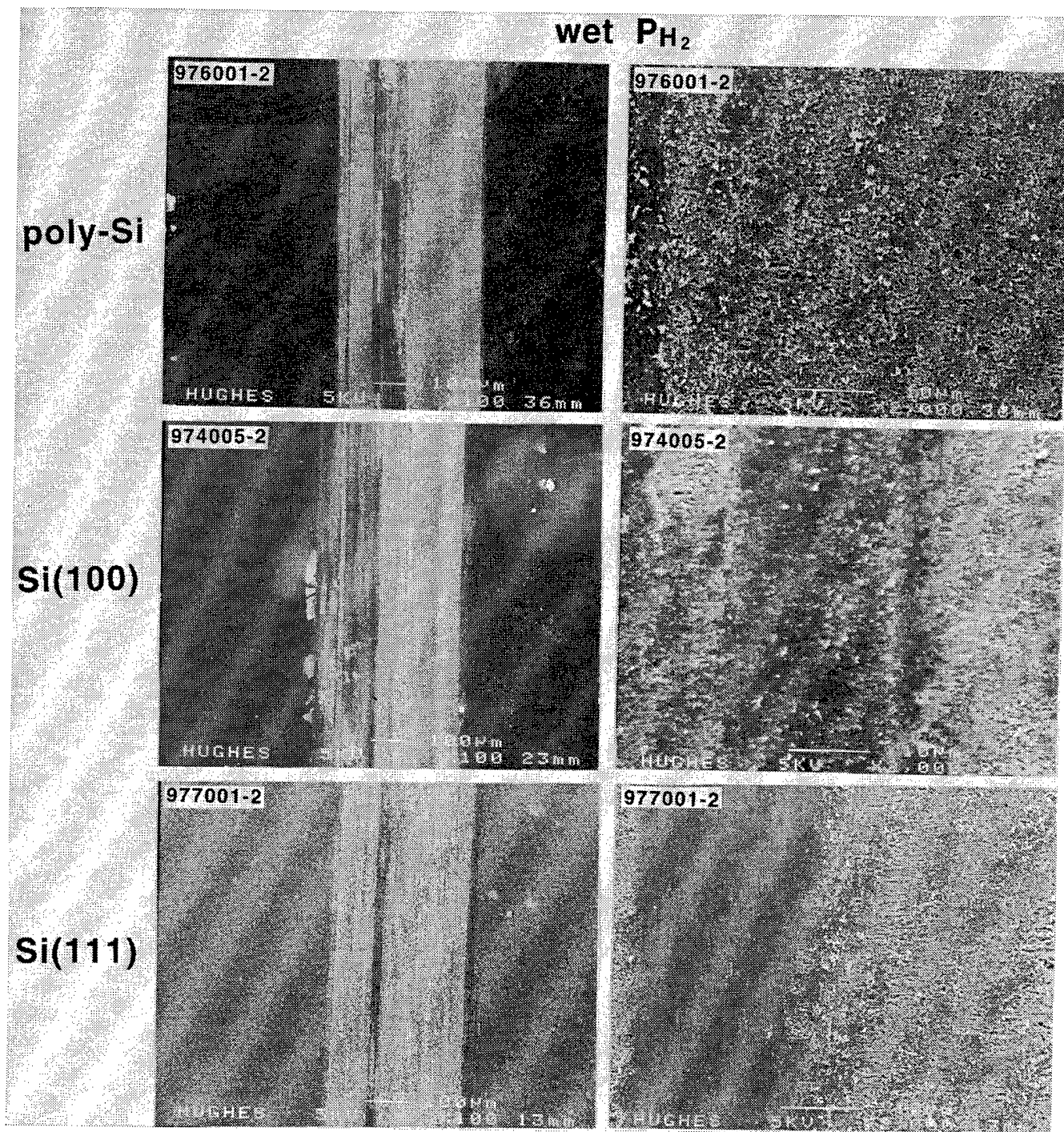


Figure 24. SEM photomicrographs of Si flat wear scars at 100x and 2000x mags., after the respective 15 g load wet P_{H_2} RT "grind" + 15 g load standard thermal ramp experiments. Photos of matching pin tip scars at 100x mag. in Fig. 22.

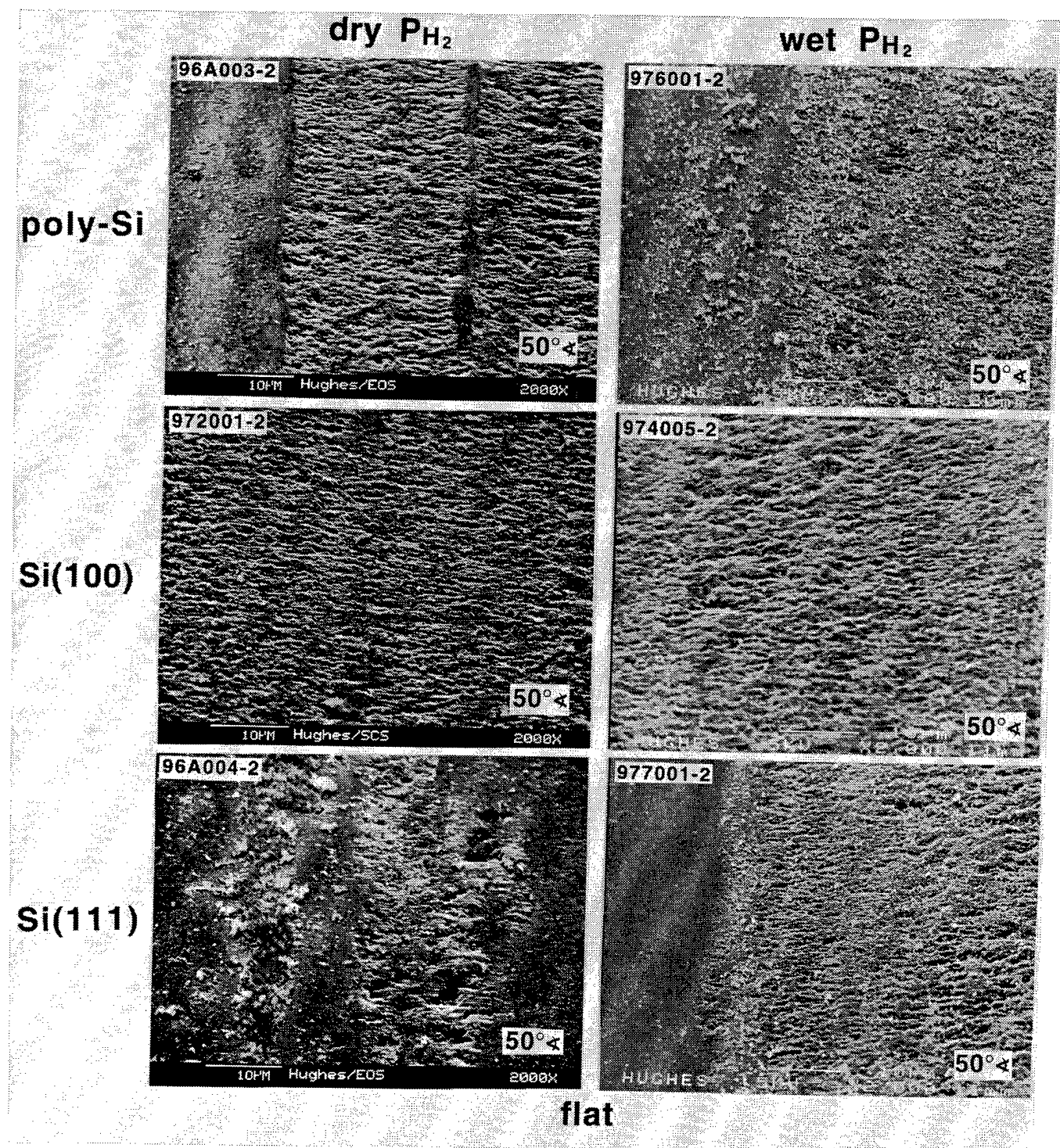


Figure 25. SEM photomicrographs of Si flat wear scars at 2000x mag., after the respective 15 g dry and wet P_{H_2} RT "grind" + 15 g load standard thermal ramp experiments. Photos show typical tensile microcracking of the respective surfaces.



PIN

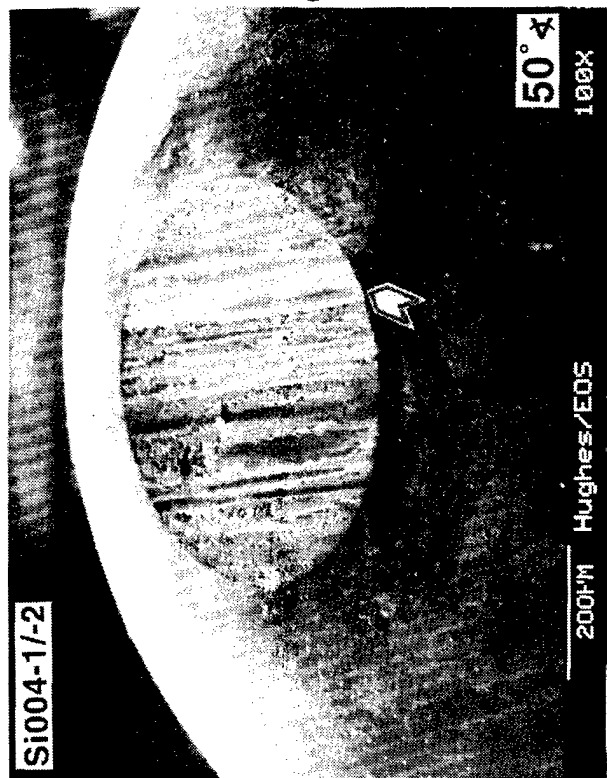


FLAT

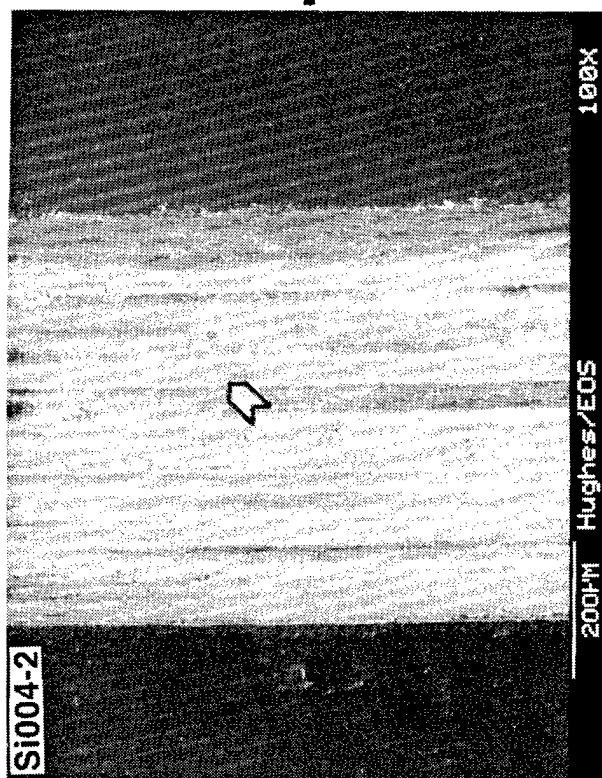


POLY-XTL Si vs. POLY-XTL Si (repeat) **(15 g = 0.15 N)**

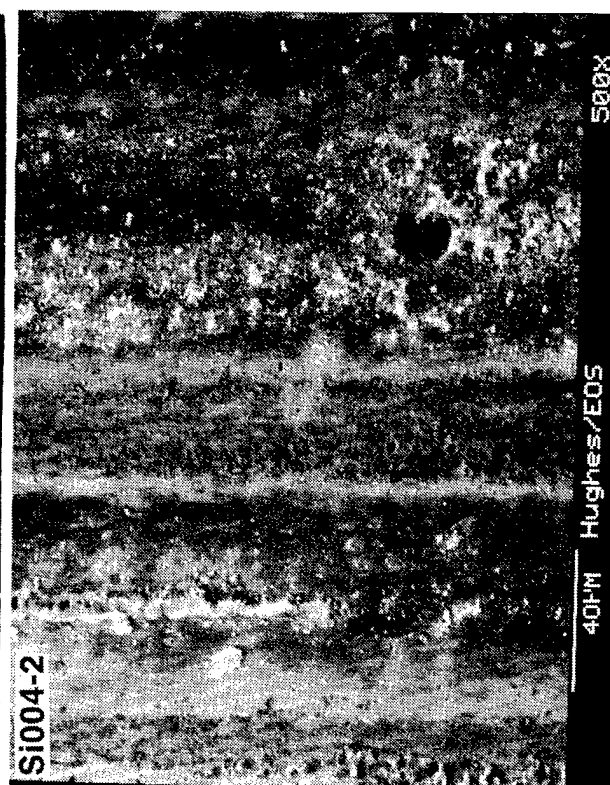
Figure 26. SEM photomicrographs of poly-Si pin tip and flat wear scars at 100x and 500x mags., after the respective 15 g load RT "grind" + 15g load standard thermal ramp experiments in vacuum.



PIN

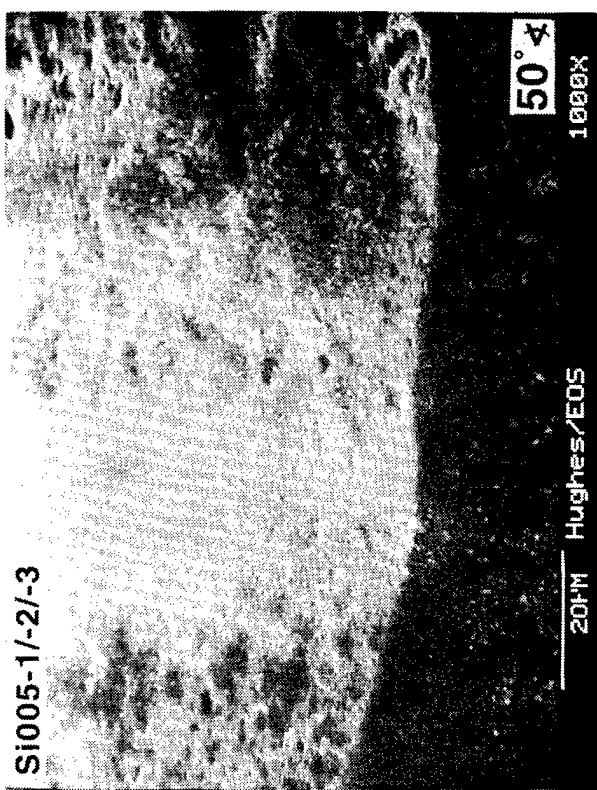


FLAT

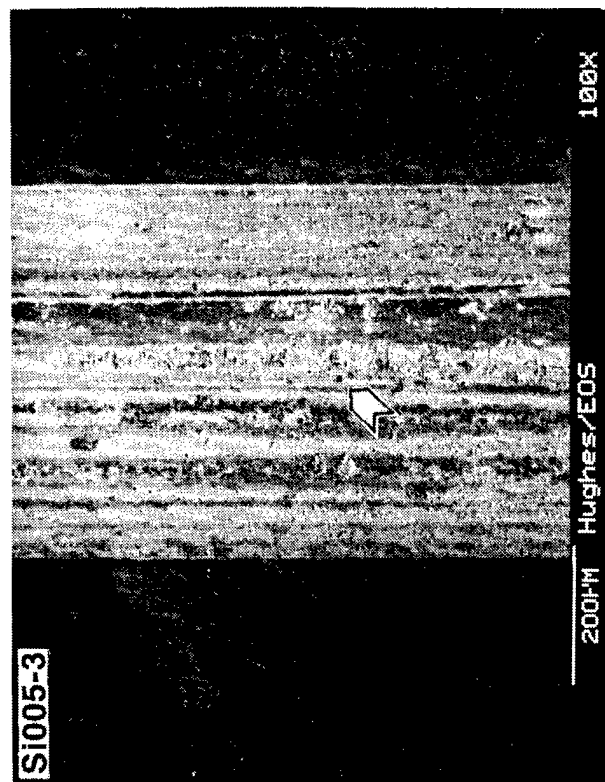


Si (100) vs. Si (100) (repeat) (15 g = 0.15 N)

Figure 27. SEM photomicrographs of Si(100) pin tip and flat wear scars at 100x and 500x mags., after the respective 15g load RT "grind" + 15g load standard thermal ramp experiments in vacuum.



PIN

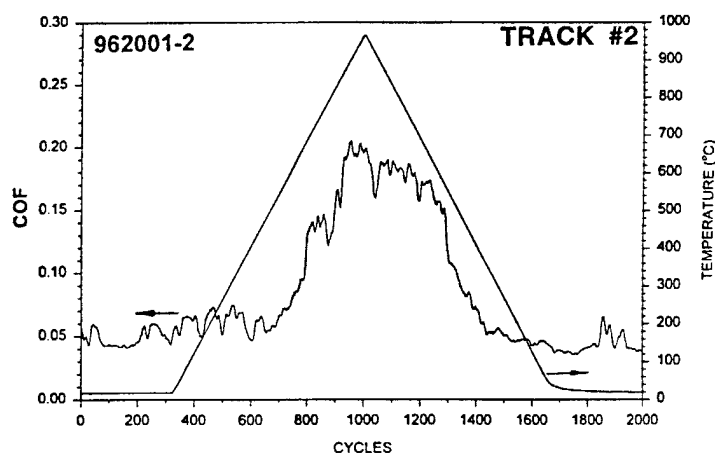


FLAT

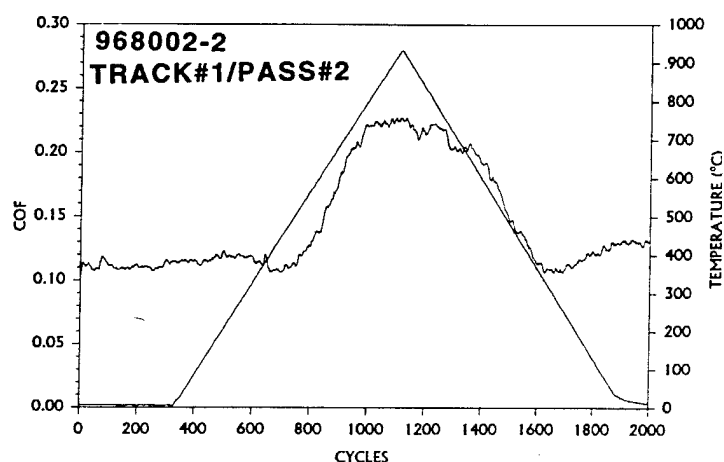
Si (111) vs. Si (111) + Si (111) vs. Si (111) (repeat) + Si (111) vs. Si (111) (3rd test)
(15 g = 0.15 N) (15 g = 0.15 N) (15 g = 0.15 N)

Figure 28. SEM photomicrographs of Si(111) pin tip and flat wear scars at 100x and 500x mags., after the respective 15g load RT "grind" + 15g load standard thermal ramp experiments in vacuum.

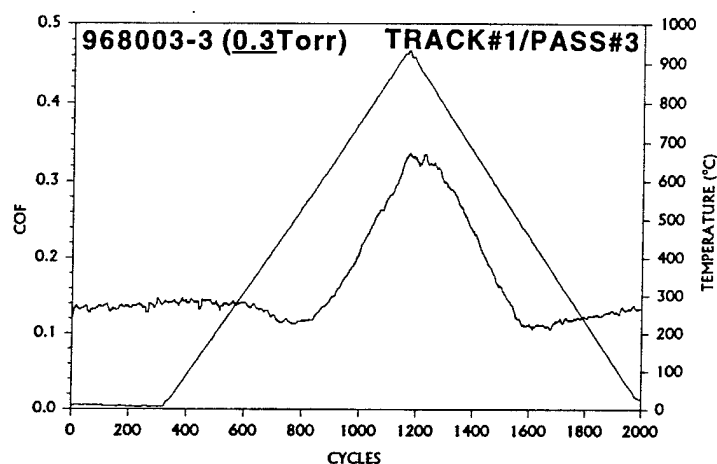
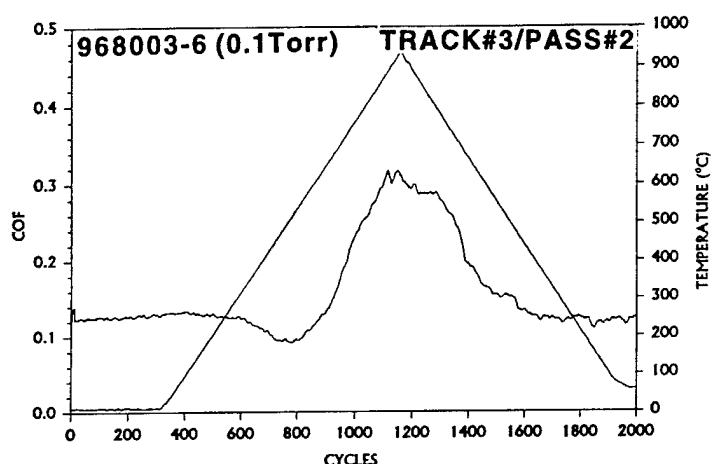
0.2 TORR P_{H2} (first round)



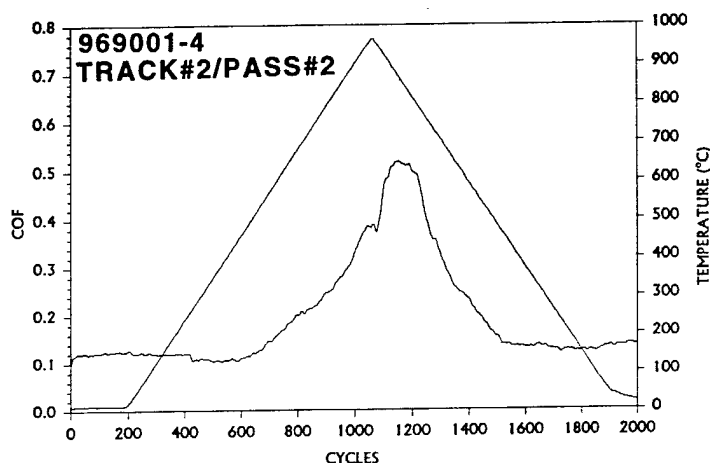
0.2 Torr P_{H2} (third round)



0.1 and 0.3 Torr P_{H2} (fourth round)



0.1 Torr P_{H2} (fifth round)



0.18 Torr P_{H2} (sixth round)

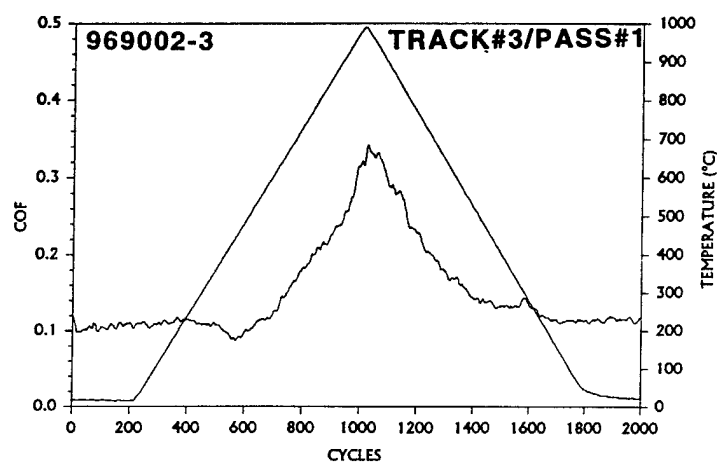
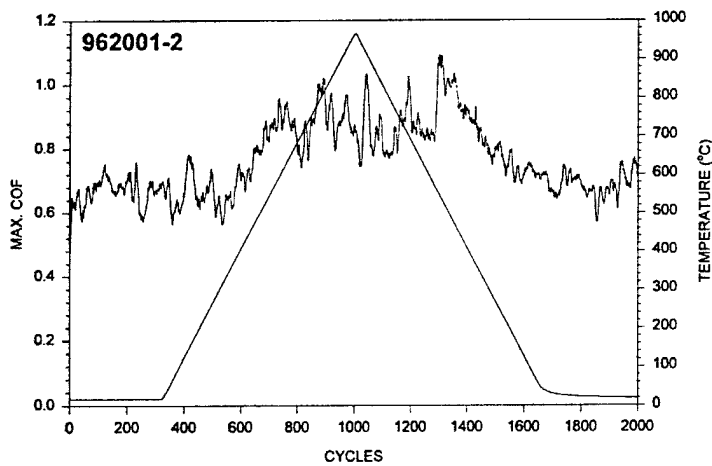
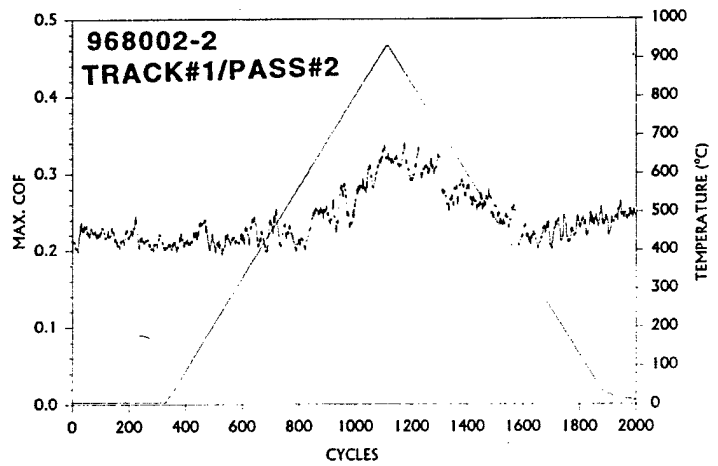


Figure 29. Typical peak-type PCD_{C(100)} COF curves taken from the various 28 g load dry P_{H2} standard thermal ramp test rounds described more thoroughly in [2], not showing re(de)constructions troughs previously depicted in Fig. 2.

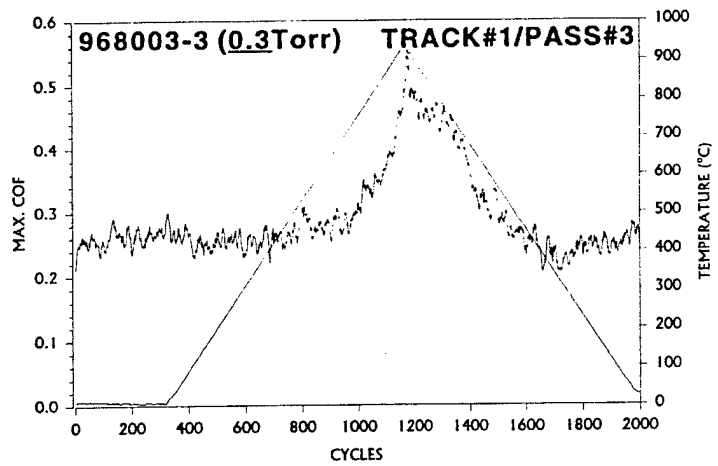
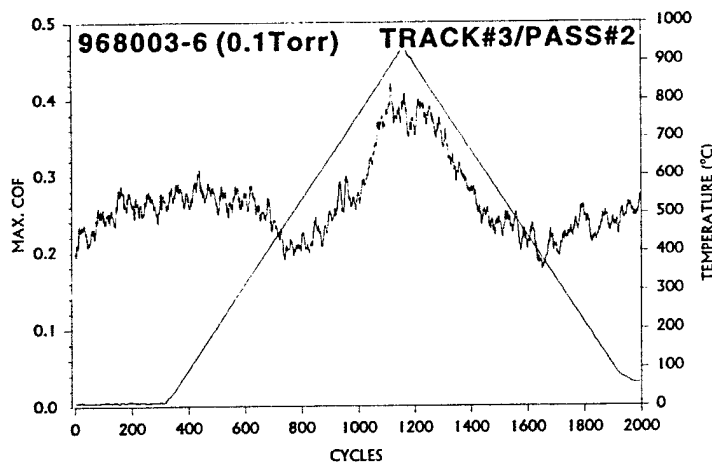
0.2 TORR P_{H_2} (first round)



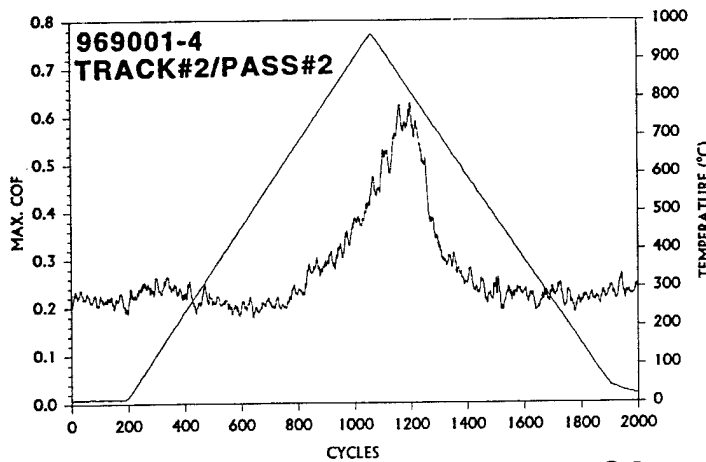
0.2 Torr P_{H_2} (third round)



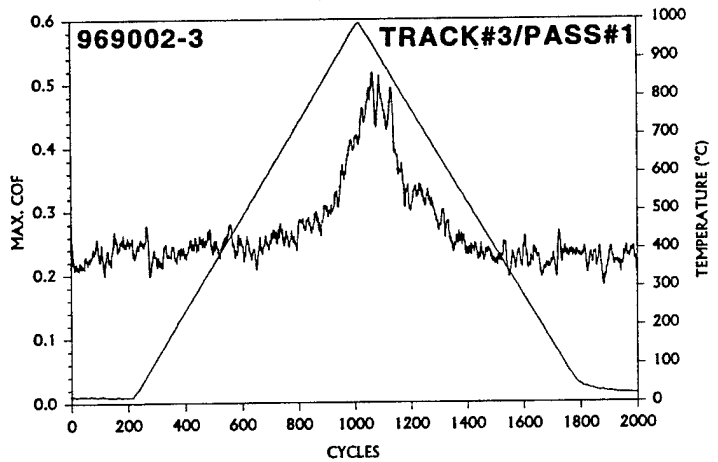
0.1 and 0.3 Torr P_{H_2} (fourth round)



0.1 Torr P_{H_2} (fifth round)



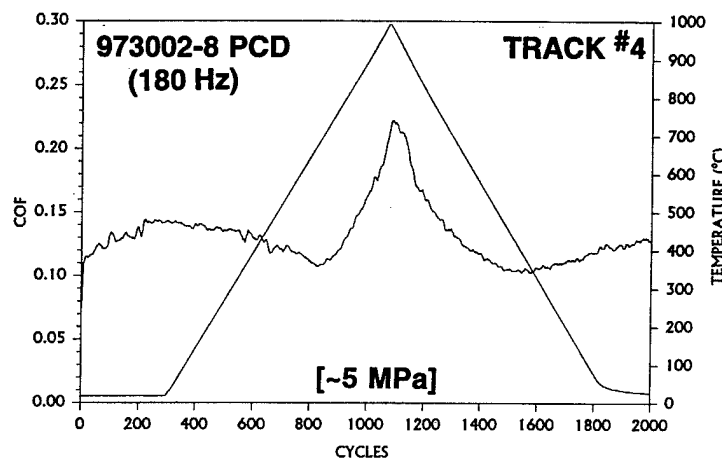
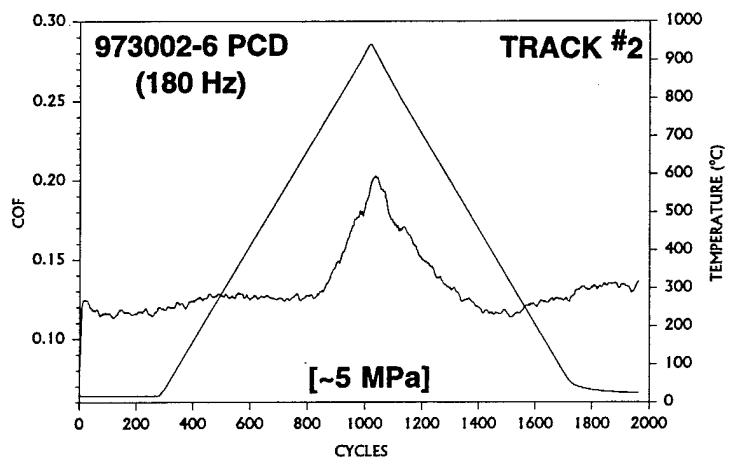
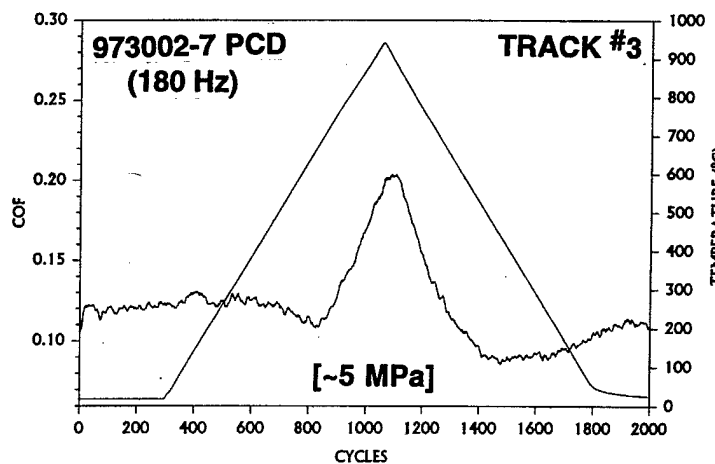
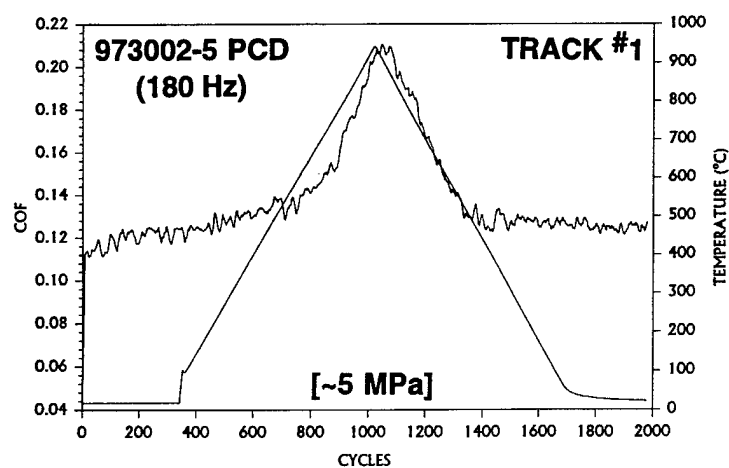
0.18 Torr P_{H_2} (sixth round)



28 g LOAD

Figure 30. Typical peak-type $PCDC_{(100)}$ MAX.COF curves taken from the various 28 g load dry P_{H_2} test rounds described more thoroughly in [2], not showing re(de)constructions troughs previously depicted in Fig. 2. Equivalent COF curves in Fig. 29.

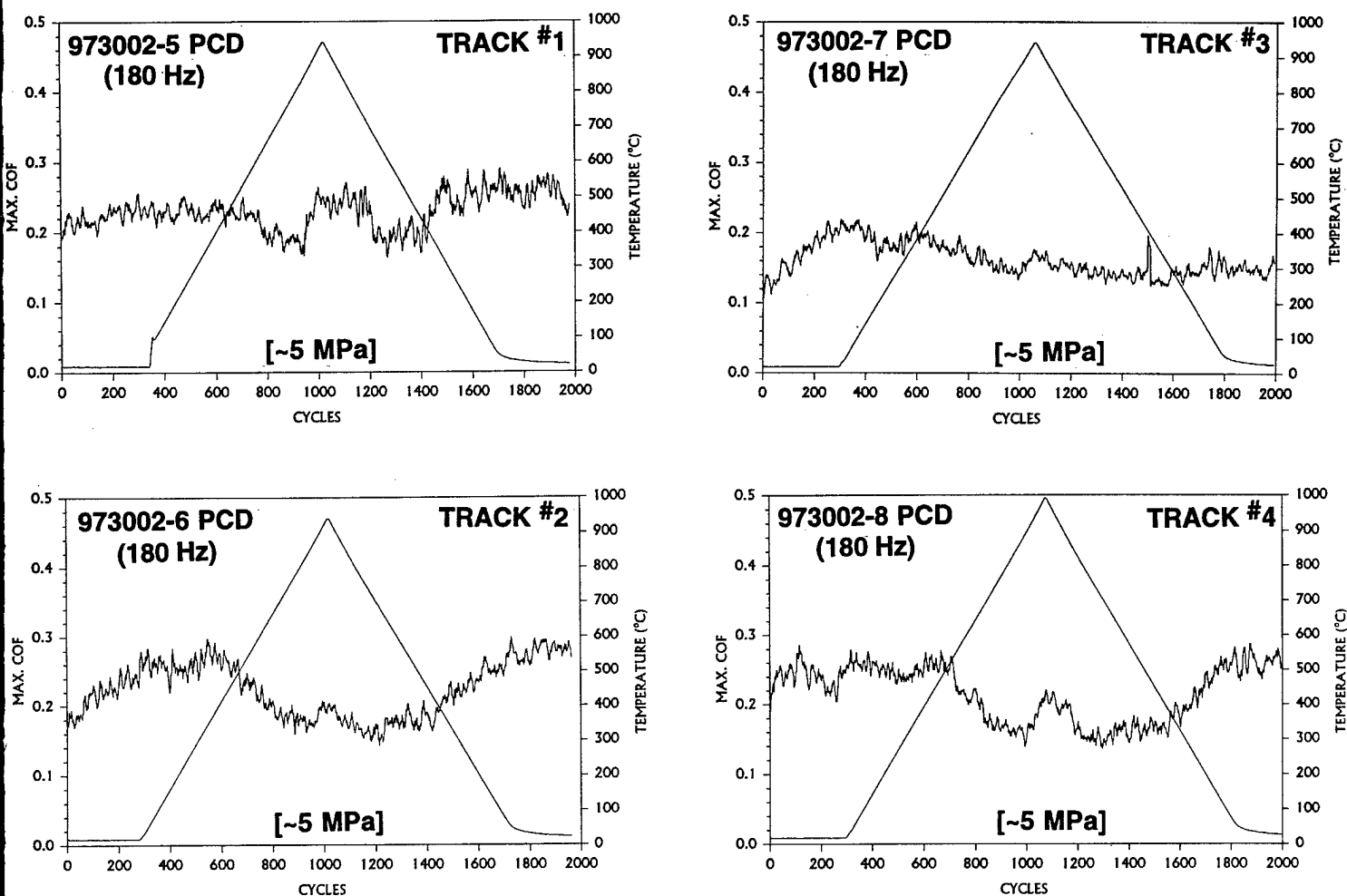
in 0.2 Torr wet H₂ ($P_{H_2O} \cong 0.02$ Torr)



28 g LOAD

Figure 31. All PCD_{C(100)} COF curves taken from the 28 g load wet P_{H₂} experiments.

in 0.2 Torr wet H_2 ($P_{H_2O} \cong 0.02$ Torr)



28 g LOAD

Figure 32. All $PCD_{C(100)}$ MAX.COF curves taken from the 28 g load wet P_{H_2} experiments.

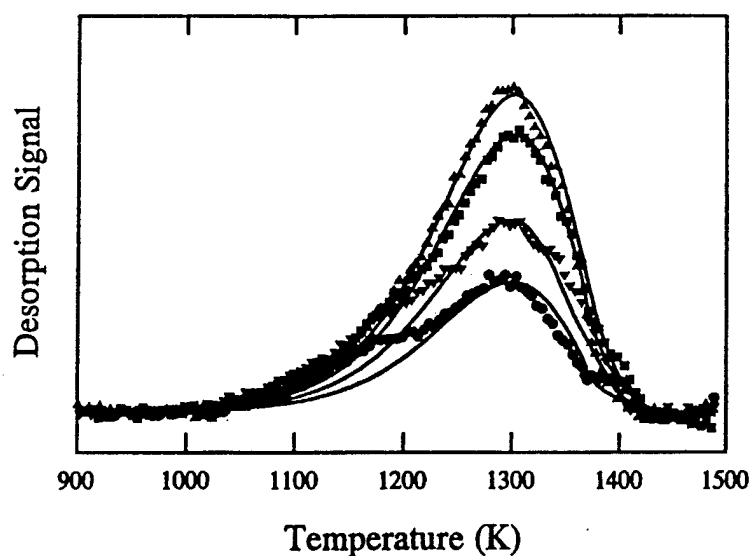


Figure 33. Temperature programmed desorption spectra (symbols) and first order fits (solid lines) off PCD for initial deuterium coverages of 0.27 ML (●), 0.40 ML (▼), 0.52 ML (■), and 0.57 ML (▲). The fit parameters are $E_a = 51$ kcal/mol and $\nu = 5 \times 10^7$ s⁻¹; from [78].

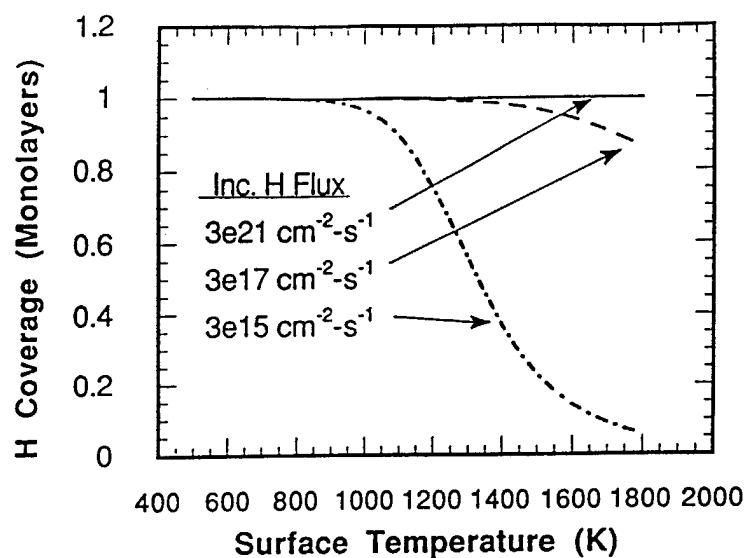


Figure 34. Calculated coverage of atomic hydrogen on C(100) as a function of surface temperature for three values of H atom flux shown; from [79].

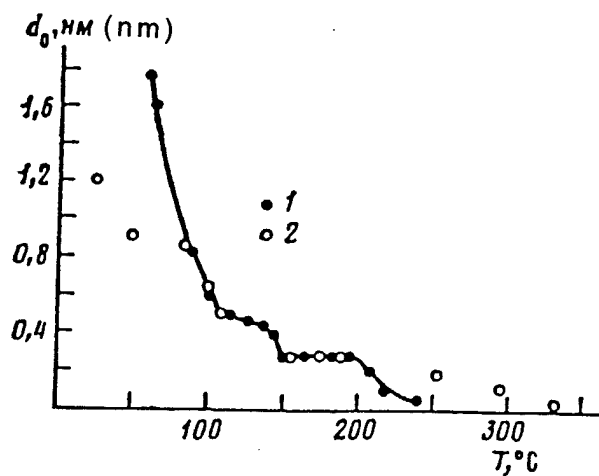


Figure 35. Thickness of titanium oxide (1) and silicon oxide (2) layers produced by surface hydration as a function of temperature; from [82].

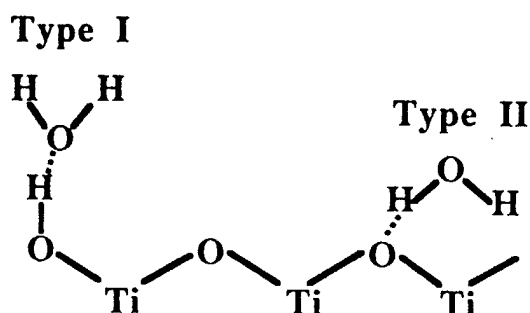


Figure 36. Schematic representation of the types of water adsorbed on TiO_2 : Type I is hydrogen-bonded to surface hydroxyl groups, whereas Type II is hydrogen-bonded to a bridging oxygen atom; from [83].

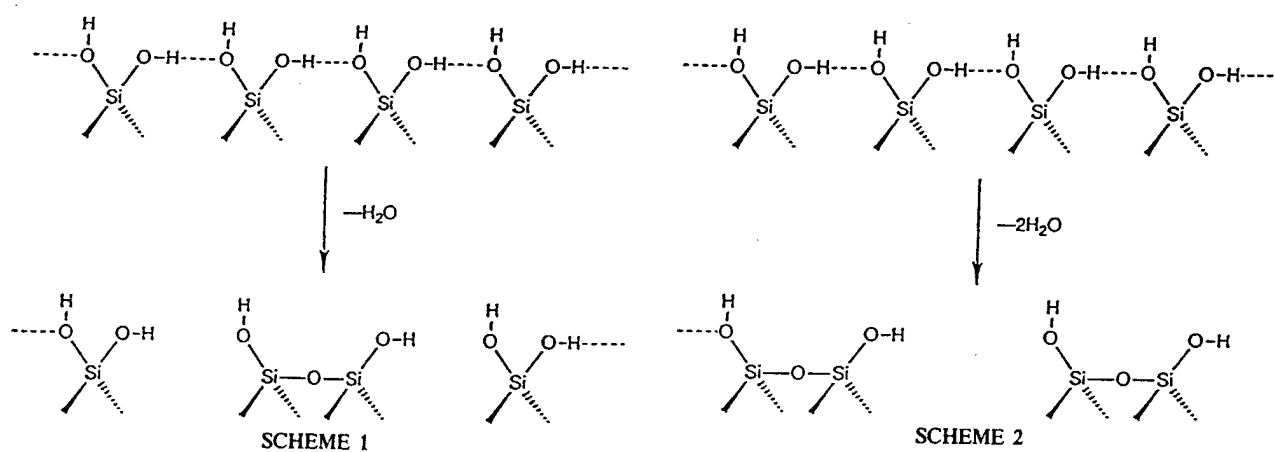


Figure 37. Modeled schemes of surface hydroxylations and partial dehydroxylations; from [84].

APPENDIX: M.N. Gardos, "Advantages and Limitations of Silicon as a Bearing Material for MEMS Applications," invited paper presented at the NSF/AFOSR/ASME Workshop *Tribology Issues and Opportunities in MEMS*, Nov. 9-11, 1997, Columbus, OH; to be published in a book by Kluwer Academic Publishers (in press).

ADVANTAGES AND LIMITATIONS OF SILICON AS A BEARING MATERIAL FOR MEMS APPLICATIONS

M. N. GARDOS

Hughes Aircraft Company, Components & Materials Laboratory
El Segundo, CA 90245

Abstract

The useful life of rotating-sliding Si MEMS moving mechanical assembly (MEMS-MMA) machine elements is short. This is attributed to high wear exacerbated by high coefficients of friction (COF) measured during actual micromachine operation *and* during bench-top tribometry, even under the relatively mild environmental stresses of room-ambient conditions. A summary of recent SEM tribometric experiments is given to show that high friction and wear are caused by a variety of factors related to the low cohesive energy density and surface chemistry of poly-Si, Si(100) and Si(111). Compared to polycrystalline diamond (PCD) films, Si performs poorly as a MEMS bearing material. In particular, the 1.8-times strength of the C-C bond in PCD as opposed to the Si-Si bond in bulk silicon translates into more than 10,000 times lower PCD wear rates under thermal ramping to 850°C, in vacuum. This major difference in behavior has been ascribed to the way Si and diamond interact with the environment. The respective material removal rates are controlled by shear-induced surface cracking superimposed by the adhesive interaction caused by the incipient linkage of dangling bonds between the sliding counter-faces, generated by heating in vacuum above the desorption temperature of adsorbates. The magnitude of the COF is material-specific, generally defined by the number and distribution of dangling (high friction), reconstructed (reduced friction) or adsorbate-passivated (low friction) surface bonds, as a function of temperature and the atmosphere. Even in the benign atmospheric environment of a 0.2 Torr partial pressure of hydrogen gas (P_{H_2}), the COF of the various Si crystallinities at the 15 g (low) SEM tribometer load is as high or higher than in vacuum and significantly higher than those of the PCD under a 28 g load. There is, however, a remarkably repeatable reduction in COF_{Si} within a narrow thermal range at that low load, just below the desorption temperature of hydrogen, indicating the same type of heating- and sliding-catalyzed dissociative chemisorption of H_2 previously observed with PCD. In contrast with PCD, deconstructed (*dangling*) Si bonds do not seem to react with H_2 on cooling, leaving the COF at high values. Only the Si(100) benefited somewhat from P_{H_2} in terms of some wear rate reduction. The other crystallinities exhibited essentially the same wear rates in vacuum and P_{H_2} on thermal ramping to 850°C (near $10^{-12} \text{ m}^3/\text{N}\cdot\text{m}$, 10^4 -times more than PCD), although the rates were reduced during testing at room temperature by one to two orders-of-magnitude. These values could be further diminished by keeping the COF_{Si} the lowest by staying within the 250°C to 450°C temperature range of the tribocatalytic reaction region. The results indicate that operating in the right thermal-atmospheric environment may extend the life of Si MEMS-MMAs sufficiently for a variety of practical applications.

1. Introduction

The production processes used for the fabrication of Si-based integrated circuits have also been employed with increasing finesse to make micron-sized Si mechanical structures combined with electronic circuitry on the same piece of semiconductor. As summarized in [1-5] and reiterated here, the useful life of rotating Si micromachines and other MEMS-sized moving mechanical assemblies (MEMS-MMAs) is not nearly long enough for practical applications. They are considered as demonstration hardware only due to excessive wear of Si exacerbated by high coefficients of friction (COF). These unsuitable parameters were measured during both actual micromachine operation *and* bench-top tribometry, even under the relatively mild environmental stresses of room-ambient conditions.

This paper also contains a brief review and critique of the friction and wear testing techniques most often used to characterize and screen MEMS-MMA bearing materials. Atomic force microscopy, friction force microscopy or molecular tribometry are deemed insufficient to approximate the actual contact conditions of most MEMS-MMAs. To present data more representative of the conditions and degradation found in micromechanisms, the results of recent scanning electron microscope (SEM) tribometric experiments are summarized. It is demonstrated that high friction and wear are caused by a variety of factors related to the low cohesive energy density and surface chemistry of Si crystallinities such as undoped Si(100), Si(111) and polycrystalline silicon (poly-Si). Compared to polycrystalline diamond (PCD) films, all Si crystallinities perform poorly as MEMS bearing materials. In particular, the 1.8-times strength of the C-C bond in PCD as opposed to the Si-Si bond in bulk silicon translates into more than *10,000 times* lower PCD wear rates under thermal ramping to 850°C, in vacuum. The extraordinarily low wear of PCD is surprising in view of its flexural strength being only 20-times, the hardness 10-times and the fracture toughness about 5-times higher than those of Si.

This major difference in behavior has been ascribed to the way Si and PCD interact with the environment. The respective material removal rates are controlled by shear-induced microcracking of the relatively low tensile strength surfaces. The dominant failure mode is the drastically increased adhesive interaction via the incipient linkage of dangling σ bonds between the sliding counterfaces, especially above the desorption temperature of adsorbates in vacuum. The magnitude of the COF is material-specific, generally defined by the number of dangling (high friction), reconstructed (reduced friction) or adsorbate-passivated (low friction) surface bonds as a function of temperature and test atmosphere.

New SEM-tribometric results are also given in this paper, indicating that Si micromachine elements operated in the right thermal-atmospheric environment may result in much longer MEMS-MMA lifetimes, without having to apply self-assembled monolayers as lubricants. A remarkably repeatable reduction in COF and wear of all examined Si crystallinities, in a narrow temperature range just below the thermal desorption temperature in a low partial pressure (0.2 Torr) of hydrogen (P_{H_2}), appears to be advantageous. It is hypothesized that in this limited regime, heating- and rubbing-catalyzed dissociative chemisorption of molecular hydrogen turns H_2 into an atomic-level lubricant.

2. Current State of Si MEMS-MMA Improvements

To date, measures aimed at mitigating the high COF and wear of Si for MEMS applications included (a) implantation with carbon [6], boron [7,8] or phosphorus [8] ions, (b) dry oxidative generation or CVD deposition of SiO_2 [8], and (c) coating Si with thin layers of metals such as Ag, Cu, Sn or Zn [10]. These methods have been offered as partial solutions to the tribological misbehavior of Si MEMS-MMAs, despite the fact that oxidized Si surfaces are hydrophilic. Hydrated surfaces and capillary water cause high "stiction" (break-away friction force) in micromotors [11]. Replacement of Si with bare-metallic bearing surfaces (e.g., LIGA-processed Ni coatings deposited on the microelements) also resulted in extremely high friction and wear [12].

Some promise has been shown by recently fabricated electrostatic micromotors spun up to $>100,000$ rpm, using metals and polymers as bearings. However, lifetimes greater than 6 months could be achieved only when the speeds were reduced to 10,000 rpm [13]. Yet, in many applications, sufficiently high drive torques can only be provided by much higher rotational velocities to compensate for the small rotor mass. By appropriately designing the involute profiles of Si microgears, Sniegowski [14] reported $>2.3 \times 10^9$ revolutions with 66,300 start/stop cycles for gear trains driven at 200,000 rpm, in air. If such high speeds were a design requirement for the performance of a MEMS motor and gear train assembly, the time of continuous operation before failure would be only 8 days. This still-impressive achievement represented the best results among several attempts, with other gear trains failing after much shorter periods of time. No adequate explanation was given for the lack of repeatability.

At first glance, a simple solution is to hydrogenate all the Si surface bonds before use [15]. This technique might be useful for static release applications in the absence of prolonged contact with water vapor, but it cannot provide repassivation of the wear-generated dangling bonds throughout the tribological process. Another way of lengthening the life of Si MEMS-MMAs appears to be the application of hydrophobic, self-assembled (low surface energy) monolayers on the bearing surfaces [11,16-19]. Again, for static release applications this may be fine, but in the sliding or rolling mode the tribooxidative stability of these thin (mostly hydrocarbon-based) lubricating films, especially with their degradation catalyzed by active surface sites at elevated flash (and environmental) temperatures, is in question. Also, as enumerated in [19], some of these layers are incompatible with certain MEMS materials of construction. The presence of SiO_2 is tribologically undesirable, because "stiction" is caused by hydrogen bonded or capillary water trapped within the bearing interfaces. The formation of surface silica is exacerbated by enhanced tribooxidation of Si when water vapor is there.

The presence of SiO_2 is ubiquitous. It is either an integral part of the MEMS fabrication process or an unavoidable byproduct generated during handling, storage or operation of Si-based MEMS-MMAs, even if only in room temperature air and humidity. The rubbing-enhanced reaction of Si with water vapor to generate $\equiv\text{Si-OH}$ groups at the interface changes both the chemistry and the morphology of the surfaces. It is the precursor of oxide-hydroxide wear debris formation. In spite of the "lubricating" effects of high partial pressures of water previously shown to provide low friction via the mechanism of $\text{Si} \rightarrow \text{SiOH} \rightarrow \text{SiO}_2 \rightarrow$ hydrated SiO_2 during bench-top tribometry at RT [20], the MEMS literature is awash with reports of the harmful effects of ordered molecular layers of hydrogen-bonded H_2O or worse, capillary (bulk) water and grease-like hydrated silica trapped within the exceedingly small clearances of Si MEMS-MMAs.

Friction-induced energy dissipation on the atomic-molecular-scale and the lubrication of solids with low shear strength surfactant monolayers in benign environments are reasonably well understood [21,22]. Nevertheless, the application of this knowledge towards reducing the high stiction/friction of Si-based MEMS-MMA devices is scarce, even for applications at RT. Instead, more attention has been paid to mitigating the problem by reducing the real area of contact (A_r) through a controlled increase of surface microroughness [23-30]. This methodology is presently used with computer hard discs. Microscopic texture marks are purposely stamped on the disc to reduce A_r between it and the head, and thus mitigate stiction during head lift-off and touchdown, i.e., start-up and shut-down of the computer [23]. Nanoscale scribing of Si microbearing surfaces to reduce A_r with some control (similar to efforts with computer discs) has also been attempted [28]. In both macroscopic [27] and microscopic [4] tribosystems, surface pores and asperity valleys act as debris traps. The depressions keep abrasive debris away from the load-carrying A_r .

Even though surface roughness is an important parameter, the stiction/friction-increasing or reducing effects of any interfacial layer (unavoidably generated by tribochemical reactions with atmospheric adsorbates or purposely preapplied as a lubricant) cannot be considered separately from the roughness [30,31]. The main reason is embodied in the simple and well-known equation $F_k = \tau_s \cdot A_r$, where F_k = friction force, and τ_s = shear strength of the surface layer (A_r as previously defined). Both τ_s and A_r must be controlled simultaneously. Electrostatic effects, which also have to be taken into account as a contributing factor to the residual adhesion and/or repulsion of MEMS surfaces in contact, are closely related to asperity height and shape as well as charge bleed-off [29,31]. The interaction of all these parameters is complex. Even the most thoroughly constructed predictive models can deal with well-defined, statically contacting surfaces only [31]. The initial conditions change radically with progressive wear, rendering the practicality of such models for operating MEMS-MMAs questionable.

These problems stand unresolved. To make matters worse, current research on advanced MEMS still use Si almost exclusively for MMA construction [13,14,32]. The troubling status of MEMS bearing materials is well-represented by the tacit admission in [32]: "...Silicon was selected as the bearing material for its micromachinability, although it is not necessarily the ultimate material of choice for micromachine bearing components." The problem of rapid wear-out and high friction remains pervasive, because the vast majority of these MEMS-MMA devices are still based on Si due to the technological know-how accumulated on manipulating, machining and manufacturing this widely used microelectronics material. The fact is that very few of the practical MEMS incorporate sliding or rolling parts under load, because their wear lives are not long enough. Yet, in many cases, dynamic (tribological) assemblies such as a single micromotor can do the same job better than a large array of static devices [14, 33-38].

3. Tribometric Characterization of MEMS-MMA Bearing Materials

At the present time, atomic force microscopy/friction force microscopy (AFM/FFM) [39] and molecular tribometry (MT) [40-43] are most often used or recommended for approximating MEMS-MMA conditions by bench-testing in the lab. Even a cursory review of the systems aspects of this approach indicates that AFM/FFM and/or MT may be necessary but are not sufficient for the task. The surface behavior of those MEMS micro-

elements which move (but just bend or twist) or even if they touch a counterface (e.g., in sensors, membrane pumps or microtweezers) is vastly different from those that slide-roll under surprisingly high Hertzian stresses (e.g., in micromotors and actuators). Tribometers must be able to reveal the adhesive and friction forces as well as the realistic surface damage (wear) resulting from these particular contact conditions. The essential differences lie in the presence or absence of shear under load and the associated roughening of the worn bearing surfaces and the formation of wear debris, all in the presence of chemical bonds ranging from the weak van der Waals to strong covalent bonding affected by the environment. The combined macroscopic effects of hydration, capillary and electrostatic forces are superimposed on the compaction, plowing and rejection of wear debris from the contacts and the attendant loss of tolerances by wear.

In nearly all MEMS-MMAs the interaction is within area contacts, under a variety of normal loads. As an example, the 16% wear-induced increase in just 5 minutes of the originally 28 μm inside (bearing hole) diameter of an air-driven, Si microturbine wheel driving nothing but itself at 150,000 rpm [44] is not approximated by the action of a sharp AFM/FFM Si, diamond or any other tip brought close to a highly flat Si surface. On the other hand, the hydrogen-bonding-induced hydration forces causing MEMS stiction failures such as Si microtweezers not being able to completely release sapphire microbeads [29] or other similar adhesion problems related to handling of microparts [45] can be quantified by AFM/FFM [46]. Significant differences have been shown between thin hydrocarbon or fluorocarbon lubricant layers serving as stiction-reducing surface films [47]. A properly instrumented AFM/FFM tip can help determine (a) the shear strength of an MoO_3 island displaced laterally on a basal plane of MoS_2 or those of (b) a Nb_2O_3 island similarly sheared off its own disulfide basal plane [48,49], or (c) a C_{60} buckyball island sheared on the basal plane of graphite [47,50].

As to present-day MT apparatus, their crossed-cylinder contacts invariably consist of mica. Although the Hertzian contact area and the related unit stress are controlled better than those of an AFM tip occasionally penetrating (scratching) the counterface on purpose, mica is not a MEMS-MMA bearing material. Molecular tribometry is of little use, unless the surface energy-related friction of ultra-thin fluid lubricant layers deposited on mica are the data of interest [43].

Therefore, at interfaces where the degree of adhesion ("stiction" or repulsion) of essentially statically contacting surfaces is the critical value for MEMS operation, AFM/FFM is useful. Even MT might be applicable, provided the specimen materials were changed from mica to more realistic candidates (e.g., Si). It is essential to recognize that the performance of macroscopic sliding-rolling interfaces is controlled by adhesion, friction and wear in a load range where Amonton's Law is followed. In nanotribometry, the friction force is *not* linearly proportional to the normal load, however [51]. Approximating MEMS-MMA bearing surface behavior at a bench top level needs more suitable test machines.

The scanning electron microscope (SEM) tribometer schematically described in Fig. 1a was specially designed and constructed to fill the gap between an AFM/FFM or MT and a benchtop-type, conventional friction and wear tester. Its primary purpose has been to help reveal tribological effects of bearing material surface chemistry influenced by elevated temperatures and various gas atmospheres, under realistic engineering Hertzian stresses. Transcending the microscopic region into the macroscopic regime, a small (7 mm x 5 mm x 2 mm) flat is oscillated against a hemispherically tipped and dead-weight-loaded pin (2 mm dia.), either in the vacuum of the SEM column ($\sim 1 \times 10^{-5}$ Torr; over 90% water vapor in the residual gas atmosphere at room temperature) or in a lidded, Knud-

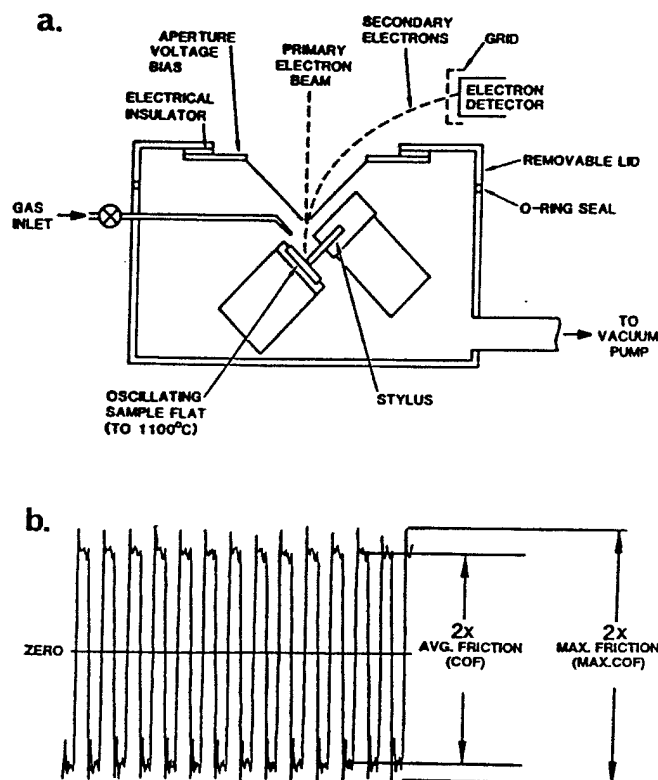


Figure 1. The SEM tribometer: (a) tester schematic, and (b) an idealized friction trace depicting twice the COF and MAX.COF about the zero friction baseline during oscillatory sliding. MAX.COF values are not reported in this paper.

sen cell-like subchamber backfilled and purged with low partial pressures of selected gases such as H_2 , He, N_2 and O_2 . Depending on the modulus, Poisson's ratio and wear rate of the specimen materials, the Hertzian contact stresses range from GPa to MPa (from many thousands to hundreds of psi) values. The flat may be held at RT or heated to as high as $\sim 1100^\circ C$ during tribometry. The normal load-force and the average friction force are logged and converted to the average coefficient of kinetic friction (designated as COF in the present paper, see Fig. 1b) by a tabletop computer using commercial data logging and analysis software. This apparatus has been employed to test SiC and intercalated graphites [51], substoichiometric rutile-based lubricious oxides [51-56], MoS_2 [57,58], carbon-graphite seal materials [59,60], as well as Si and PCD for MEMS-MMA bearing material applications [1-5].

4. SEM Tribometry of Si in Vacuum and Hydrogen

SEM tribometric data are presented here on poly-Si, Si(100) and Si(111) (a) heated to 850°C, then cooled to room temperature (RT) at a relatively rapid (40°C/min) thermal ramping rate in $\sim 1.33 \times 10^{-3}$ Pa = 1×10^{-5} Torr vacuum (over 90% residual H₂O), followed by similar experimentation in 26 Pa (0.2 Torr) partial pressures of 99.999%-pure H₂ (PH₂), (b) slowly thermal-ramped to adsorbate (hydrogen) desorption temperatures in PH₂, and (c) kept at RT during sliding in PH₂. Mainly, we wanted to examine the possibility of using molecular hydrogen as an atomic level lubricant, chemisorbed on the dangling bonds generated on rubbed Si surfaces.

The most promising analogous experiments to date have shown that H₂ became dissociatively chemisorbed on PCD in certain temperature ranges, providing the lowest COF measured with PCD sliding against itself [4]. The wear rates in vacuum and in PH₂ were in the low 10^{-16} m³/N·m regime, about 10⁴-times less than those of the various Si crystallinities examined in vacuum. According to the basic hypothesis governing the fundamental tribological behavior of diamond and Si described in [1-4], the degree of wear is controlled by high COF-induced surface (tensile) cracking directly resulting from the extent of the adhesive interaction caused by the incipient linkage of dangling bonds between the sliding counterfaces.

The magnitude of adhesive COF of PCD and Si are essentially defined by the number of dangling (high friction), reconstructed (reduced friction) or adsorbate-passivated (low friction) surface bonds. Incipient linking of the sliding counterfaces by unsaturated bonds on heating to sufficiently high temperatures, and their passivation by benign adsorbates on cooling, have been suggested as the main causes of radically increased and reduced adhesion and friction, respectively. Strong circumstantial evidence has also been repeatedly given for a trough-like "bathtub" curve dip in the COF at the highest temperatures, attributed to surface re(de)construction. Continued heating of the progressively degased and worn PCD and Si surfaces in vacuum appears to dimerize the dangling bonds to lower the surface energy, unhindered by the ongoing tribological action. However, once the heating stops and the rubbed surfaces cool below a certain temperature, the loss of activation energy needed to keep the bonds reconstructed causes a significant rise from the deepest part of the COF trough due to deconstruction. This rise culminates in another COF peak, where the surface adsorbates rapidly passivate the reappearing dangling bonds to lower the COF once more on further cooling to RT. The best examples of such ideal stepfunction-with-trough COF signatures to date have been generated during SEM tribometry of the mechanically polished and hot chromic acid-cleaned, C(100)-textured PCD films [4]. These layers were sliding against each other under thermally ramped conditions, both in $\sim 1 \times 10^{-5}$ Torr vacuum and in low PH₂ (Fig. 2). The offset of the peaks between COF trough (the first forms at a higher temperature than the second) was attributed to the known thermal-atmospheric stability of the reconstructed surfaces.

During SEM tribometry to $\sim 800^\circ\text{C}$ and cryogenic wear testing of well-characterized amorphous and turbostratic carbons sliding against α -SiC in vacuum, PH₂ and PHe also showed that a 0.2 Torr PH₂ environment was particularly able to reduce the room temperature COF and wide temperature range wear rate of these materials [59-61]. This reduction was attributed to their low sp²/sp³ ratio and the passivation of a significant number of dangling carbon σ (and π) bonds on the wear-torn surfaces.

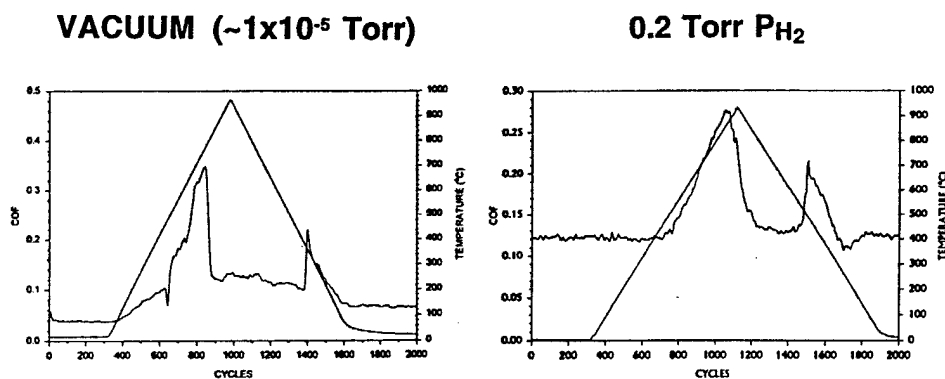


Figure 2. Typical stepfunction-with-re(de)construction trough COF_{PCD} signatures generated by SEM tribometry in vacuum and partial pressure of hydrogen; from [4].

If the dangling (but less energetic) Si σ bonds generated on the sliding counterfaces were also able to break the stable H-H bonds to create the reactive hydride intermediates and hydrogen radicals needed for surface passivation, both the high COF and the frictional tensile stress-induced cracking (i.e., incipient wear) could be mitigated. This way, artificial generation of the reactive hydrogen species in the vicinity of MEMS-MMAs e.g., with hot filaments or UV lamps (convoluted and potential harmful techniques not readily tailorable to the task at hand [62]) would be avoided. MEMS-MMAs fabricated from Si might then be transplanted from the narrow realm of demonstration mechanisms into the ranks of practical hardware.

As a secondary benefit, operating rapidly spinning MEMS components in low PH₂ could reduce the extent of wind resistance they normally suffer in atmospheric air or high P_{gas}. Instrument (ball) bearing-operated gyroscopes are routinely rotated in low P_{He} to mitigate such parasitic viscous losses [63]. Inasmuch as the diffusivity of molecular hydrogen through poly- and single-crystal Si is low [64-67], hermetic enclosure of ultrahigh speed microrotors in low PH₂ is feasible.

4.1. TEST METHODOLOGY

During the low-load (15 g = 0.15 N) Si vacuum experiments more thoroughly described in [1,2], each test was started at RT, followed by heating to 850°C at a 40°C/min ramping rate. From there, the flat was cooled at the same rate to near RT. Each test lasted for 2000 cycles in vacuum (~1 x 10⁻⁵ Torr of the SEM column). A pin was tested four times: twice against one flat on progressively fresh test paths starting at a 15 g (the lowest reliable) normal load, in two pumpdown and backfill cycles. After the first test, the flat was moved sideways with a second, built-in x-y stage housing the heater to expose a fresh wear path for the second test. The first two tests yielded usable wear rate (\mathcal{W}) data, but only unreliable COF signatures due to the high initial wear of the pin. These experiments were followed by (a) disassembly, photomicrography and HF+H₂O etch/rinse cleaning of the used pin and a new flat (also to simultaneously achieve complete hydrogenation of the surface bonds), and (b) two additional tests with the used pin against fresh

wear tracks in separate pumpdown cycles. Repeated testing with the same pin but several successive wear paths on two flats were found necessary to enlarge the wear scar and to mitigate the effects of excessive wear debris formation and plowing of the compacted debris into furrows. These approaches were needed to provide the largest and most debris-free apparent and real areas of contact (A_{app} and A_r) for clearer COF signatures that are footprints of the varying magnitudes of adhesion at the atomic level.

During the following three rounds of PH_2 tests, we tried several techniques to eliminate the need for the two starting experiments with each Si specimen pair. These initial tests were only used to enlarge the wear scars. During the fourth round, slow thermal ramping was performed to the temperature signalling the mass desorption of hydrogen to confirm a remarkably repeatable reduction in COF found during the first three rounds. The lowest COFs_i ever measured appeared in a narrow thermal range immediately preceding this temperature of sudden COF increase. The W within this beneficial region was also measured and compared to the W obtained during (a) conventional high temperature (850°C) thermal ramping in vacuum and in PH_2 , and (b) the RT "grinds" in PH_2 . Since it is unlikely that silicon would serve in MEMS anywhere near 850°C in any atmosphere, the SEM-tribometric W values determined at RT are deemed more representative of the W found with conventional Si MEMS-MMAs.

4.1.1. First Round (Room Temperature "Grind" and Standard Thermal Ramp in PH_2)

Here, scars equivalent to some minimum size were prepolished on the tip in an attempt to shorten the overall procedure. The prepolished pin and its mating flat were (HF+H₂O)-rinsed to hydrogenate the surface bonds before testing. Next, the plane-parallelism of each artificial "scar" mated to its flat still had to be assured by a 1000-cycle "grind" under the 15 g = 0.15 N load, before the first real test was performed under the same load in an unbroken PH_2 atmosphere. As explained before, two marginally useful "grinding" tests had to be performed first during the previous vacuum tests before any valid COF results could be generated.

The seating "grind" in PH_2 was done only after several pumpdown and backfill cycles with 99.999%-pure H₂ issued from a lecture bottle, following the procedure delineated in [4]. The lidded tribometer subchamber, with its own separate mechanical vacuum pump continually removing the admitted H₂, was repeatedly purged at gas pressures low enough so that the turbomolecular pump of the SEM column could handle the spill-over H₂ load emanating through the pinhole of the subchamber lid. The thorough H₂ purge cycles removed as much residual air and moisture as possible mainly by momentum transfer, without having to bake the subchamber. After "grinding", the flat was moved sideways with a second motorized stage to expose a new wear path for the first 15 g test, without disturbing the PH_2 atmosphere. As in [4], SEM imaging was not done in PH_2 to preclude any H-H bond-breaking or desorption assist by the e-beam.

It was found after Round 1 with all three Si crystallinities that the slight shift of each wear scar on the flat that suddenly developed due to the equally slight (but nevertheless detrimental) wobbling of the oscillating sample stage. No sharp scar boundaries were on the flat. Since both the "grind" and the following test were done in an unbroken PH_2 atmosphere with no disassembly and photography in-between, well-defined boundaries were essential for accurate estimation of W . As an additional problem, the 1000-

cycle "grind" did not render the artificial scar sufficiently plane-parallel with the flat, despite of the otherwise good alignment of the pin secured in its well-fitting holder. For these reasons, the Round 1 tests generated valid COF results, but \mathcal{W} could not be calculated with confidence.

4.1.2. Second Round (Room Temperature "Grind" and Standard Thermal Ramp in PH_2)

The observations during Round 2 and photography of the worn specimens indicated again that prepolishing the starting pin tip scars did not work as well as originally anticipated. Furthermore, relubricating the main stage jackscrew could not completely eliminate the stage wobble problem. Therefore, the estimation of reliable \mathcal{W} data was again prevented, although some good COF curves (not reported here), similar to those in Round 1, were generated.

4.1.3. Third Round (Room Temperature "Grind" and Standard Thermal Ramp in PH_2)

"Grinding" at RT, but only for 2000 cycles (2000 cycles less than in vacuum) was tried again in the hope that less (and less harmful) debris would be caught between the counter-faces in PH_2 than in vacuum. This procedure did provide a starting pin tip scar large and debris-free enough (although not as large as those worn in vacuum or the prepolished scars during the first two rounds in PH_2) to yield meaningful COF data for the immediately following thermal-ramp test. We also developed an accurate scar width measurement procedure after the "grind" to allow the estimation, for the first time, of \mathcal{W} in RT PH_2 . Knowing the "ground" scar size on the pin tip further permitted the calculation of \mathcal{W} during the thermal ramp test that followed. It was discovered that the pin could be removed and reassembled from/into the friction force transfer arm for photography after "grind" without losing conformity between the pin scar and the flat. The close tolerances of the pin holder's tightly-fitting dovetail that slides securely into the end of the arm may have been responsible for this serendipitous find. However, disassembly had to be followed by another pump-and-purge cycle, introducing an added time penalty to the new procedure.

The wear scar measurement problem was resolved by this revised procedure. However, the slight but persistent stage wobble and the resulting smearing of the wear scars on the flat to a width greater than the width of the pin tip scar were still not eliminated. Additional testing revealed that the wobble of the oscillating stage was not caused by reduced lubrication or increasing wear of its jackscrew. It was the activation of the second stage, used to move the flat sideways between tests without breaking atmosphere, that imparted the skewed motion of the flat during the next experiment. An inexplicably developed backlash of the drive gears and/or the jackscrew of the secondary stage seemed to have affected the behavior of the primary stage. Even though this problem no longer prevented the measurement of the pin tip \mathcal{W} due to the newly devised tip removal and photographic technique after "grinding", the wobble was nevertheless circumvented by manually moving the flat sideways to expose a fresh track for the next test on the same flat. The second motorized stage originally designed for the job was simply not activated. Inasmuch as the pin had to be removed for post-"grind" photography anyway, repositioning the flat in its holder and tightening it down against the heater strip simply became part of the overall test procedure. As a result, the pin scar width could be reconciled with the scar widths on the flat, and Round 3 yielded the best Si friction and wear results gene-

rated in PH_2 to date. It also gave the first set of reliable RT \mathcal{W} values measured during the initial "grind" cycles, in PH_2 .

4.1.4. Fourth Round (Room Temperature "Grind" and Slow Thermal Ramp in PH_2)

Using ad-hoc thermal ramping procedures tailored to the general friction behavior of each Si crystallinity, the temperature of the flats was slowly raised to the point of drastic COF increase. We aimed to duplicate the unusual COF reduction in this apparently beneficial thermal-atmospheric regime, and show a possible parallel reduction in \mathcal{W} . The RT "grind" cycles preceding the slow-ramp procedures were also meant to yield additional RT \mathcal{W} values, complementing those measured during the Round 3 "grinds".

5. Test Results

5.1. FRICTION DATA

The COF of the Si crystallinities measured in vacuum and those obtained during the Round 1 PH_2 tests are compared in Fig. 3. The Round 1 and 3 PH_2 experiments are juxtapositioned in Fig. 4 to show the extent of COF repeatability in light of the differences in scar size: those in Round 1 were somewhat larger than during Round 3. Although the stepfunction-with-re(de)construction trough COF signatures previously also observed with PCD in vacuum and PH_2 (Fig. 2) manifest themselves with Si as well, there are some important modifications to the curve shapes:

- a. There is a remarkable and repeatable reduction in the COF_{Si} in PH_2 at the estimated surface temperatures of 250°C to 450°C. The relatively high starting RT COF (as high as 0.45) is reduced there to near 0.1, as low as 0.02. This low friction region occurs just below the temperature of drastic COF increase attributed mainly to the removal of surface hydrogen by thermal desorption. The same type of COF reduction below the thermal desorption temperature of hydrides was observed with PCD in PH_2 , but not in vacuum [4]. Apart from this beneficial region, the COF_{Si} at all other temperatures are generally higher in PH_2 than in vacuum.
- b. There was some reduction in COF_{Si} on cooling in vacuum, but the final values are not as low as those at the onset at RT. This was attributed to the considerable increase in both A_{app} and A_{r} due to the high \mathcal{W} of Si producing larger wear scars (see the low average Hertzian stresses associated with each test, given in brackets within the respective COF curves). In contrast, the final COF values in PH_2 came down only in the case of poly-Si (Round 1). For all other tests, the final RT COF in PH_2 was significantly higher than in vacuum, in spite of the smaller scars (i.e., smaller A_{app} or A_{r}) producing larger Hertzian stresses.
- c. The true surface temperature of the flat is heavily influenced by the thermal conductivity of the test atmosphere [60]. Considering the ~200°C ΔT between the heater thermocouple and the estimated surface temperature of the flat in vacuum, but only a ~100°C ΔT in 0.2 Torr H_2 [4,60], the presence of PH_2 increases the approximate

hydrogen desorption temperatures of Si from about 300° to 400°C in vacuum to 400° to 500°C in PH_2 . This phenomenon was observed with PCD as well [4].

- d. The thermal range of the re(de)construction-attributed troughs observed in vacuum shifted to higher values during the Round 1 Si(111) PH_2 test only. However, the troughs invariably shifted in the same direction during *all* tests of Round 3. The final COF remained characteristically high in PH_2 , with no reduction on cooling.

The COF charts of the Round 4 slow-ramp experiments are presented in Fig. 5. The data reconfirm the unusual thermal-atmospheric region where COF is significantly reduced, especially in the case of poly-Si. This crystallinity also yielded the lowest COF in the beneficial region during both Rounds 1 and 3. The adsorbate desorption temperatures rank qualitatively with the strengths of the respective surface hydrides-to-Si bonds: $\text{SiH}_2\text{-on-Si}(100) < \text{SiH-on-Si}(111)$, with the poly-Si desorption temperature in-between.

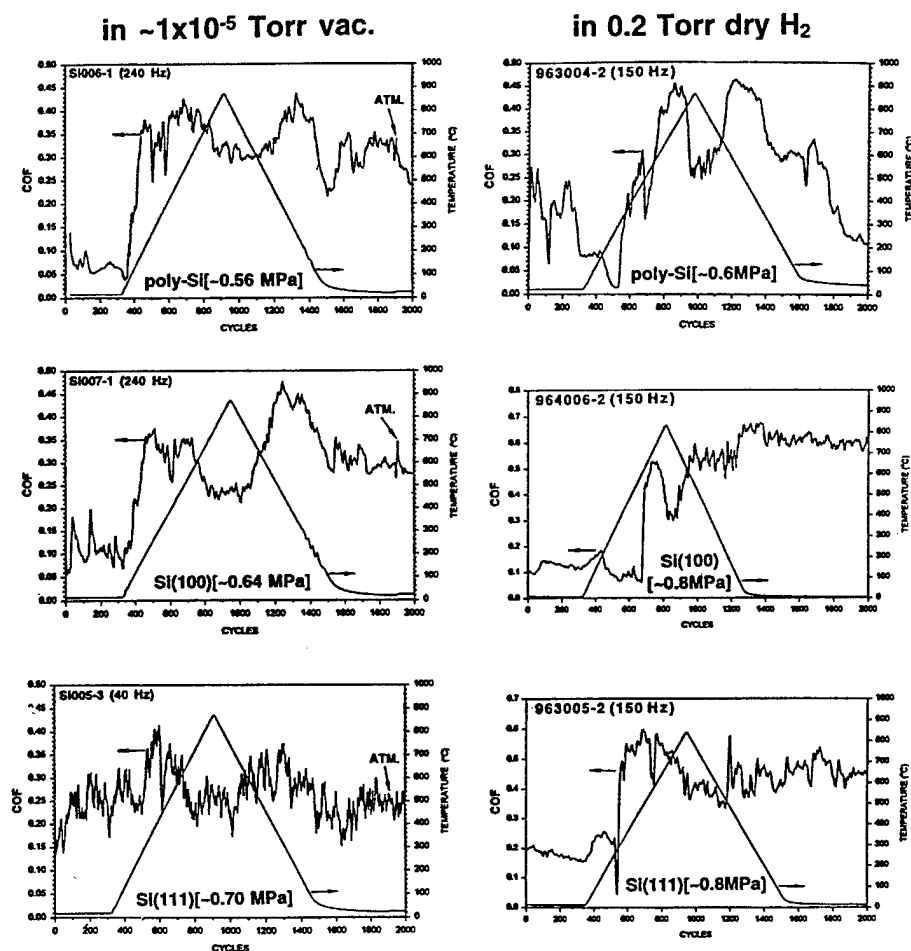


Figure 3. COF of the various Si crystallinities in vacuum and PH_2 (Round 1) under standard thermal ramping (Hertzian stresses calculated by wear scar diameters).

in 0.2 Torr dry H_2

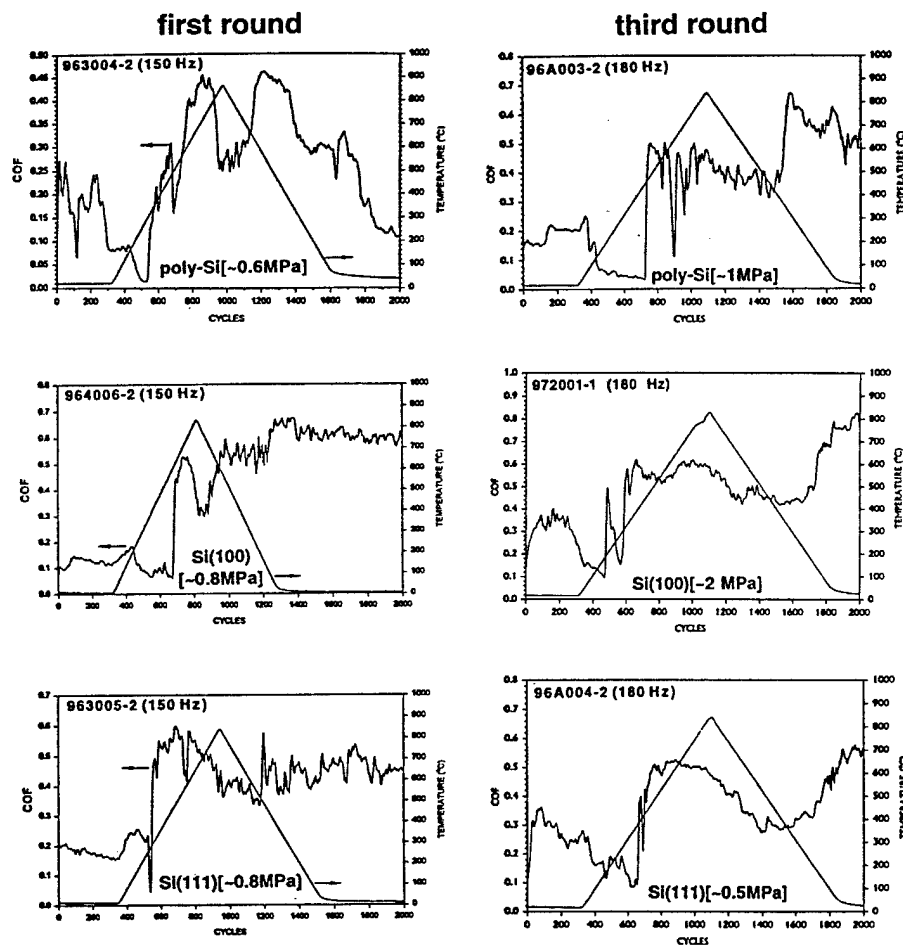


Figure 4. Comparison of COFs_i During Round 1 and 2 in PH_2 under standard thermal ramping (Hertzian stresses calculated by wear scar diameters).

The low desorption temperature of the Si(100) in Fig. 5 is the same as that indicated by the first desorption peak of the Si(100) doublet in Fig. 4, but does not agree with the Si(100) singlet temperature in Fig. 3.

Since these experiments were not duplicated, the origin and cause of the particular COF variations in Fig. 5, such as the unusually repeatable oscillations with Si(111) or the appearance of multiple desorption peaks are not speculated upon at this time.

0.2 Torr P_{H2}

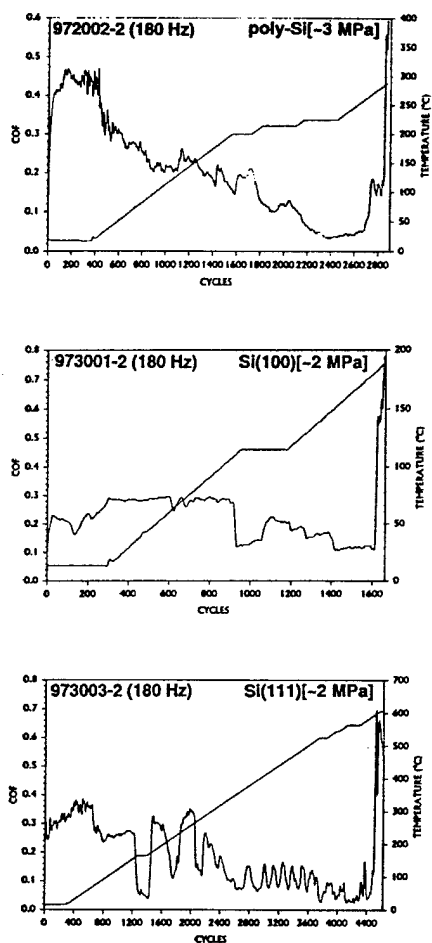


Figure 5. COF of the various Si crystalinities in P_{H2} under *slow* thermal ramping (Hertzian stresses calculated by wear scar diameters).

5.2. WEAR RATE (\mathcal{W}) DATA

The \mathcal{W} of the sliding combinations thermally ramped to/from 850°C in vacuum and in P_{H2} (designated as TR), "ground" at room temperature in P_{H2} (RT) and tribocatalytically slow-ramped (TCSR) to hydrogen desorption temperatures are presented in Table 1. The results indicate that during the TR tests, only the Si(100) benefited from the atmosphere of rarified hydrogen. The other two crystallinities exhibited essentially the same \mathcal{W} both in vacuum and P_{H2}. In P_{H2}, sliding at RT does reduce \mathcal{W} from the TR level of $\sim 10^{-12}$ m³/N·m by one to two orders-of-magnitude. *Operating in the P_{H2} TCSR regime yields the lowest friction and wear in each case.* The poor repeatability of the duplicated RT Si(100) \mathcal{W} cannot be explained until (a) more tests are run, and (b) the SEM photomicrographs depicting the appearance of the scars on the pins and flats are examined.

Even in the absence of these data, it is known that the precision and accuracy of the \mathcal{W} associated with the RT and TCSR experiments is low due to the small size of the pin scar and the error involved in measuring the small scar diameter from SEM photos.

Table 1. The wear rate (\mathcal{W}) of the various silicon crystallinities in vacuum and PH_2 under thermally ramped to/from 850°C (TR), room temperature (RT) "grinding" and tribocatalytically slow-ramped (TCSR) conditions.

Pin/Flat	Atm./Test Type	Stress (MPa)		Pin Wear Rate* ($\text{m}^3/\text{N}\cdot\text{m}$)	No. of cycles
		Start	End		
Si(100)	Vac./TR	0.8	0.5	2.82×10^{-12}	2000
	dry PH_2 /TR	3.3	0.8	6.2×10^{-13}	2000
	dry PH_2 /RT	430	3.3	3×10^{-14}	2000
		430	108	$(3 \times 10^{-17})^*$	2000
	dry PH_2 /TCSR	108	57	$(9 \times 10^{-17})^*$	1625
Si(111)	Vac./TR	1.0	0.8	9.7×10^{-13}	2000
	dry PH_2 /TR	2.5	0.9	1.45×10^{-12}	2000
	dry PH_2 /RT	430	2.5	2.9×10^{-13}	2000
		430	2.8	8×10^{-14}	2000
	dry PH_2 /TCSR	2.8	2.0	$(2 \times 10^{-15})^*$	4600
poly-Si	Vac./TR	0.8	0.6	1.62×10^{-12}	2000
	dry PH_2 /TR	132	1.1	1.27×10^{-12}	2000
	dry PH_2 /RT	430	132	1×10^{-14}	2000
		430	3.5	3×10^{-14}	2000
	dry PH_2 /TCSR	3.5	2.9	$(9 \times 10^{-15})^*$	2850

* values in parentheses are reported to a larger number of significant figures due to the extremely small wear rates; precision/accuracy are poorer.

6. Discussion

6.1. DISSOCIATIVE CHEMISORPTION OF MOLECULAR HYDROGEN ON Si

The general thermodynamic concepts of hydrogen de(re)sorption off/on Si appear simple (Fig. 6), but they are not. The activation energy of the respective sorption paths vary widely and the hypothesized reactive hydride intermediates interacting with the Si surface during either direction have not been clearly elucidated [2,69]. The desorption kinetics themselves vary from one cleavage plane to another: first-order kinetics were observed for Si(100), but second order for Si(111) [69].

Notwithstanding the variation in activation energies and the differences in the kinetic paths that involve hydride intermediates, it is easier to desorb the surface hydrides during heating where sufficient thermal energy is available than to re(chemi)sorb molecular hydrogen during cooling. It is empirically known that H_2 molecules have very low sticking probability on clean Si(100)-2x1. Theoretical calculations [68] yielded a ~ 46 kcal/mol

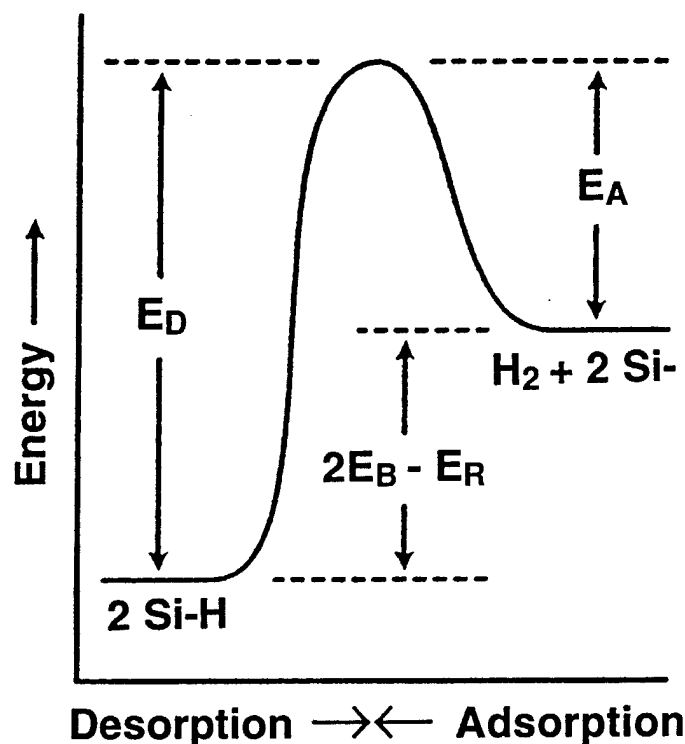


Figure 6. Bond and activation energies of hydrogen desorption and adsorption off/on Si surfaces (E_D = activation energy of desorption, E_A = activation energy of adsorption, E_R = H-H bond energy and E_B = Si-H bond energy); after [68].

activation energy for dissociative adsorption of H_2 onto Si(111), and between 15 and 19 kcal/mol for Si(100) [71,72]. In practice, Si surface bonds are capped with hydrogen mostly by HF rinses or using atomic H generated via plasmas or hot filaments [68,70]. Instead of all surface atoms becoming fully hydrogen-capped, Si(100) flats reconstruct to (2x1) upon baking in H_2 at high ($\geq 1100^\circ\text{C}$) temperatures [73]. Reconstruction is maintained even in air and atmospheric moisture for surprisingly long periods of time [73].

However, the high stability of the (2x1) structure was not always observed [74], especially not in progressively higher relative humidities [75]. In ultrahigh vacuum (UHV), molecular dynamics simulations predicted and experiments showed that Si(100) wafers pressed together statically (no sliding) spontaneously bonded covalently at RT [76]. These wafers were previously dehydrogenated in UHV and exhibited a (2x1) reconstruction pattern before contact. As early as in 1967, a paper dealing with the passivation of dangling Si bond defects at the Si/SiO₂ interface demonstrated that baking in H_2 at temperatures between 1000° and 1200 °C negated the effects of electron trapping at the interface [77]. A patent was granted along the same lines in 1979, teaching that passivation could be achieved between 650° and 950°C already [78]. Others have adapted this

method of reducing the number of charge carrier traps at the Si/SiO₂ interface [79,80]. Annealing of Si solar cells in H₂ similarly improved device performance [81,82]. The ability of both *atomic* and *molecular* hydrogen to passivate dangling bonds at the grain boundaries of poly-Si was similarly evaluated. The H₂ deactivated the free radicals during elevated temperature annealing, but not as effectively as H [82].

Epitaxial growth studies of Si [83] also deal with the dissociative chemisorption of H₂ [83]. Even Ref. 73, showing stable reconstruction of Si on hydrogen-annealing at elevated temperatures, contains a passing reference to some H₂ instability in terms of possible chemisorption: "...During the high temperature stage of the H₂ anneal the small steps on the silicon surface become unstable and by fast surface diffusion between the step edges larger flat terraces are formed so that the step density is minimized. Simultaneously or during the cooling down the surface reconstructs to the 2x1 structure, hydrogen is dissociatively absorbed [*sic*] on this surface during the cooling in the H₂ atmosphere." Heating of lapping-damaged Si surfaces in molecular hydrogen to temperatures as low as 380°C already started passivating dangling bonds, as attributed to either H₂ entering strained Si-Si bonds [81], or simply passivating the Si₃≡Si- dangling bonds on the surface [79,80]. Just plain heating Si to 810°C in vacuum alone was shown to deplete Si interstitials from the surface region and thus reduce dangling-bond-containing point defects [81].

Although these data show some ability on the part of molecular hydrogen to chemisorb on Si, they do not indicate unambiguously whether thermodynamic or kinetic factors control the decomposition of H₂, especially in the presence of the highly active dangling bonds continuously generated by wear.

As to *chemically induced* surface attrition (wear), annealing Si in H₂ at high temperatures (a) removes any oxide that formed during boule growth, originating from residual oxygen and moisture in the reactor [85], or (b) strips the thin native oxide that invariably forms on Si in air [86]. Further etching of the bare Si by hydrogen via the generation of volatile SiH₄ or by plain volatilization of the Si atoms is negligibly small below ~1000°C, but is observable above this temperature [86]. This is confirmed by other etching and Si evaporation data [87,88], where etching of the Si(100) surface was predicted to be nearly three-times faster than that of Si(111). The intermediate hydride products are apparently more readily stabilized on the Si(100) surface [87]. In contrast, surface cracking induced *mechanical* wear of Si should be higher in H₂ than in vacuum. Cracks forming in the wake of a high friction tribocontact act as important precursors to the wear of Si and PCD both in vacuum and PH₂. These cracks propagate faster in PH₂ (at least in the case of Si), because hydrogen passivates the dangling bonds that would otherwise hold the crack walls together [89].

6.2. RECONCILIATION WITH THE SEM TRIBOMETRIC DATA

The COF results are in line with the sorption data in the literature. The heating- and sliding-catalyzed dissociative chemisorption of H₂ in the thermal regime just before the mass desorption of the surface hydrides appears to be responsible for the lowest COF measured for all Si crystallinities in PH₂. The presence of hydrogen also skewed the surface desorption and the reconstruction temperatures to values higher than those observed in vacuum, in spite of more effective heat transfer between the heater strip and the flat in PH₂. The increase in the desorption temperatures may be explained by the LeChâtelier

Principle, a basic law of chemical equilibrium adapted to the present case: if a reaction (here, the desorption of an adsorbate) results in a gas (H_2) as a product, increasing the partial pressure of this gas in the reaction chamber will retard the reaction (i.e., desorption will occur at higher temperatures). A similar argument may also be applicable to the skewed re(de)construction troughs in PH_2 . Gas-phase reactions at the highest temperatures may have also hindered the formation and eventual dimerization of dangling bonds.

The COF remained high on cooling in PH_2 , because the chemisorption energy hill could not be overcome in the absence of sufficient thermal energy, the sliding induced flash temperatures and the presence of wear-generated dangling bonds notwithstanding. Therefore, on the first order, the tribocatalytic activation in the absence of external heating should be equal to or less than 46 kcal/mol on Si(111) and 15 to 19 kcal/mol on Si(100).

Yet, there was a passivating reaction with the small amount of residual water in the moderate SEM column *vacuum* during the cooling cycles (Fig. 3). This indicates that dissociated water vapor may also be a good atomic level lubricant for Si, provided the amount present in the test environment is below a certain partial pressure. The small amount of residual H_2O (on the order of 10^{-5} Torr) remaining in the SEM column readily sorbs onto the rubbed Si surface, in contrast with the severely hindered adsorption of the <1 ppm of H_2O remaining in the 99.999%-pure PH_2 . The residual H_2O molecules in PH_2 are unable to compete effectively with the much larger number of H_2 molecules for the surface. This concept of competitive sorption was previously explained in [58]. Therefore, the low starting and final RT COF in the SEM column vacuum may indicate some lubricating usefulness of even very small ($\sim 10^{-5}$ Torr) PH_2O interacting with the rubbed Si surfaces, provided that the thermal environment is below the desorption temperature of water. This hypothesis is now being tested for all three Si crystallinities by introducing a small PH_2O into the 0.2 Torr H_2 atmosphere of the SEM tribometer sub-chamber during standard thermal ramping (TR) to/from 850°C.

The fact that only Si(100) has benefited some from the PH_2 atmosphere in terms of reduced W during TR may be associated with the lowest surface energy of a fully H-terminated Si(100) [2,15], maintained longer to some extent by the effects of the LeChâtelier Principle. With the rest of the crystallinities, any wear reduction under the benign conditions of the tribocatalytic hydrogen chemisorption region is probably counteracted by the otherwise generally high COF and more extensive surface microcracking in PH_2 . As a combined result, the W_{TR} appeared to be the same for poly-Si and Si(111) both in vacuum and PH_2 . Examination of the photomicrographic appearance of the worn pin and flat scars as well as the morphology, amount and distribution of the wear debris may shed additional light on the differences and/or similarities in the respective wear mechanisms.

7. Conclusions

A review of the tribometric techniques used for the characterization of MEMS-MMA bearing materials (mainly Si) indicates that at interfaces where the proper degree of adhesion ("stiction" or repulsion) of essentially statically contacting surfaces is the critical value for MEMS operation, AFM/FFM is useful. Even MT might be made acceptable, if the specimen materials were changed from mica to more realistic candidates. However,

where the performance of the sliding-rolling interfaces is controlled by adhesion, friction and wear, more appropriate test machines are needed.

A summary of recent SEM tribometric experiments more suitable to the task is also given to show that high friction and wear are caused by a variety of factors related to the surface chemistry and low cohesive energy density of poly-Si, Si(100) and Si(111). Compared to PCD films, Si does not perform nearly as well as a MEMS bearing material. This major difference in behavior has been ascribed not just to the large difference in cohesive energy density, but also to the way Si and diamond interact with the environment. The respective W are controlled by shear-induced surface cracking superimposed by the adhesive interaction caused by the incipient linkage of dangling bonds between the sliding counterfaces. These bonds are generated by heating in vacuum or in PH_2 above the desorption temperature of the surface adsorbates and by wear. The validity of this hypothesis will be further scrutinized by the photographic examination of the PH_2 -worn scars.

The magnitude of the COF is material-specific, generally defined by the number and distribution of dangling (high friction), reconstructed (reduced friction) or adsorbate-passivated (low friction) surface bonds, as a function of temperature and the atmosphere. In PH_2 , the COF of the various Si crystallinities is as high or higher than in vacuum and significantly higher than those of the PCD. However, there is a remarkably repeatable reduction in COF_{Si} in a narrow temperature range just below the thermal desorption temperature of hydrogen, indicating the same type of heating- and sliding-catalyzed dissociative chemisorption of H_2 previously observed with PCD. Unlike PCD, however, the deconstructed (dangling) Si bonds do not react with H_2 on cooling, leaving the final COF at very high values.

Only the Si(100) appears to benefit, to a limited extent, from PH_2 in terms of some reduction in W . The other crystallinities exhibited essentially the same W in vacuum and PH_2 on standard thermal ramping to 850°C (near $10^{-12} \text{ m}^3/\text{N}\cdot\text{m}$, 10^4 -times more than PCD), although the wear rates were reduced during RT testing by about a factor of 10 to 100. *The wear rates could be further lowered by keeping COF the smallest by staying within the temperature range of the tribocatalytic reaction region.* The results indicate that operating Si MEMS-MMAs in the right thermal-atmospheric environment may lengthen their useful lifetimes sufficiently for a variety of practical applications, provided the MEMS electronics on the same chip can withstand the same temperatures.

Acknowledgments

The author would like to thank Messrs. S. Gabelich, L. Melton, B. Buller and G. Meldrum of Hughes Aircraft Company for performing the SEM tribotests with consummate skill and reducing the data to publishable form. Prof. Jiri Jonas (Beckmann Inst., U. of Illinois Champaign-Urbana) provided invaluable references essential to one of the main themes of the present paper. This research was completed under AFOSR Contract No. F49620-95-C-0002 managed by Maj. Hugh C. De Long at AFOSR/NL.

References

1. Gardos, M.N. (1996) Surface chemistry-controlled tribological behavior of Si and diamond, *Tribol. Lett.*, **2**, 173-187.
2. Gardos, M.N. (1996) Tribological behavior of polycrystalline and single-crystal silicon, *Tribol. Lett.*, **2**, 355-373.
3. Gardos, M.N. (1997) Tribological behavior of polycrystalline diamond films, in "Protective Coatings and Thin Films," *Proc. NATO Adv. Res. Workshop, May 30 - June 5, 1996, NATO ARW Series*, Y. Pauleau and P.B. Barna (eds.), Kluwer Academic Publishers, Dordrecht, The Netherlands, pp.185-196.
4. Gardos, M.N. (in press) Re(de)construction-induced friction signatures of polished polycrystalline diamond films in vacuum and hydrogen, *Tribol. Lett.*.
5. Gardos, M.N. (in press) Silicon and diamond for MEMS bearing applications in extreme environments, in *Proc. Fifth Int. Symp. on Diamond Materials*, 192nd Joint International Meeting of the Electrochem. Soc., Aug. 31-Sept. 5, 1997, Paris, France.
6. Gupta, B.K., Chevallier, J., and Bhushan, B., (1993) Tribology of ion bombarded silicon for micromechanical applications, *Trans. ASME, J. Tribol.*, **115**, 392-399.
7. Gupta, B.K., Bhushan, B., and Chevallier, J. (1994) Modification of tribological properties of silicon by boron ion implantation, *Tribol. Trans.*, **37**, 601-607.
8. Bhushan, B., and Li, X. (1997) Micromechanical and tribological characterization of doped single-crystal silicon and polysilicon films for microelectromechanical systems devices, *J. Mat. Res.*, **12**, 54-63.
9. Bhushan, B., and Koinkar, V.N. (1994) Tribological studies of silicon for magnetic recording applications, *J. Appl. Phys.*, **75**, 5741-5746.
10. Jang, D.-S., and Kim, D.-E. (1996) Optimum film thickness of thin metallic coatings on silicon substrates for low load sliding applications, *Tribol. Int.*, **29**, 345-356.
11. Alley, G.R.L., Cyuan, J., Howe, R.T., and Komvopoulos, K. (1992) The effect of release etch processing on surface microstructure stiction, in *Tech. Digest, 1992 IEEE Solid-State Sensor and Actuator Workshop* (June 21-25, 1992, Hilton Head Island, NC), pp. 202-207.
12. Mathieson, D., Beerschwinger, U., Yang, S.J., Reuben, R.L., Taghizadeh, M., Eckert, S., and Wallrabe, U. (1996) Effect of progressive wear on the friction characteristics of nickel LIGA processed rotors, *Wear*, **192**, 199-207.
13. Anon.(1996) Micromotor's lifetime exceeds six months, *Micromachine Devices (R&D Magazine Newsletter)*, **1**(3), Nov. 1996, p.2.
14. Sniegowski, J.J. (1996) Shrinking microdesigns in microdevices: surface micro-machined gearboxes, locks and mirrors, in *Proc. NAS/AVS/JPL Micromachining Workshop III*, Sept. 25-26, 1996, Anaheim, CA.; Miller, S.L., Sniegowski, J.J., LaVigne, G., and McWhorter, P.J. (1996) Performance tradeoffs for a surface micromachined microengine, *Micromachined Devices and Components II*, SPIE Proc. Vol. **2882**, 182-191.
15. Houston, M.R., Howe, R.T., and Maboudian, R. (1997) Effect of hydrogen termination on the work of adhesion between rough surfaces, *J. Appl. Phys.*, **81**, 3474-3483.

16. Tsukruk, V.T., Bliznyuk, V. N., Visser, D., and Hazel, J. (1996) Reconstruction of fluid Langmuir monolayers under shear forces, *Tribol. Lett.*, **2**, 71-80; Tsukruk, V.V., Bliznyuk, V.B., and Everson, M.P. (1996) Nanotribology of composite molecular layers, *Polymer Prepr.*, **37**, 557-558.
17. Wang, D., Thomas, S.G., Wang, K.L., Xia, Y., and Whitesides, G.M. (1997) Nanometer scale patterning and pattern transfer on amorphous Si, crystalline Si, and SiO₂ surfaces using self-assembled monolayers, *Appl. Phys. Lett.*, **70**, 1593-1595.
18. Abeln, G.C., Lee, S.Y., Lyding, J.W., Thompson, D.S., and Moore, J.S. (1997) Nanopatterning organic monolayers on Si(100) by selective chemisorption of norbornadiene, *Appl. Phys. Lett.*, **70**, 2747-2749.
19. Maboudian, R., and Howe, R.T. (1997) Stiction reduction processes for surface micromachines, *Tribol. Lett.*, **3**, 215-221.
20. Zanolari, E.S., Danyluk, S., and McNallan, M.J. (1995) Formation of cylindrical sliding-wear debris on silicon in humid conditions and elevated temperatures, *Tribol. Trans.*, **38**, 721-727.
21. Yoshizawa, H., Chen, Y.-L., and Israelaschvili, J. (1993) Recent advances in molecular level understanding of adhesion, friction and lubrication, *Wear*, **168**, 161-166.
22. Klein, J., Kumacheva, E., Mahalu, D., Perahla, D., and Fetters, L.J. (1994) Reducing the frictional forces between solid surfaces bearing polymer brushes, *Nature*, **370**, 634-636.
23. Elings, V.B., and Gurley, J.A. Scanning tunneling microscopy in research and development, *Res. & Dev.*, Feb. 1989, pp. 126-129.
24. Alley, R.L., Mai, P., Komvopoulos, K., and Howe, R.T. (1993) Surface roughness modification of interfacial contacts in polysilicon microstructures, in *Proc. 7th Int. Conf. Solid-State Sensors and Actuators, TRANSDUCERS '93*, June 7-10, 1993, Yokohama, Japan.
25. Suh, N.P., Moshleh, M., and Howard, P. S. (1994) Control of friction, *Wear*, **175**, 151-158.
26. Kotwal, C.A., and Bhushan, B. (1996) Contact analysis of non-Gaussian surfaces for minimum static and kinetic friction and wear, *Tribol. Trans.*, **39**, 890-898.
27. Dubruejaud, B., Vardavoulis, M., and Jeandin, M. (1994) The role of porosity in the dry sliding wear of a sintered ferrous alloy, *Wear*, **174**, 155-161.
28. Ando, J., Ino, Y., Ishikawa, Y., and Kitahara, T. (1996) Friction and pull-off force on silicon surface modified by FIB, in *Proc. Ninth Ann. Int. Workshop on Micro Electro Mechanical Systems*, San Diego, CA Feb. 11-15, 1996, IEEE Cat. No. 96CH35856, ISSN 1084-6999, pp. 349-353.
29. Arai, F., Andou, D., and Fukuda, T. (1996) Adhesion forces reduction for micro manipulation based on micro physics, in *Proc. Ninth Ann. Int. Workshop on Micro Electro Mechanical Systems*, San Diego, CA Feb. 11-15, 1996, IEEE Cat. No. 96CH35856, ISSN 1084-6999, pp. 354-359.
30. Stanley, H.M., Etsion, I., and Bogy, D.B. (1990) Adhesion of contacting rough surfaces in the presence of sub-boundary lubrication, *Trans. ASME, J. Tribol.*, **112**, 98-104; Jeng, Y.-R., (1996) Impact of Plateaued Surfaces on Tribological Performance, *Tribol. Trans.*, **39**, 354-361.
31. Komvopoulos, K., and Yan, Y. (1997) A fractal analysis of stiction in micromechanical systems, *Trans. ASME, J. Tribol.*, **119**, 391-400.
32. Anon. (1996) Kona conference raises 4 issues about commercialization of MEMS, *Micromachine Devices (R&D Magazine Newsletter)*, **1**(2), Oct. 1996, p. 2.

33. Helvajian, H., and Robinson, E.Y. (eds.) (1993) Micro- and nanotechnology for space systems: an initial evaluation, *ATR-93(8349)-1*, The Aerospace Corp., El Segundo, CA, 1993; Scott, W.B. Micromachines Hold Promise for Aerospace, *Aviation Week*, March 1, 1993, p. 36.
34. Helvajian, H. (ed.) (1995) Microengineering technology for space systems, *ATR-95(8168)-2*, The Aerospace Corp., El Segundo, CA, 30 Sept. 1995.
35. Hawkey, T.J., and Torti, R.P. (1993) Integrated microgyroscope, in *Proc. Workshop on Microtechnologies and Applications to Space Systems*, JPL Publ. 93-8, NASA CR-195688, June 15, 1993, pp.257-264.
36. Yates, R., Williams, C., Shearwood, C., and Mellor, P. (1996) A Micromachined rotating yaw rate sensor, *Micromachined devices and Components II*, SPIE Proc. Vol. 2882, 161-168.
37. Legtenberg, R., Berenschot, E., Elwenspoek, M., and Fluitman, J. (1996) Electrostatic microactuators with integrated gear linkages for mechanical power transmission, in *Proc. Ninth Ann. Int. Workshop on Micro Electro Mechanical Systems*, San Diego, CA Feb. 11-15, 1996, IEEE Cat. No. 96CH35856, ISSN 1084-6999, pp. 204-209.
38. Bright, V.M., Reid, J.R., and Comtois, J.H. (1996) Polysilicon thermal actuator arrays and applications, in *Proc. NAS/AVS/JPL Micromachining Workshop III*, Sept. 25-26, 1996, Anaheim, CA.
39. Bhushan, B. (1996) Nanotribology and nanomechanics of MEMS devices, in *Proc. Ninth Ann. Int. Workshop on Micro Electro Mechanical Systems*, San Diego, CA Feb. 11-15, 1996, IEEE Cat. No. 96CH35856, ISSN 1084-6999, pp. 91-98.
40. Israelaschvili, J.N., and McGuiggan, P.M. (1990) Adhesion and short-range forces between surfaces. Part I: New apparatus for surface force measurements, *J. Mater. Res.*, 5, 2223-2231; *ibid*, Part II: Effects of surface lattice mismatch, 2232-2243.
41. Van Alsten, J., and Granick, S. (1989) Friction measured with a surface forces apparatus, *Tribol. Trans.*, 32, 246-250.
42. Hirano, M., Shinjo, K., Kaneko, R., and Murata, Y. (1991) Anisotropy of frictional forces in muscovite mica, *Phys. Rev. Lett.*, 67, 2642-2645.
43. Matsuoka, H., and Kato, T. (1996) Discrete nature of ultrathin lubrication film between mica surfaces, *Trans. ASME, J. Tribol.*, 118, 832-838.
44. Gabriel, K.J., Behi, F., Mahadevan, R., and Mehregany, M. (1990) In-situ friction and wear measurements in integrated polysilicon mechanisms, *Sensors and Actuators*, A21-A23, 184-188.
45. Fearing, R.S. (1995) Survey of sticking effects for micro parts handling, in *Proc. 1995 IEEE/RSJ Int. Conf. on Intelligent Robotics and Systems*, Vol. 2, 212-217.
46. Noy, A., Frisbie, C.D., Rozsnyai, L.F., Wrighton, M.S., and Lieber, C.M. (1995) Chemical force microscopy: exploiting chemically-modified tips to quantify adhesion, friction, and functional group distributions in molecular assemblies, *J. Am. Chem. Soc.*, 117, 7943-7951; Thomas, R.C., Houston, J.E., Crooks, R.M., Kim, T., and Michalske, T.A. (1995) Probing adhesion forces at the molecular scale, *J. Am. Chem. Soc.*, 117, 3830-3834.
47. Meyer, E., Lüthi, R., Howald, L., Gutmannsbauer, W., Haefke, H., and Güntherodt, H.-J. (1996) Friction force microscopy on well-defined surfaces, *Nanotechnology*, 7, 340-344.
48. Kim, Y., Huang, J.-L., and Lieber, C.M. (1991) Characterization of nanometer scale wear and oxidation of transition metal dichalcogenide lubricants by atomic force microscopy, *Appl. Phys. Lett.*, 59, 3404-3406.

49. Lieber, C.M., and Kim, Y. (1991) Characterization of the structural, electronic and tribological properties of metal dichalcogenides by scanning probe microscopies, *Thin Solid Films*, **206**, 355-3590.
50. Lüthi, R., Meyer, E., Haefke, H., Howald, L., Gutmanns Bauer, W., and Güntherodt, H.-J. (1994) Sled-type motion on the nanometer scale: cohesive energies of C₆₀, *Science*, **266**, 1979-1981.
51. Feldman, K., Fritz, M., Hahner, G., Marti, A., and Spencer, N.D. (1997) Surface forces, surface chemistry, and tribology," invited paper presented at the First World Tribology Congress, Sept. 8-12, 1997, London, England, in *New Directions in Tribology*, Mech. Eng. Publ. Ltd., London, England, 1997, pp. 347-353.
52. Gardos, M.N. (1990) Determination of the tribological fundamentals of solid lubricated ceramics, Volume 1: Summary, *WRDC-TR-90-4096*, Nov. 1990, Hughes Aircraft Co., El Segundo, CA, USA.
53. Gardos, M.N. (1988) The effect of anion vacancies on the tribological properties of rutile (TiO_{2-x}), *Tribol. Trans.*, **31**, 427-436; also see discussions on this paper (1989) *Tribol. Trans.*, **32**, 30-31 ; Gardos, M.N., Hong, H.-S., and Winer, W.O. (1990) The Effect of anion vacancies on the tribological properties of rutile (TiO_{2-x}), Part II: Experimental evidence, *Tribol. Trans.*, **32**, 209-220.
54. Gardos, M.N. (1989) The Tribooxidative behavior of rutile-forming substrates, in *Mat. Res. Soc. Symp. Proc., New Materials Approaches to Tribology: Theory and Applications*, L. E. Pope, L. L. Fehrenbacher and W. O. Winer, (eds.) Vol. **140**, 325-338.
55. Gardos, M.N. (1993) The Effect of Magnéli phases on the tribological properties of polycrystalline rutile (TiO_{2-x}), in *Proc. 6th Int. Congr. on Tribology, Eurotrib '93*, M. Kozma (ed.), Vol. **3**, Aug. 30 - Sept. 2, 1993, Budapest, Hungary, pp. 201-206.
56. Gardos, M.N. (1994) Determination of the tribological fundamentals of solid lubricated ceramics, Part III: Molecular engineering of rutile (TiO_{2-x}) as a lubricious oxide, *WL-TR-94-4108*, Hughes Aircraft Company, El Segundo, CA, USA, Oct. 1994.
57. Didziulis, S.V., Fleischauer, P.D., Soriano, B.L., and Gardos, M.N. (1990) Chemical and tribological studies of MoS₂ films on SiC substrates, *Surf. Coat. Technol.*, **43/44**, 652-662.
58. Gardos, M.N. (1995) Anomalous wear behavior of MoS₂ Films in moderate vacuum and dry nitrogen, *Tribol. Lett.*, **1**, 67-85.
59. Gardos, M.N., Adams, P.M., Barrie, J.D., and Hilton, M.R. (1997) Crystal-structure-controlled tribological behavior of carbon-graphite seal materials in partial pressures of helium and hydrogen. I. Specimen characterization and fundamental considerations, *Tribol. Lett.*, **3**, 175-184.
60. Gardos, M.N., Davis, P.S., and Meldrum, G.R. (1997) Crystal-structure-controlled tribological behavior of carbon-graphite seal materials in partial pressures of helium and hydrogen. II. SEM tribometry, *Tribol. Lett.*, **3**, 185-198.
61. Gardos, M.N., and Buller, B.W. (1997) Crystal-structure-controlled tribological behavior of carbon-graphite seal materials in partial pressures of helium and hydrogen. III. Cryogenic (100 K) wear tests, *Tribol. Lett.*, **3**, 199-204.
62. Uchida, Y., Deane, S.C., and Milne, W.I. (1992) Posthydrogenation of low-pressure chemical vapor deposited amorphous silicon using a novel internal lamp system and its application to thin-film transistor fabrication, *J. Appl. Phys.*, **72**, 3150-3154.

63. Gardos, M.N., and Meeks, C.R. (1984) Solid lubricated rolling element bearings, Part I: Gyro bearings and the associated solid lubricants research, *Vol. I: Summary*, AFWAL-TR-83-4129, Final Report, Hughes Aircraft Company, El Segundo, CA, February 1984.
64. Abrefah, J., Olander, D.R., and Balooch, M. (1990) Hydrogen dissolution in and release from nonmetals. II. Crystalline silicon, *J. Appl. Phys.*, **67**, 3302-3310.
65. Beyer, W. (1991) Hydrogen effusion: a probe for surface desorption and diffusion, *Physica B*, **170**, 105-114.
66. Stutzman, M., Beyer, W., Tapfer, L., and Herrero, C.P. (1991) States of hydrogen in crystalline silicon, *Physica B*, **170**, 240-244.
67. Jackson, W.B., Johnson, N.M., Tsai, C.C., Wu, I.-W., Chiang, A., and Smith, D. (1992) Hydrogen diffusion in polycrystalline silicon thin films, *Appl. Phys. Lett.*, **61**, 1670-1672.
68. Myers, S.M., Follstaedt, D.M., Stein, H.J., and Wampler, W.R. (1992) Hydrogen interaction with cavities in helium-implanted silicon, *Phys. Rev. B*, **47**, 13,380-13,394.
69. Wu, C.J., Ionova, I.V., and Carter, E.A. (1994) First-principles-derived rate constants for H ad-atom surface diffusion on Si(100)-2x1, *Phys. Rev. B*, **49**, 13,488-13,500.
70. Wu, C.J., Ionova, I.V., and Carter, E.A. (1993) Ab initio H₂ desorption pathways for H/Si(100): the role of SiH₂(a), *Surf. Sci.*, **295**, 64-78.
71. Sinniah, K., Sherman, M.G., Lewis, L.B., Weinberg, W.H., Yates, J.T. Jr., and Janda, K.C. (1989) New mechanism for hydrogen desorption from covalent surfaces: the monohydride phase on Si(100), *Phys. Rev. Lett.*, **62**, 567-570.
72. Sinniah, K., Sherman, M.G., Lewis, L.B., Weinberg, W.H., Yates, J.T. Jr., and Janda, K.C. (1990) Hydrogen desorption from the monohydride phase on Si(100), *J. Chem. Phys.*, **92**, 5700-5711.
73. Bender, H., Verhaverbeke, S., Caymax, M., Vatel, O., and Heynes, M.N. (1994) Surface reconstruction of hydrogen annealed (100) Silicon, *J. Appl. Phys.*, **75**, 1207-1209.
74. Ibach, H., Wagner, H., and Bruchman, D. (1982) Dissociative chemisorption of H₂O on Si(100) and Si(111) - a vibrational study, *Solid State Commun.*, **42**, 457-459.
75. Sakuraba, M., Murota, J., and Ono, S. (1994) Stability of the dimer structure formed on Si(100) by ultraclean low-pressure chemical-vapor deposition, *J. Appl. Phys.*, **75**, 3701-3703.
76. Gösele, U., Stenzel, H., Martioni, T., Steinkirchner, J., Conrad, D. and Schneeschmidt, K. (1995) Self-propagating room-temperature silicon wafer bonding in ultrahigh vacuum, *Appl. Phys. Lett.*, **67**, 3614-3616.
77. Hofstein, S.R. (1967) Stabilization of MOS devices, *Solid State Electronics*, **10**, 657-670.
78. Levinstein, H.J., and Sinha, A.K. (1979) Hydrogen annealing process for stabilizing metal-oxide-semiconductor structures, *U.S. Patent No. 4,151,007*, Apr. 24, 1979.
79. Bower, K.L., and Myers, S.M. (1990) Chemical kinetics of hydrogen and (111)Si-SiO₂ interface defects, *Appl. Phys. Lett.*, **57**, 162-164.
80. Mrstik, B.J., and Rendell, R.W. (1991) Model for Si-SiO₂ interface state formation during irradiation and during post-irradiation exposure to hydrogen environment, *Appl. Phys. Lett.*, **59**, 3012-3014.

81. Babsail, L.S., and Morrison, S.R. (1991) The Effect of hydrogen treatment on damaged and undamaged metal-insulator-semiconductor solar cells, *J. Appl. Phys.*, **70**, 259-265.
82. Kazmerski, L.L. (1988) Investigation of impurity neutralization and defect passivation in polycrystalline silicon solar cells, in *Mat. Res. Soc. Symp. Proc.*, Vol. **106**, 199-211.
83. Wolff, S.H., and Wagner, S. (1989) Hydrogen surface coverage: raising the silicon epitaxial growth temperature, *Appl. Phys. Lett.*, **55**, 2017-2019.
84. Gossman, H.-J., Rafferty, C.S., Unterwald, F.C., Boone, T., Mogi, T.K., Thompson, M.O., and Luftman, H.S. (1995) Behavior of intrinsic Si point defects during annealing in vacuum, *Appl. Phys. Lett.*, **67**, 1558-1560.
85. Yanase, Y., Horie, H., Oka, Y., Sano, M., Sumita, S., and Shigematsu, T. (1994) Atomic force microscopy observation of Si(100) surface after hydrogen annealing, *J. Electrochem. Soc.*, **141**, 3259-3263.
86. Gallois, B.M., Besmann, T.M., and Stutt, M.W. (1994) Chemical etching of Silicon(100) by hydrogen, *J. Am. Ceram. Soc.*, **77**, 2949-2952.
87. Wei, L. Li, Y., and Tsong, I.S.T. (1995) Etching of Si(111)-(7x7) and Si(100)-(2x1) surfaces by atomic hydrogen, *Appl. Phys. Lett.*, **66**, 1818-1820.
88. Zhong, L., Fujimori, H., Shimbo, M., Kashima, K., Matsushita, Y., Aiba, Y., Hayashi, K., Takeda, R., Shirai, H., Saito, H., Matsushita, J.-I., and Yoshikawa, J. (1995) Determination of Si evaporation rate at 1200°C in hydrogen, *Appl. Phys. Lett.*, **67**, 3951-3953.
89. Thouless, M.D., and Cook, R.F. (1990) Stress-corrosion cracking in silicon, *Appl. Phys. Lett.*, **56**, 1962-1964; Lu, X., Cheung, N.W., Strathman, M.D., Chu, P.K., and Doyle, B. (1997) Hydrogen induced silicon surface layer cleavage, *Appl. Phys. Lett.*, **71**, 1804-1806.